UNIVERSITÄT OSNABRÜCK

Simultaneous optical and electrical recordings in horizontal lipid bilayers

Membrane dynamics and protein interactions

Dissertation

Presented to the department of Biology/Chemistry,
University of Osnabrueck in partial fulfillment of the requirements for the degree of '*Doctor Rerum Naturalium*'

by

Alf Honigmann

Osnabrueck
June 2010

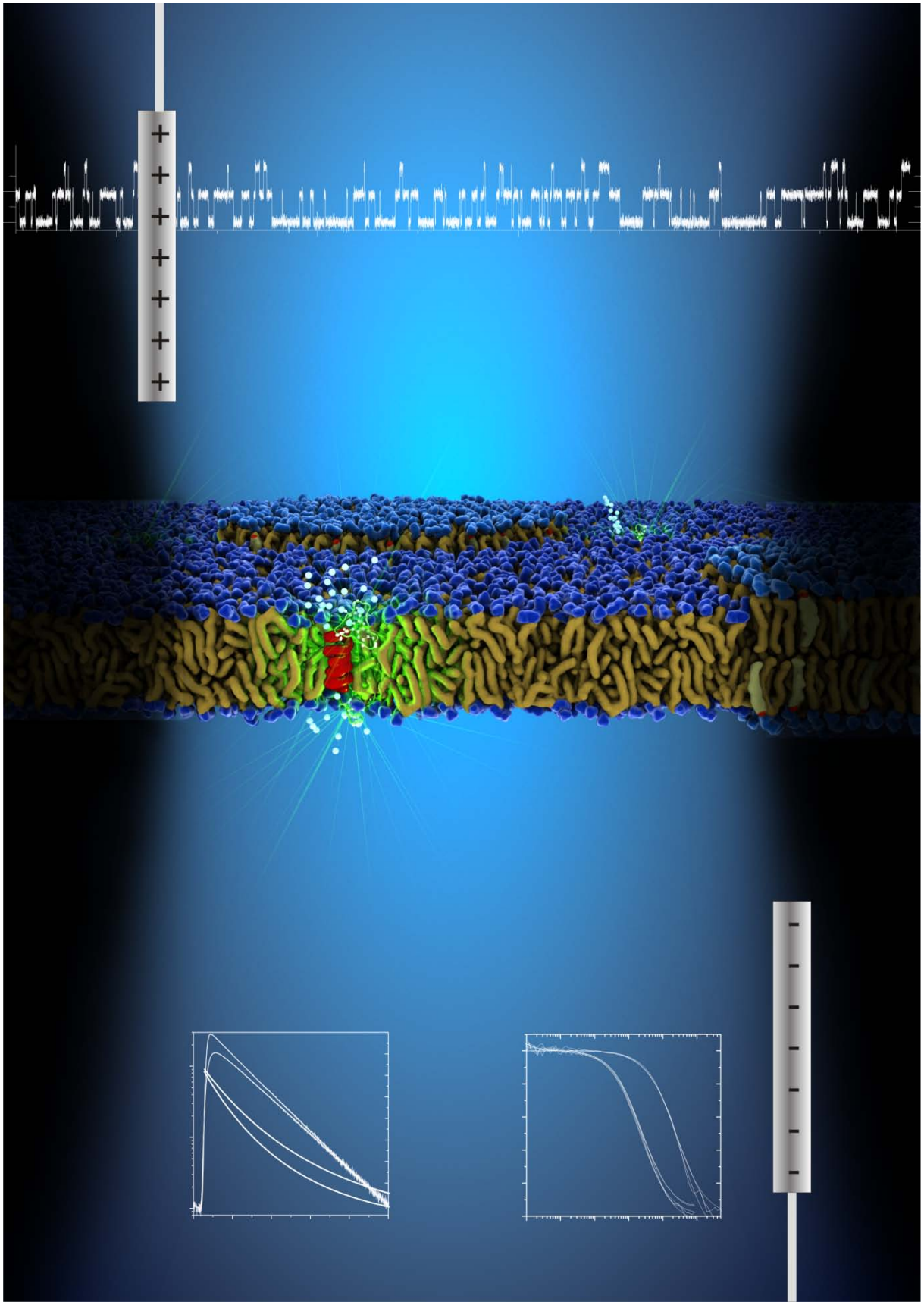

Table of Contents

1. Introduction 1

1.1 Preface 1
1.2 Biological membranes 2
1.3 Membrane model systems 3
1.4 The planar lipid bilayer technique 5
1.5 Electro-optical studies on lipid bilayers 8
1.6 The electro-optical bilayer setup 8
1.7 Fluorescence fluctuation spectroscopy (FFS) 10
1.7.1 Fluorescence correlation spectroscopy (FCS) 11
1.7.2 Confocal fluorescence lifetime analysis (cFLA) and time resolved anisotropy (cTRA) 12
1.8 Objectives of this thesis 15
1.9 References 16

2. Characterization of horizontal lipid bilayers as a model system to study lipid phase separation 23

2.1 Abstract 23
2.2 Introduction 23
2.3 Material and methods 25
2.3.1 Chemicals 25
2.3.2 Horizontal lipid bilayers 25
2.3.3 Confocal microscopy 27
2.3.4 Time resolved anisotropy (TRA) 27
2.3.5 Fluorescence correlation spectroscopy (FCS) 28
2.3.6 Steady state anisotropy 29
2.3.7 Temperature Control 30
2.3.8 Bilayer viscosity determination 30
2.3.9 L_o domain tracking 30
2.3.10 Gramicidin A labeling and electrophysiological activity 31
2.4 Results 32
2.4.1 Effect of hydrocarbon solvents on lipid mobility in horizontal bilayers 32
2.4.2 Phase separation 33
2.4.3 Lateral mobility of lipid probes in L_o and L_d phase 33
2.4.4 Rotational diffusion in the L_d and L_o phase 34

2.4.5 Dipole-orientation of Atto647N-Lipids 36
2.4.6 Steady state anisotropy 37
2.4.7 FCS diffusion laws in lipid domains and temperature dependence 38
2.4.8 Hydrodynamic viscosity of planar bilayers in the L_d phase 40
2.4.9 Electrical resistance of binary and ternary lipid mixtures 42
2.4.10 Partitioning and electrical activity of gramicidin A in lipid domains 43
2.5 Discussion 45
2.6 References 46
3. Membrane binding and channel formation of Colicin A studied with an electro-optical approach 53
3.1 Abstract 53
3.2 Introduction 53
3.3 Material and Methods 55
3.3.1 Chemicals 55
3.3.2 Mutagenesis, preparation and purification of ColA 56
3.3.3 Fluorescence labeling of single cysteine ColA mutants 57
3.3.4 Horizontal lipid bilayers and electrophysiology 57
3.3.5 Confocal microscopy setup 57
3.3.6 Fluorescence correlation spectroscopy (FCS) 58
3.3.7 Fluorescence cross-correlation spectroscopy (FCCS) 58
3.3.8 Confocal fluorescence lifetime measurements 59
3.3.9 Steady state fluorescence measurements 59
3.3.10 Calcein efflux from liposomes incubated with ColA 59
3.4 Results 61
3.4.1 Membrane binding of ColA is pH dependent 61
3.4.2 Electrophysiological properties of single ColA channels 63
3.4.3 Oligomerization measurements of ColA 65
3.4.4 ColA induces calcein efflux from liposomes at acidic pH 68
3.4.5 The membrane bound state of ColA 68
3.5 Discussion 71
3.5.1 pH dependence of membrane binding 71
3.5.2 Electrophysiological properties of the ColA-channel 72
3.5.3 ColA induced Calcein efflux from liposomes 72
3.5.4 ColA is a monomer in aqueous solution as well as in a membrane environment 73
3.5.5 The membrane bound conformation of ColA 73

3.5.6 The open channel conformation of ColA 75
3.6 References 75
4. Conclusion 81
4.1 Limitations of HLBs in combination with FFS 82
4.1.1 The size relation problem 82
4.1.2 Incorporation of functional ion channels into HLBs 83
4.1.3 Detection of non electrolyte transport through the bilayer 84
4.1.4 Lifetime of HLBs 85
4.2 Outlook 85
4.2.1 Lipid domain partitioning of KV-channels 85
4.2.2 Calmodulin binding to Sec61 86
4.2.3 Single particle tracking 86
4.3 References 87
5. Summary 91
6. Appendix 93
6.1 Construction plans of the horizontal bilayer chip 93
6.1.1 Component assembly 93
6.1.2 PTFE Chamber 94
6.1.3 Upper adhesive tape 95
6.1.4 PTFE foil 96
6.1.5 Lower adhesive film 97
6.1.6 Temperature control 98
6.2 Publications 99
6.3 Index of figures and tables 99
6.4 Abbreviations 100
6.5 Software 102

1. Introduction

1.1 Preface

In this thesis the deployment of a methodological combination of two single molecule techniques, the planar bilayer technique and fluorescence fluctuation spectroscopy, is presented. The newly devised electro-optical setup will serve as a sophisticated model system for electrical excitable biological membranes. The expectation on a combined electro-optical setup is to be able to correlate the function of membrane channels (electrical activity) with its structural properties (fluorescence assays).

The thesis is grouped into four chapters: A general introduction, providing the biological and methodological background, is followed by two studies on the application of the electro-optical setup in the field of membrane biophysics. In the first study the electrical and diffusion properties of planar bilayer membranes made of simple and ternary lipid mixtures are characterized. Additionally, the influence of temperature dependent lipid phase separation on the electrical activity of the ion channel gramicidin A is studied. The second study addresses the conformational changes of the pore-forming toxin Colicin A during membrane binding and ion channel formation. Finally, the potentials and the limitation of the presented setup are discussed.

1.2 Biological membranes

Every living cell is separated from its dissipating environment by at least one membrane (plasma membrane) which selectively controls the exchange of material. Additionally, eukaryotic cells contain systems of internal membranes which form specialized compartments within the cytoplasm. Besides the obvious role of a lipid membrane as a permeability barrier, a variety of other vitally important processes occur in and at membranes, to name a few: signaling and sensing, energy conversion and electrical action potential propagation. To constitute this variety of functions each membrane type is a composite of a dedicated ensemble of lipids, sugars and proteins [1, 2].

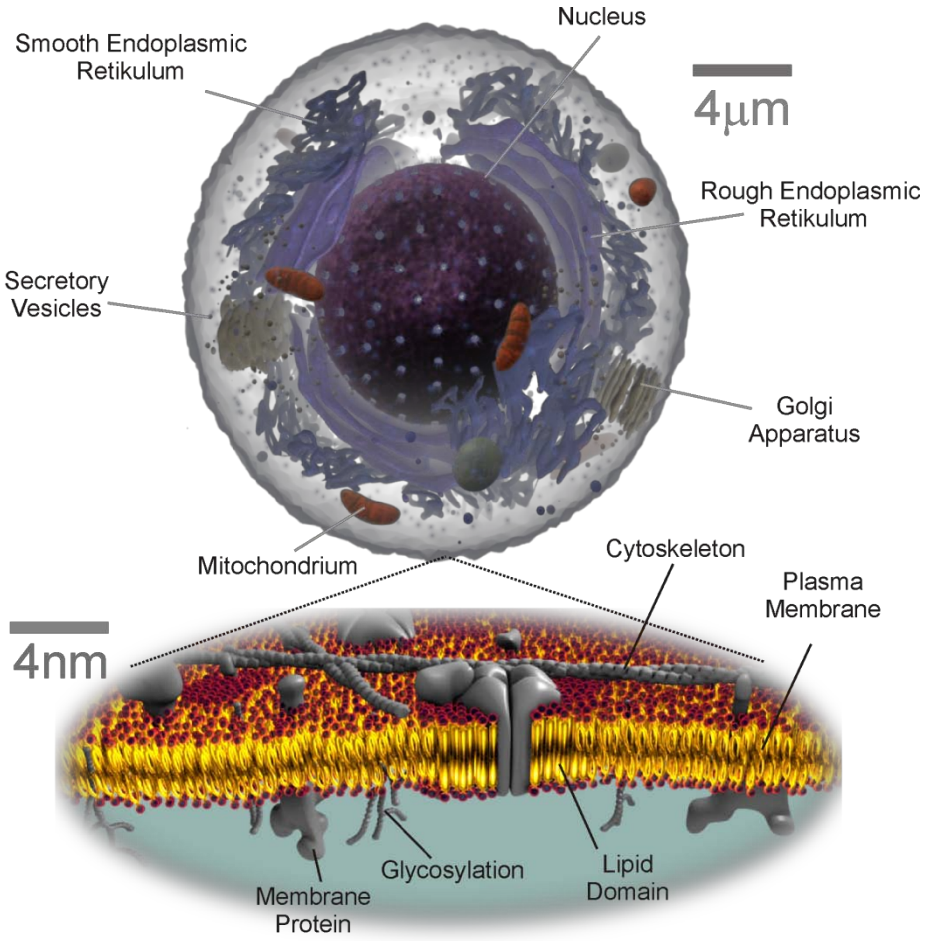

FIGURE 1.1 Cartoon of a eukaryotic cell showing the various compartments, which are set up by different types of membranes. The lower panel shows a magnification of the plasma membrane. The lipid bilayer is shown in red/gold. Membrane proteins and glycosylations are shown in gray. For clarity membrane associated and cytosolic proteins are omitted.

Understanding the mechanisms of membrane organization and the regulation of membrane functions is an important part in the field of molecular biology. The first generally accepted model for cell membranes, the fluid mosaic model, was proposed by Singer and Nicolson in

1972 [3]. In this model the cell membrane is described as a fluid bilayer of lipids in which the hydrophobic integral membrane proteins are freely diffusing.
In the last three decades, with its technical improvements, the simple view of the bilayer as a passive carrier for proteins has been gradually expanded by a more interactive relation between the lipid composition of the bilayer and the function of proteins [2, 4-6]. The free diffusion of membrane constituents, as suggested by the fluid mosaic model, seems to be restricted / regulated by different processes. As 15 % – 30 % of cell membrane surface area is estimated to be occupied by proteins, one can expect that the properties of the bilayer will be greatly influenced by its protein content [7]. In fact the high protein density itself restricts the fluidity of the bilayer and leads to molecular crowding effects [8, 9]. Additionally, many membrane proteins are organized in oligomeric complexes or even super-complexes of multiple different oligomeric proteins, which often interact with protein components on both sides of the membrane (e.g. cytoskeleton). Thus, the position of these proteinaceous sites is virtually anchored in the membrane [10, 11].
The heterogeneous distribution of proteins in the bilayer was suggested to be related to the local lipid environment [12]. This theory was based mainly on two findings. Firstly, a certain fraction of membrane proteins can be purified together with a sphingolipids and cholesterol enriched lipid phase (DRMs). Secondly, sphingolipids, saturated phospholipids and cholesterol were shown to phase separate into lipid domains in an unsaturated lipid model membrane environment [12, 13]. In many studies on cell membranes indications have been found that proteins and lipids are indeed organized into nano-meter sized domains [14-16]. Lipid phase separation is thought to influence the sorting of specific proteins to specialized patches in the membrane [17-19].
Generally, as more details are revealed by higher resolution and more advanced techniques, the simplified view of biological membrane has to be gradually extended. The various forces affecting the functional organization of biological membranes are still topic of current research. New methods are required for a comprehensive understanding of the structure function relationship of biological membranes.

1.3 Membrane model systems

Since the complexity of the biological membrane content renders an in vivo analysis of single functional aspects very difficult, model systems have been used to reconstitute specific components of a biological membrane in vitro. To give a short overview, the benefits and drawbacks of the most popular membrane model systems will be briefly discussed.
The simplest and most widely used model system is the liposome (also referred to as unilamellar vesicles) (Fig. 1.2*A*). According to the size of the liposomes three classes are distinguished: small unilamellar vesicles (< 100 nm SUV), large unilamellar vesicles (≈ 200 nm LUV) and giant unilamellar vesicles (> 1 µm GUV).SUVs and LUVs are

suited for ensemble spectroscopy, while GUVs can be imaged by microscopy techniques. The reason for the popularity of using SUVs and LUVs as model systems is that they are easy to produce and membrane proteins can be functionally incorporated by detergent reconstitution methods [20]. In contrast the preparation of GUVs is technically more challenging and in most cases requires a dehydration step of lipids which makes reconstitution of proteins more complicated. The most efficient technique to produce GUVs is electro-formation [21, 22]. GUVs have been extensively employed in the field of lipid phase separation, because most parts of the membrane are free standing and lipid domains can be imaged by confocal microscopy [23, 24].

Immobilized membranes which are deposited e.g. by vesicle fusion on a solid support [25] are referred to as supported lipid bilayers (SLB) (Fig. 1.2*B*). Generally, SLBs are rather stable and can be studied with high resolution, surface sensitive methods such as total internal reflection microscopy (TIRFM) or atomic force microscopy (AFM) [26, 27]. Since one leaflet of SLBs directly interacts with the supporting material, only one side of the membrane is accessible to modifications during an experiment. Furthermore, unspecific interactions between the support material and membrane components may cause artifacts. To minimize surface interactions a layer of polymer tethers can be placed between the support and the membrane [28].

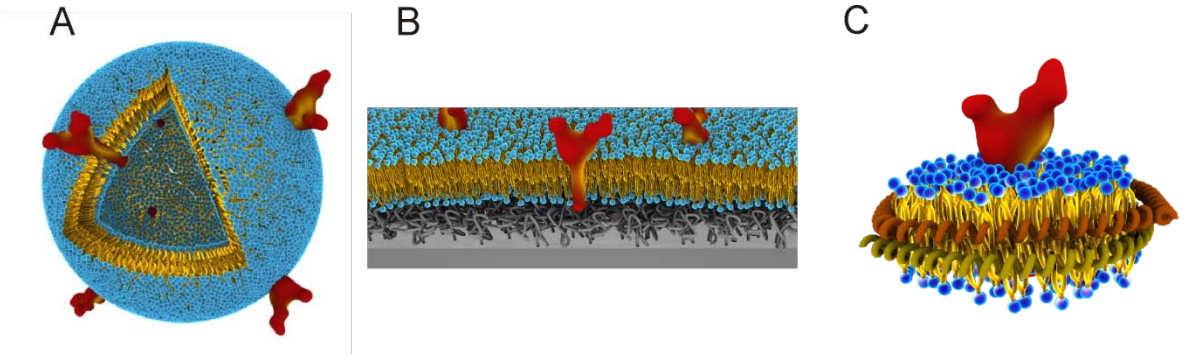

FIGURE 1.2 Model membrane systems: (A) Unilamellar vesicles with reconstituted membrane proteins. (B) Supported lipid bilayer on a tethered polymer support with reconstituted membrane proteins. (C) Phospholipid bilayer nano-disc shaped by scaffolding proteins. The nano-disc contains one reconstituted membrane protein.

As an alternative to SUVs lipid nano-discs have been established. The bilayer nano-discs were derived from high-density lipoprotein particles which are involved in cholesterol and fatty acids homeostasis in the blood cycle [29]. The nano-discs are shaped by the protein apo A-1 which acts as a scaffold surrounding a number of lipids. Purified and lipid reconstituted apo A-1 nano-discs were shown to have a mono-disperse size distribution ($Ø \approx 10$ nm), which is an advantage in many structural analysis techniques. Also, the planarity of the disc may be an advantage compared to liposomes, because both side of the disc are accessible

during an experiment. Membrane proteins can be added to nano-disc by detergent reconstitutions methods comparable to liposomes. However, the restricted small size of nano-discs may hamper reconstitution of large protein complexes.

1.4 The planar lipid bilayer technique

The electrophysiological properties of a lipid membrane can be studied with the planar bilayer technique, also referred to as black lipid membranes (BLM) [30, 31]. This membrane model system will be introduced in more detail, because it is a precursor of the finally presented electro-optical bilayer technique.

In a typical BLM setup two aqueous compartments are separated by a free standing, vertical, planar lipid bilayer. Via electrodes in both compartments the membrane is voltage clamped such that its electrical properties can be monitored (Fig. 1.3).

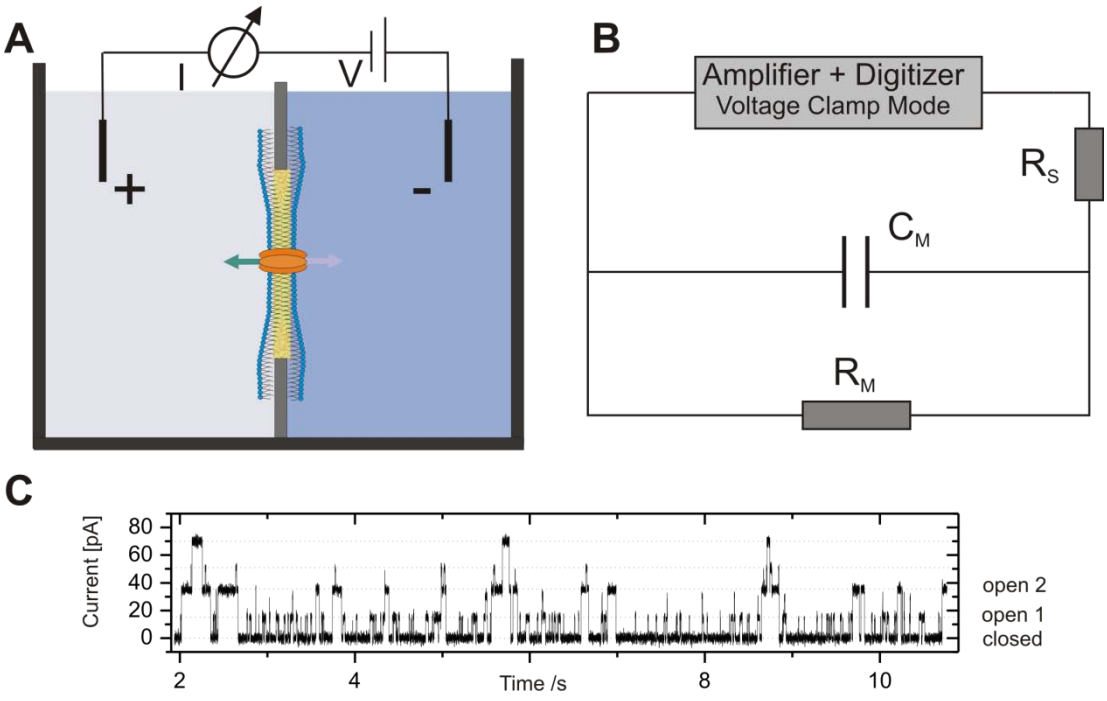

FIGURE 1.3 BLM setup. (A) Scheme of a bilayer chamber with the planar lipid membrane separating the *Cis* and *Trans* compartment. The bilayer is formed form a hydrocarbon solvent mixture. The transition of the 5 nm thick bilayer to the 25 µm thick PTFE-sheet is formed by a torus containing the hydrocarbon solvent. An incorporated ion channel can be studied by voltage clamp recordings using Ag/AgCl electrodes (black). (B) Electrical circuit diagram of the bilayer setup. The lipid membrane has the electrical characteristics of a capacitor ($C_M \approx 1$ µF/cm^2) and a resistor ($R_M \approx 1 \cdot 10^8$ Ω·cm^2) in parallel connection. The resistance of the remaining setup (R_S , buffer solutions and the electrodes) is negligible. If an ion conducting protein channel is incorporated in the bilayer, R_M will drop according to the conductance value of the open ion-channel. (C) Current trace of a single ion channel. Channel openings are visible as current jumps. The corresponding conductance states can be extracted by a statistical analysis of single gating events (Ohms law).

The signal to noise ratio of a BLM setup allows for detection of single ion channel gating events (Fig. 1.3*C*) [32]. The electrophysiological analysis of single ion channels can be used to determine the ion conductance states, the ion selectivity, the dwell time of gating and the voltage dependent open probability under precisely controlled conditions [33].
The BLM method was introduced by Mueller et al. 1962 [31]. Mueller's first technique to prepare the artificial membrane is referred to as 'painting technique', because a lipid/solvent solution is painted over a small aperture (see Fig. 1.4*A*). A major critique point of the painting BLM technique was the use of the hydrocarbon solvent, which is not present in biological membranes.

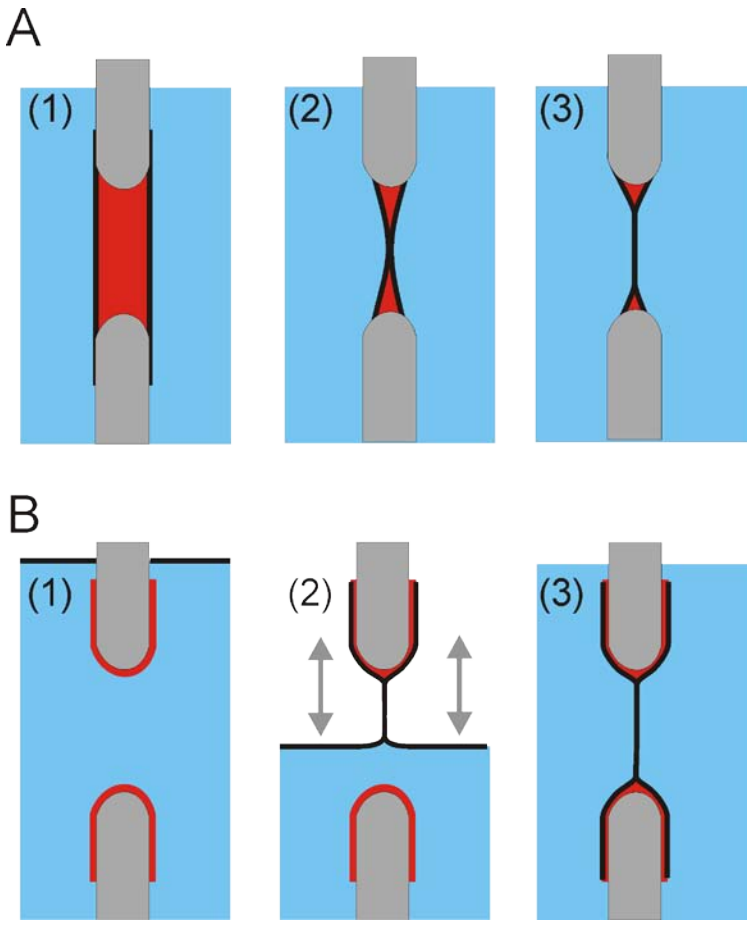

FIGURE 1.4 BLM formation techniques. (A) 1. According to the painting technique a lipid (black)/solvent (red) mixture is spread across a hydrophobic aperture (Ø ≈ 100 µm). 2. Thinning out of the bulk solvent results in the spontaneous formation of a bilayer. (B) 1. Using the monolayer folding technique the aperture is pretreated with a hydrocarbon solvent (red). Lipid monolayers (black) are spread on the water/air interface using a volatile solvent. 2. After solvent evaporation the water levels in the *Cis* and *Trans* compartment are simultaneously lowered and raised. 3. A bilayer is formed from the two contacting monolayers.

Therefore, Montal and Mueller developed a second bilayer formation method which is based on lipid monolayer folding [34] (Fig. 1.4*B*). Since most of the solvent is evaporated before

the bilayer is formed, the resulting bilayer was assumed to be solvent free. However, also with the monolayer folding technique the aperture has to be pretreated with a hydrocarbon solvent, to form a transition region (torus) between the bilayer and the aperture material [35].

Incorporation of purified ion channel proteins into the planar lipid bilayer was first demonstrated by Bean et al. [36]. Generally, the incorporation method depends on the properties of the respective ion channel. The easiest incorporation method is to add the protein to the lipid/hydrocarbon mixture before preparing the actual bilayer. Unfortunately, this method works only for small peptides or very robust proteins. Most proteins will lose its activity during this process. The second approach is to add detergent solubilized protein directly in front of the prepared bilayer [37]. Some of the protein may spontaneously incorporate into the bilayer before it denatures in the aqueous solution. However, the use of detergents in combination with the lipid bilayer is dangerous, because the planar bilayer can easily rupture. The most gentle method to incorporate a protein into the bilayer, is to fuse a proteo-liposome with the planar bilayer [38, 39]. The fusion can be facilitated by an osmotic gradient between this *Cis* and *Trans* side of the bilayer.

When a liposome, which contains an open ion channel, binds to the bilayer, water will flow into the liposome along the osmotic gradient. The liposome will swell until it ruptures and spontaneously fuses with the bilayer (Fig. 1.5).

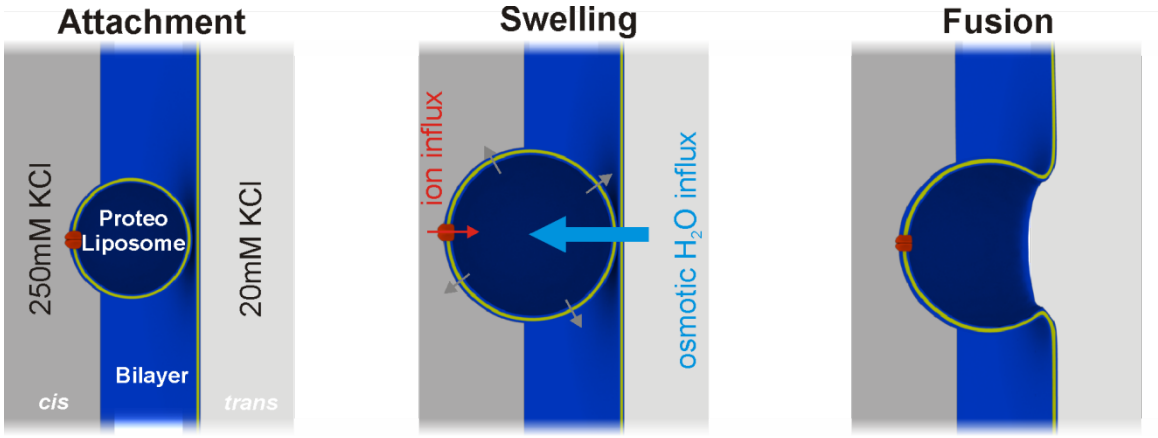

FIGURE 1.5 Proteo-liposome fusion to a BLM. After a proteo-liposome attaches to the bilayer through electrostatic interactions, which can be facilitated by Ca^{2+}, the liposome starts to swell, due to water influx from the *Trans* compartment. If an open ion channel (red) is present in the liposome, swelling will proceed, because the ion concentration in the liposome will be in balance with the *Cis* compartment. Finally, the liposome ruptures and spontaneously fuses with bilayer.

The main drawbacks of the planar bilayer technique may be the stability of the bilayer itself, solvent partition effects and the susceptibility to protein impurities originating from the lipid

preparation and/or the protein purification. Additionally, the quantitative incorporation of none channel proteins in a BLM is not easy.

1.5 Electro-optical studies on lipid bilayers

In this thesis the BLM technique is combined with fluorescence fluctuation spectroscopy. The vision of a combined electro-optical method is to correlate fluorescence- with electrical signals from single proteins, which may ultimately result in new insights into structure function relations of ion-, metabolite- and protein-conducting channels. The idea of a combined electro-optical measurement technique is not new. In pioneering studies the planar bilayer technique has been combined with fluorescence microscopy / spectroscopy using different methodical approaches. Already in the 1970s, the first diffusion measurements on fluorescent lipid analogues were performed using fluorescence correlation spectroscopy (FCS) combined with BLMs [40]. Also during this time, the mechanism of ion channel formation of the peptide gramicidin was elucidated by a combination of ensemble fluorimetry and electrophysiology [41]. The experimental effort to build an electro-optical setup was enormous at that time, mainly because the optical components such as detectors and cameras were not sensitive enough to study single molecule signals. During the 1990s high sensitive photon multipliers and avalanche photodiodes were developed which allowed for single molecule detection. Yet, it took another 10 years until the first opto-electrical setup which was sensitive for single molecules both electrically and optically was presented in 2000 [42]. Ide et al used a single molecule tracking setup combined with BLMs which were oriented horizontally to perform diffusion measurement on electrically active single ion channels. However, in this study no correlation between optical and electrical signals was achieved. In 2003, Borisenko et al conducted simultaneous optical and electrical recording of single gramicidin channels in horizontal lipid bilayers (HLBs) [43]. They were able to show that single current gating events (open or closure of a channel) correlated with FRET signals which indicated that gramicidin monomers assembled into dimers to form an active channel. Until now, other successful examples of combined electro-optical studies are rare [44, 45].

1.6 The electro-optical bilayer setup

To perform electro-optical measurements, we developed a horizontal planar bilayer chip, which is a modification of the traditional (vertical) bilayer setup shown in Fig. 1.6 and is based on the works of Ide et al. and Borisenko et al. [42, 43]. To achieve optical access to the bilayer by a high numerical aperture objective, a PTFE-foil is sandwiched between a cover slide and the chip-body (Fig. 1.6). The detailed construction plans of the horizontal bilayer chip can be found in the appendix (6.1). Using this construction a freestanding planar bilayer can be prepared 100 µm above a cover slide by the painting technique [31]. In contrast to previously presented setups, both compartments (*Cis* / *Trans*) of the chip are perfusable during a measurement session.

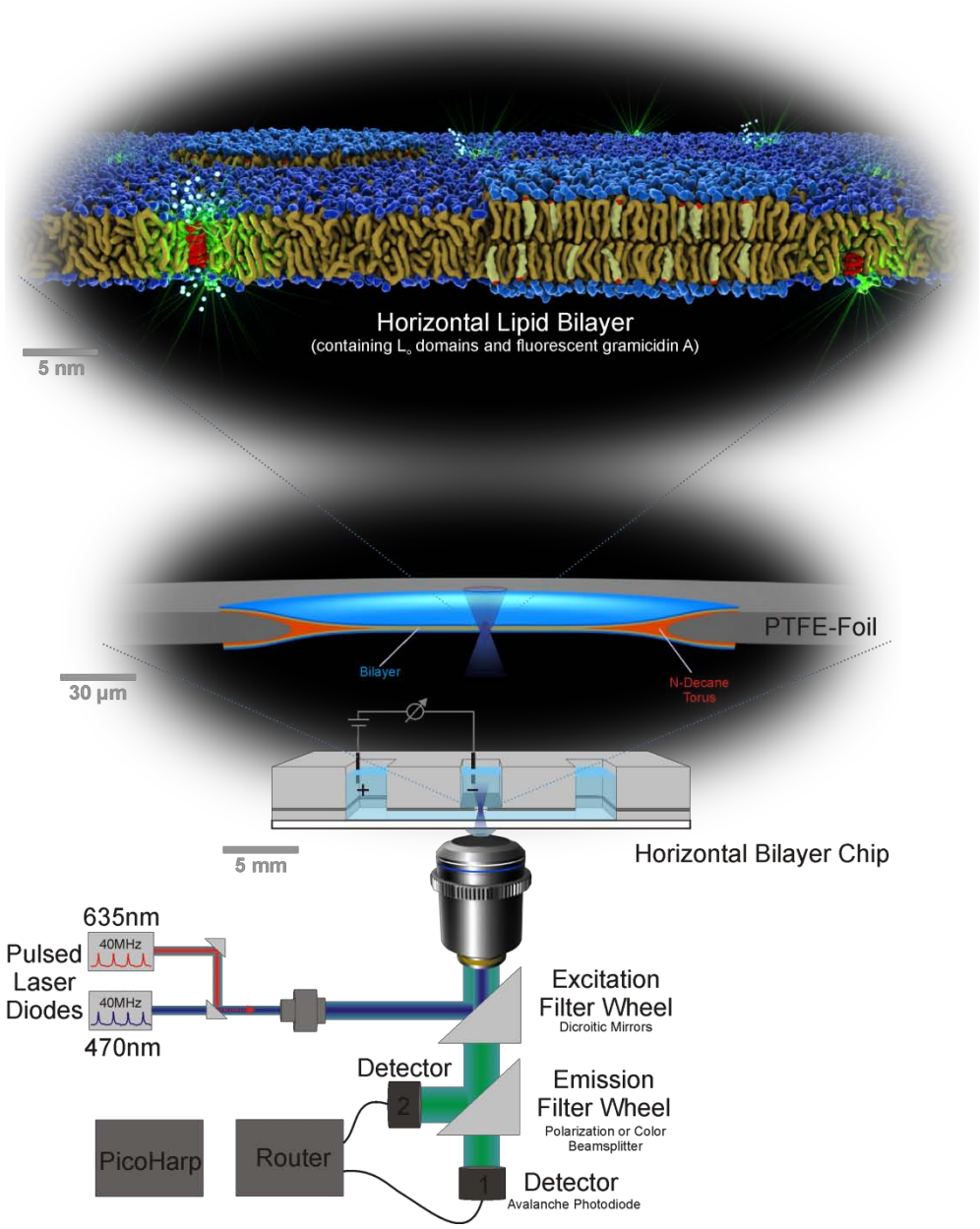

FIGURE 1.6 Scheme of the horizontal lipid bilayer setup. At the bottom the basic optical components of the laser scanning microscope with a single photon counting detection unit are shown: The excitation laser beam is focused through the objective to a diffraction limited spot. The scanning unit is omitted for clarity. The fluorescence emission can be split according to polarization or wavelength and is detected independently on two detectors. The horizontal bilayer chip is mounted on the LSM. The confocal detection volume can be positioned in the *Cis/Trans* compartments or directly in the HLB. The electrophysiological measurement equipment is denoted by the electrodes. Above the bilayer chip a magnification of the PTFE-foil with the $Ø \approx 100$ µm aperture containing the HLB is depicted. At the top a molecular representation of the bilayer is shown. The bilayer contains liquid ordered domains which are segregated from the liquid disordered phase. A fluorescent ion channel is present (gramicidin A) which can be detected electrically and optically at the same time.

Electrical access to the bilayer is obtained by Ag/AgCl electrodes which are connected to standard electrophysiological equipment. A small faraday cage is used to shield the bilayer and electrodes from undesirable electrical noise. The time resolution of the electrical equipment combined with the horizontal bilayer chip is 100 µs with noise amplitude (rms) of 10 pA, which is sufficient to resolve gating events of single ion channels reconstituted in the HLB. The circuit diagram of the electrical components of the bilayer setup is equivalent to vertical setup shown in Fig. 1.3*B*.

For simultaneous optical recordings a modified Insight Cell 3D microscope (Evotech Technologies) is used. Two pulsed laser diodes (470 nm and 635 nm) are used as excitation sources. The combined laser beams are focused to a refraction limited spot through a 40x water immersion objective (NA = 1.15). 3D scanning of the confocal spot is achieved by tilting the laser beam in XY direction and moving the objective in Z-direction. Both moving directions are piezo controlled, which offers nano-meter precise positioning.

The actual fluorescence fluctuation measurement is based on the diffusion or transport of fluorescent molecules through the confocal volume. As a fluorescent dye passes the excitation volume it is excited and emits photons. The collected fluorescence emission can be split up onto two single photon counting detectors according to polarization or wavelength of the emission light. The amplified photon signals are recorded by a combination of a PHR800 router (PicoQuant) and a PicoHarp 300 real-time processor (PicoQuant) connected to a personal computer. The optical setup allows recording fluorescence lifetime histograms with a time resolution of 16 ps and photon fluctuations traces with 100 ns time resolution.

The fluorescence signals from single molecules passing the excitation volume may be used to determine lateral diffusion (see 1.7.1) and rotational (see 1.7.2) diffusion constants and the fluorescence lifetime (see 1.7.2). Additionally, complex formation of binding partners can be studies using the two color setup.

1.7 Fluorescence fluctuation spectroscopy (FFS)

FFS is a collective term for a number of techniques which are based on evaluating fluorescence signals from single molecules passing a small excitation volume [46]. With the development of modern confocal microscopy and single photon counting detectors it became possible to resolve the fluorescence emission of single molecules in solution and membranes. Typically, a laser is focused to a diffraction limited spot, which spatially confines the excitation for fluorescent molecules. If the concentration of fluorescent molecules is small, single molecule transients through the excitation volume will be visible as photon bursts in the recorded fluorescence emission time-trace. These fluorescent fluctuations contain information about molecular properties, which can be extracted by

applying different evaluation methods. In contrast to fluorescence ensemble measurements, different molecular species may be resolved with FFS, which would be averaged out by ensemble spectroscopy. The most popular FFS technique is fluorescence correlation spectroscopy (FCS) which is used to determine lateral diffusion properties and the concentration of fluorescent molecules. The rotational diffusion and the fluorescence lifetime of fluorescent molecules can be determined by confocal time resolved anisotropy (cTRA) measurements. The molecular brightness of fluorescent molecules may be determined with fluorescence distribution analysis (FIDA) or photon counting histograms (PCH) [47, 48]. Each of these techniques may be used to study molecular binding or other biological relevant interactions directly *in vivo* in living cells or *in vitro* using model systems.

1.7.1 Fluorescence correlation spectroscopy (FCS)

In this work the photon data recorded by FFS will be mainly evaluated by FCS. FCS is a statistical analysis of the mean time a fluorescent particle resides in the confocal volume (τ_D = diffusion time) and the mean number of particles in the confocal volume (N) [49-51].

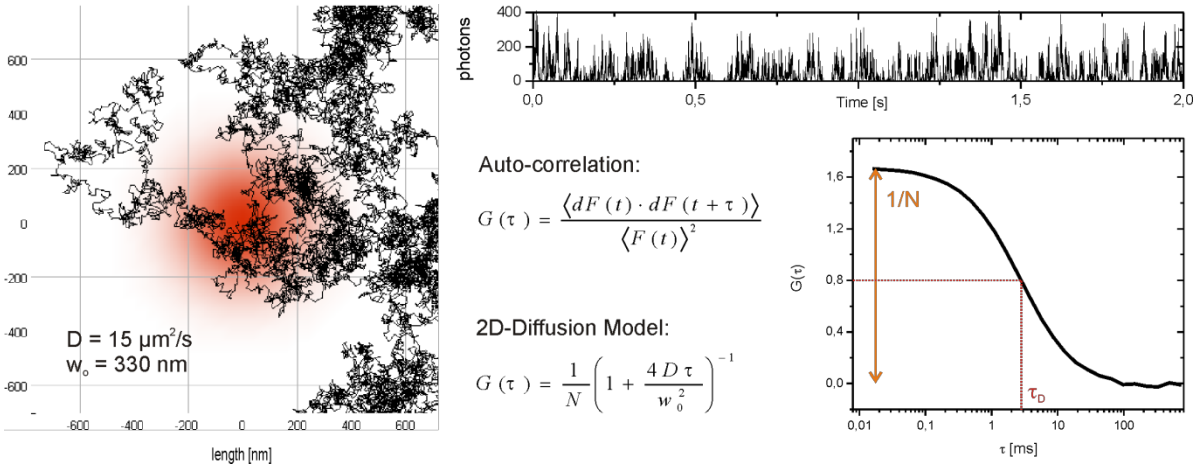

FIGURE 1.7 Fluorescence correlation spectroscopy. The principal of FCS is shown using a 2D diffusion simulation. Fluorescently labeled particles perform a random walk in a simulation box of 2 µm (left). The laser excitation is shown in red. When a particle crosses the excitation volume it will emit photons with a certain probability. Repeating photon bursts result in a photon fluctuation trace (top). The whole photon trace is auto-correlated and the correlation curve is fitted to a 2D diffusion model (right). The fit yields the mean number of particles in the confocal volume (N) and the mean transition time of the particles (τ_D). A detailed description of the simulation can be found in [52].

To extract this information the recorded photon trace is auto-correlated and the correlation data are fitted to a 3D or in case of membrane diffusion to a 2D diffusion model (Fig. 1.7). Since the correlation amplitude is inverse proportional to the number of fluorescent particles in the excitation volume, the correlation signal approaches zero as the particle number (N)

increases. On the other hand a very low concentration will result in an insufficient number molecule transitions in an acceptable measurement time to be statistically evaluable. Practically a concentration range between 1–50 particles in the excitation volume yields reliable results.

One critical parameter in FCS analysis is the size of the confocal volume. Traditionally this parameter has to be determined by a calibration measurement with a standard fluorescent dye. Unfortunately, the shape and the size of the confocal volume are prone to a number of optical aberrations which can bias the resulting FCS analysis [53]. Therefore, the optical setup has to be calibrated at least once per day to keep the FCS results comparable. Recent methodic advancements in the FCS-field have overcome this limitation [54]. The confocal volume can be determined during the diffusion measurement itself either by moving the confocal volume during the measurement (Scanning FCS) [55], by using two spatially separated confocal volumes (Two-focus FCS) [56] or by performing multiple FCS measurements with different confocal sizes (Z-Scan FCS, STED-FCS) [15, 57, 58].

In this work we applied Z-Scan FCS to estimate the minimal waist size of the confocal volume (w_0) while determining the lateral diffusion constant simultaneously. Additionally, Z-Scan FCS offers the advantage that the diffusion law (free versus hindered diffusion) can be determined [58]. The principal of Z-Scan FCS is depicted in Fig. 1.8. As the confocal volume is incrementally moved through a lipid bilayer the size of the excitation area will change according to the con/divergent laser beam profile (Fig. 1.8*A*). From the stack of correlation curves the mean diffusion time and the mean number of particles are extracted for each axial position. The resulting relation between diffusion time and Z-position is fitted to the Z-Scan model which yields at the same time the minimal waist size of the confocal volume as well as the diffusion constant (Fig. 1.8B). The mode of diffusion can be estimated by plotting the diffusion time (τ_D) versus the probed area (N_{obs}/N_{min}) (Fig. 1.8*C*).

1.7.2 Confocal fluorescence lifetime analysis (cFLA) and time resolved anisotropy (cTRA)

One characteristic parameter of a fluorescent probe is the lifetime of its first excited state. Since the fluorescent lifetime is dependent on a number of intra- and inter-molecular processes, lifetime measurements may be employed to probe changes in the rate constants of the depopulating processes of the excited state [60]. For example the lifetime of an appropriate fluorescent dye may be used to explore the hydrophobicity of its local environment or to sense a fluorescence acceptor molecule in the near vicinity [61].

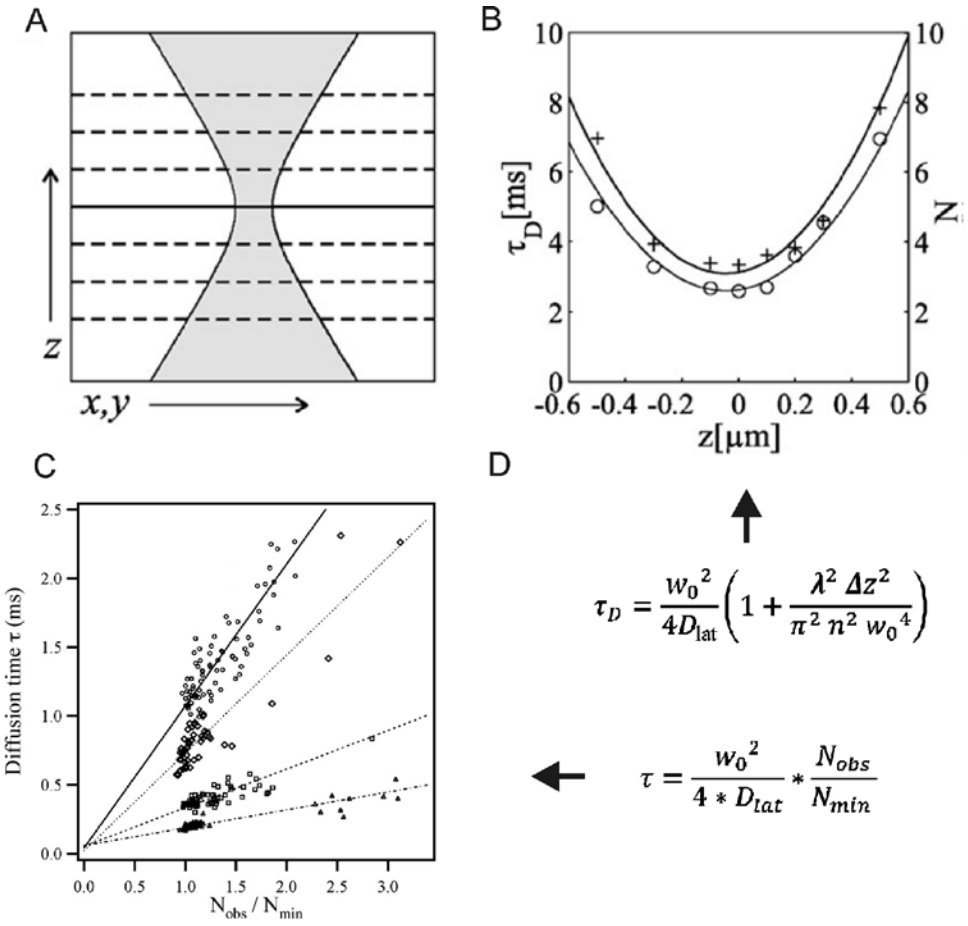

FIGURE 1.8 Z-Scan FCS. (A): A stack of correlation curves is measured at different axial positions. (B) The divergence of the laser beam leads to an increase in the particle number N (+) and diffusion time t_D (o) with distance Z from the membrane [57]. Fitting it with an appropriate model results in an estimate of the size of the laser focus and provides internal calibration. (C) The relation of diffusion time versus area (N_{obs}/N_{min}) is linear with an interception at the origin if the diffusion is free. The slope of the line is $w_0^2/4*D_{lat}$ [Gudmand2009]. (D) Z-scan equations for both modes of evaluation. Graphs in (A) and (B) were taken from [54] and (C) was taken from [59].

The fluorescence lifetimes of commonly used dyes range between 0.1-10 ns. In practice pulsed laser sources in combination with a precise photon arrival detection system are used to excite fluorescent dyes with a short pulse and measure the time it takes until a photon is emitted (Fig. 1.9). A fluorescence decay histogram is calculated from the photon arrival events. In the simplest case the lifetime can be determined by fitting the decay histogram to a first order exponential decay model (Fig. 1.9*B*).

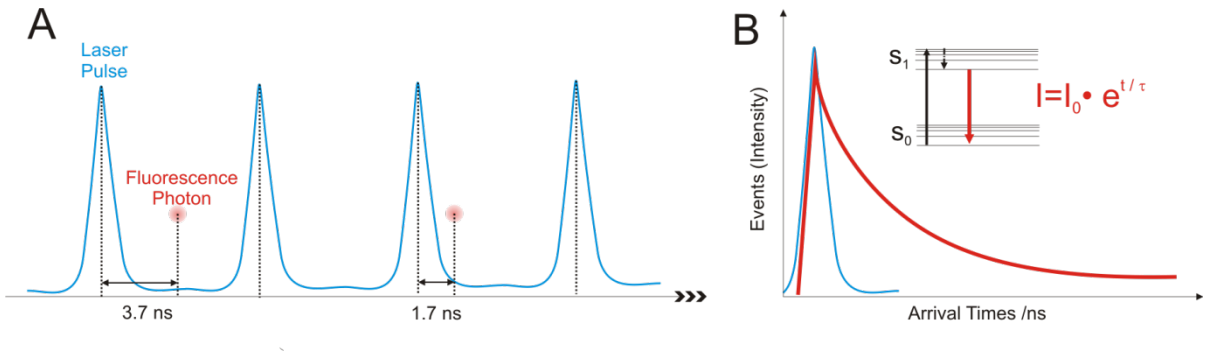

FIGURE 1.9 The principle of time-correlated single photon counting. (A) Laser pulses with a repetition rate of 40 MHz excite fluorescent dyes. The time between an excitation pulse and an arriving photon is measured using APDs and PicoQuant detection electronics. (B) The arrival times are histogramed. An exponential decay fit yields the fluorescent lifetime

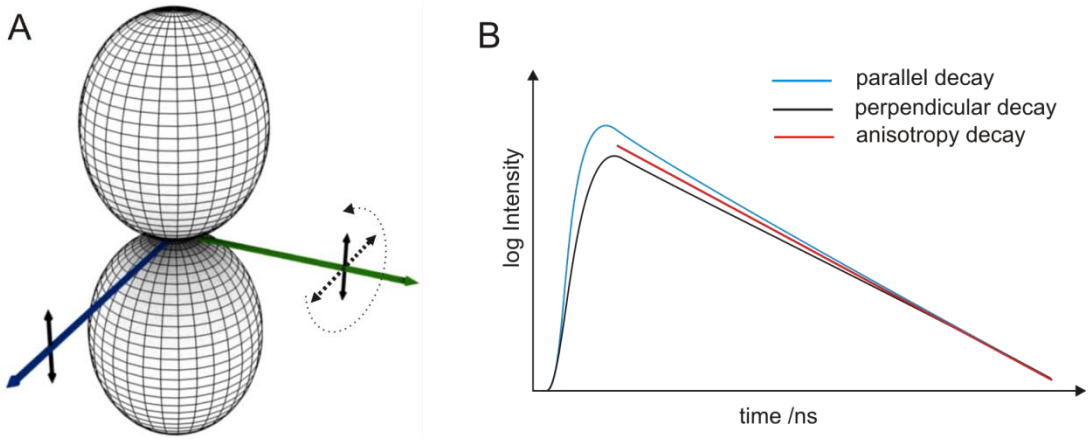

FIGURE 1.10 The principle of time resolves anisotropy. (A) The dipole of a fluorescent dye is depicted. If the dye is excited with linear polarized (black arrow) light (blue) in the dipole orientation axis, the emission light (green) will have the same polarization orientation as the excitation light provided the dye is not rotating during absorption and emission. If the dye is rotating the polarization axis of the emission light will be tilted. (B) The fluorescence emission is split up according to the polarization axis (parallel and perpendicular to the excitation), such that two decay histograms can be recorded one for the parallel and one for the perpendicular polarized emission. The difference in the decay histogram is due to rotational motion of the dye during its fluorescent lifetime.

The fast rotational diffusion of fluorescent molecules can be determined using time resolved anisotropy (cTRA), which is based on the detection of polarized fluorescence emission [60] (Fig. 1.10). Since the anisotropy decay is determined during the lifetime of the respective fluorescent probe, the rotational diffusion has to be on the same time scale as the fluorescent lifetime. If rotation is much faster the probe will seem isotropic, if the rotation is much slower the probe will seem to be stationary. In the field of membrane biophysics the anisotropy of fluorescent lipid analogues is used to determine the order of the acyl chains in a lipid bilayer [60]. However, also binding reactions can be followed using cTRA [39].

1.8 Objectives of this thesis

The aim of this project is to combine the planar bilayer technique with fluorescence fluctuation spectroscopy. At first the implementation of an electro-optical setup comprises the construction of a horizontal planar bilayer chip which is well suited for optical measurements on an inverted microscope equipped with high numerical aperture objectives.

BLMs have been long used as a model system for electrophysiological measurements, but rarely for optical measurements. Due to the special preparation of BLMs using hydrocarbon solvents, the question arises whether the biophysical properties of BLMs are the same as of solvent free model membrane systems. Therefore, I started with a characterization of the horizontal bilayer setup by determining the membrane dynamics of HLBs, which are easily accessible by FFS, and compare the properties to other model systems like GUVs and SLBs. The basic characterization of the physical properties of HLBs involves the determination of lateral and rotational diffusion coefficients of fluorescent lipid analogues, the dynamic viscosity of the bilayer and its electrical capacitance and resistance.

Going one step further HLBs were prepared which mimic the outer leaflet of eukaryotic plasma membranes. In reference to the phase diagrams derived from measurements on GUVs and SLBs large scale lipid phase separation was induced by a temperature control of the HLB. As a unique property of the HLB-setup the electrical activity of ion channels can be determined simultaneously to the fluorescence measurements. Therefore, the setup was applied to resolve the influence of lipid phase separation on the electrical properties of a model ion channel. In a simple test case study it was demonstrated that the electrical activity of gramicidin A is significantly altered during liquid phase separation, due to a lateral sorting of gramicidin A according to its affinity for the lipid domains.

In a second study the conformational changes of the pore-forming toxin Colicin A (ColA) were determined during membrane binding and subsequent ion channel formation. ColA is a well characterized water soluble protein which is known to insert in lipid bilayers in a pH and voltage dependent manner. The conformational changes that occur during membrane binding of ColA have been characterized by FRET and ESR experiments [3, 18]. However, since the open channel conformation of ColA depends on a correctly oriented membrane potential of over 60 mV, the open channel structure has not been accessible using liposome reconstitution of ColA. The electro-optical setup was used to induce channel opening of ColA by application of trans-membrane potentials and measure corresponding fluorescence signals from specific site labeling of ColA at same time.

1.9 References

1. Vance, D. E., and J. E. Vance, editors. 2008. Biochemistry of lipids, lipoproteins and membranes (5th Edn.). Elsevier.

2. Lipowsky, R., and E. Sackmann, editors. 1995. Structure and dynamics of membranes. Elsevier Science B.V.

3. Singer, S. J., and G. L. Nicolson. 1972. The fluid mosaic model of the structure of cell membranes. *Science*. 175:720–731.

4. Anderson, R. G. W., and K. Jacobson. 2002. A role for lipid shells in targeting proteins to caveolae, rafts, and other lipid domains. *Science*. 296:1821–1825.

5. Helms, J. B., and C. Zurzolo. 2004. Lipids as targeting signals: lipid rafts and intracellular trafficking. *Traffic*. 5:247–254.

6. Engelman, D. M. 2005. Membranes are more mosaic than fluid. *Nature*. 438:578–580.

7. Dupuy, A. D., and D. M. Engelman. 2008. Protein area occupancy at the center of the red blood cell membrane. *Proc Natl Acad Sci U S A*. 105:2848–2852.

8. Aisenbrey, C., B. Bechinger, and G. Gröbner. 2008. Macromolecular crowding at membrane interfaces: adsorption and alignment of membrane peptides. *J Mol Biol*. 375:376–385.

9. Zhou, H.-X. Juni 11, 2009. Crowding effects of membrane proteins. *The Journal of Physical Chemistry B*. 113:7995–8005.

10. Sako, Y., and A. Kusumi. 1994. Compartmentalized structure of the plasma membrane for receptor movements as revealed by a nanometer-level motion analysis. *J Cell Biol*. 125:1251–1264.

11. Murakoshi, H., R. Iino, T. Kobayashi, T. Fujiwara, C. Ohshima, A. Yoshimura, and A. Kusumi. 2004. Single-molecule imaging analysis of Ras activation in living cells. *Proc Natl Acad Sci U S A*. 101:7317–7322.

12. Simons, K., and E. Ikonen. 1997. Functional rafts in cell membranes. *Nature*. 387:569–572.

13. Heimburg, T., and A. D. Jackson. 2007. The thermodynamics of general anesthesia. *Biophys J*. 92:3159–3165.

14. Day, C. A., and A. K. Kenworthy. 2009. Tracking microdomain dynamics in cell membranes. *Biochim Biophys Acta*. 1788:245–253.

15. Eggeling, C., C. Ringemann, R. Medda, G. Schwarzmann, K. Sandhoff, S. Polyakova, V. N. Belov, B. Hein, C. von Middendorff, A. Schönle, and S. W. Hell. 2009. Direct observation of the nanoscale dynamics of membrane lipids in a living cell. *Nature*. 457:1159–1162.

16. Fielding, C. J., editor. 2005. Lipid Rafts and Caveolae. Wiley-VCH.

17. de Meyer, F. J.-M., M. Venturoli, and B. Smit. 2008. Molecular simulations of lipid-mediated protein-protein interactions. *Biophys J*. 95:1851–1865.

18. Killian, J. A. 1998. Hydrophobic mismatch between proteins and lipids in membranes. *Biochim Biophys Acta*. 1376:401–415.

19. Monne, M., and G. von Heijne. 2001. Effects of ’hydrophobic mismatch’ on the location of transmembrane helices in the ER membrane. *FEBS Lett*. 496:96–100.

20. Philippot, J. R., and F. Schuber. 1995. Liposomes as tools in basic research and industry. CRC Press.

21. Luisi, P. L., and P. Walde. 2007. Giant Vesicles (Perspectives in Supramolecular Chemistry, Volume 6), 1st Ed. Wiley-Interscience.

22. Girard, P., J. Pecreaux, G. Lenoir, P. Falson, J.-L. Rigaud, and P. Bassereau. 2004. A new method for the reconstitution of membrane proteins into giant unilamellar vesicles. *Biophys J*. 87:419–429.

23. Kahya, N., D. Scherfeld, K. Bacia, and P. Schwille. 2004. Lipid domain formation and dynamics in giant unilamellar vesicles explored by fluorescence correlation spectroscopy. *J Struct Biol*. 147:77–89.

24. Wesolowska, O., K. Michalak, J. Maniewska, and A. B. Hendrich. 2009. Giant unilamellar vesicles - a perfect tool to visualize phase separation and lipid rafts in model systems. *Acta Biochim Pol*. 56:33–39.

25. Tamm, L. K., and H. M. McConnell. 1985. Supported phospholipid bilayers. *Biophys J*. 47:105–113.

26. Kiessling, V., J. M. Crane, and L. K. Tamm. 2006. Transbilayer effects of raft-like lipid domains in asymmetric planar bilayers measured by single molecule tracking. *Biophys J*. 91:3313–3326.

27. Chiantia, S., J. Ries, G. Chwastek, D. Carrer, Z. Li, R. Bittman, and P. Schwille. 2006. Role of ceramide in membrane protein organization investigated by combined AFM and FCS. *Biochim Biophys Acta*. 1778:1356–1364.

28. Wagner, M. L., and L. K. Tamm. 2000. Tethered polymer-supported planar lipid bilayers for reconstitution of integral membrane proteins: silane-polyethyleneglycol-lipid as a cushion and covalent linker. *Biophys J*. 79:1400–1414.

29. Nath, A., W. M. Atkins, and S. G. Sligar. 2007. Applications of phospholipid bilayer nanodiscs in the study of membranes and membrane proteins. *Biochemistry*. 46:2059–2069.

30. Winterhalter, M. Juli 2000. Black lipid membranes. *Current Opinion in Colloid & Interface Science*. 5:250–255.

31. Mueller, P., D. O. Rudin, H. T. Tien, and W. C. Wescott. 1962. Reconstitution of cell membrane structure in vitro and its transformation into an excitable system. *Nature*. 194:979–980.

32. Hladky, S. B., and D. A. Haydon. 1970. Discreteness of conductance change in bimolecular lipid membranes in the presence of certain antibiotics. *Nature*. 225:451–453.

33. Hille, B. 2001. Ion Channels of Excitable Membranes. Sinauer Associates, Inc.

34. Montal, M., and P. Mueller. 1972. Formation of bimolecular membranes from lipid monolayers and a study of their electrical properties. *Proc Natl Acad Sci U S A*. 69:3561–3566.

35. White, S. H., D. C. Petersen, S. Simon, and M. Yafuso. 1976. Formation of planar bilayer membranes from lipid monolayers. A critique. *Biophys J*. 16:481–489.

36. Bean, R. C., W. C. Shepherd, H. Chan, and J. Eichner. 1969. Discrete conductance fluctuations in lipid bilayer protein membranes. *J Gen Physiol*. 53:741–757.

37. Rudel, T., A. Schmid, R. Benz, H. A. Kolb, F. Lang, and T. F. Meyer. 1996. Modulation of *Neisseria* porin (PorB) by cytosolic ATP/GTP of target cells: parallels between pathogen accommodation and mitochondrial endosymbiosis. *Cell*. 85:391–402.

38. Cohen, F. S., W. D. Niles, and M. H. Akabas. 1989. Fusion of phospholipid vesicles with a planar membrane depends on the membrane permeability of the solute used to create the osmotic pressure. *J Gen Physiol*. 93:201–210.

39. Lee, H. B., L. Xu, and G. Meissner. 1994. Reconstitution of the skeletal muscle ryanodine receptor-Ca^{2+} release channel protein complex into proteoliposomes. *J Biol Chem*. 269:13305–13312.

40. Fahey, P. F., D. E. Koppel, L. S. Barak, D. E. Wolf, E. L. Elson, and W. W. Webb. 1977. Lateral diffusion in planar lipid bilayers. *Science*. 195:305–306.

41. Veatch, W. R., R. Mathies, M. Eisenberg, and L. Stryer. 1975. Simultaneous fluorescence and conductance studies of planar bilayer membranes containing a highly active and fluorescent analog of gramicidin A. *J Mol Biol*. 99:75–92.

42. Ide, T., and T. Yanagida. 1999. An artificial lipid bilayer formed on an agarose-coated glass for simultaneous electrical and optical measurement of single ion channels. *Biochemical and Biophysical Research Communications*. 265:595–599.

43. Borisenko, V., T. Lougheed, J. Hesse, E. Füreder-Kitzmüller, N. Fertig, J. C. Behrends, G. A. Woolley, and G. J. Schütz. 2003. Simultaneous optical and electrical recording of single gramicidin channels. *Biophys J*. 84:612–622.

44. Harms, G. S., G. Orr, M. Montal, B. D. Thrall, S. D. Colson, and H. P. Lu. 2003. Probing conformational changes of gramicidin ion channels by single-molecule patch-clamp fluorescence microscopy. *Biophys J*. 85:1826–1838.

45. Das, S. K., M. Darshi, S. Cheley, M. I. Wallace, and H. Bayley. 2007. Membrane protein stoichiometry determined from the step-wise photobleaching of dye-labelled subunits. *Chembiochem*. 8:994–999.

46. Chen, Y., J. D. Müller, K. M. Berland, and E. Gratton. 1999. Fluorescence fluctuation spectroscopy. *Methods*. 19:234–252.

47. Kask, P., K. Palo, D. Ullmann, and K. Gall. 1999. Fluorescence-intensity distribution analysis and its application in biomolecular detection technology. *Proc Natl Acad Sci U S A*. 96:13756–13761.

48. Chen, Y., J. D. Müller, P. T. So, and E. Gratton. 1999. The photon counting histogram in fluorescence fluctuation spectroscopy. *Biophys J*. 77:553–567.

49. Magde, D., E. Elson, and W. W. Webb. 1972. Thermodynamic fluctuations in a reacting system–measurement by fluorescence correlation spectroscopy. *Physical Review Letters*. 29:705.

50. R. Rigler, W. P. K., Mets. 1993. Fluorescence correlation spectroscopy with high count rate and low background: analysis of translational diffusion. *European Biophysics Journal*. 22:169–175.

51. Schwille, P., J. Korlach, and W. W. Webb. 1999. Fluorescence correlation spectroscopy with single-molecule sensitivity on cell and model membranes. *Cytometry*. 36:176–182.

52. Wohland, T., R. Rigler, and H. Vogel. 2001. The standard deviation in fluorescence correlation spectroscopy. *Biophys J*. 80:2987–2999.

53. Enderlein, J., I. Gregor, D. Patra, and J. Fitter. 2004. Art and artefacts of fluorescence correlation spectroscopy. *Curr Pharm Biotechnol*. 5:155–161.

54. Ries, J., and P. Schwille. 2008. New concepts for fluorescence correlation spectroscopy on membranes. *Phys Chem Chem Phys*. 10:3487–3497.

55. Petrasek, Z., and P. Schwille. 2008. Precise measurement of diffusion coefficients using scanning fluorescence correlation spectroscopy. *Biophys J*. 94:1437–1448.

56. Dertinger, T., V. Pacheco, I. von der Hocht, R. Hartmann, I. Gregor, and J. Enderlein. 2007. Two-focus fluorescence correlation spectroscopy: a new tool for accurate and absolute diffusion measurements. *Chemphyschem*. 8:433–443.

57. Benda, A., M. Bene, V. Mareczek, A. Lhotsk, W. T. Hermens, and M. Hof. 2003. How to determine diffusion coefficients in planar phospholipid systems by confocal fluorescence correlation spectroscopy. *Langmuir*. 19 (10):4120–4126.

58. Humpolickova, J., E. Gielen, A. Benda, V. Fagulova, J. Vercammen, M. Vandeven, M. Hof, M. Ameloot, and Y. Engelborghs. 2006. Probing diffusion laws within cellular membranes by z-scan fluorescence correlation spectroscopy. *Biophys J*. 91:L23–L25.

59. Gudmand, M., M. Fidorra, T. Bjørnholm, and T. Heimburg. 2009. Diffusion and partitioning of fluorescent lipid probes in phospholipid monolayers. *Biophys J*. 96:4598–4609.

60. Lakowicz, J. 2006. Principles of Fluorescence Spectroscopy. Springer, Singapore.

61. Johnson, A. E. 2005. Fluorescence approaches for determining protein conformations, interactions and mechanisms at membranes. *Traffic*. 6:1078–1092.

62. Eggeling, C., K. Gall, K. Palo, P. Kask, and L. Brand. 2003. Confocal fluorescence techniques in industrial application. SPIE:101–109.

63. Cascales, E., S. K. Buchanan, D. Duche, C. Kleanthous, R. Lloubes, K. Postle, M. Riley, S. Slatin, and D. Cavard. 2007. Colicin biology. *Microbiol Mol Biol Rev*. 71:158–229.

64. Padmavathi, P. V. L., and H.-J. Steinhoff. 2008. Conformation of the closed channel state of colicin A in proteoliposomes: an umbrella model. *J Mol Biol*. 378:204–214.

2. Characterization of horizontal lipid bilayers as a model system to study lipid phase separation

2.1 Abstract

Artificial lipid membranes are widely used as a model system to study single ion channel activity with electrophysiological techniques. In this study, the properties of the artificial bilayer system were characterized with respect to its dynamics of lipid phase separation using single molecule fluorescence fluctuation and electrophysiological techniques. The rotational motions of fluorescently labeled lipids were determined on the nanosecond time scale using confocal time resolved anisotropy to probe the microscopic viscosity of the membrane. Simultaneously, long range mobility was investigated by the lateral diffusion of the lipids using fluorescence correlation spectroscopy. Depending on the solvent used for membrane preparation, lateral diffusion coefficients between $D_{lat} = 10 – 25\ \mu m^2/s$ and rotational diffusion coefficients of $D_{rot} = 2.8 \times 10^7\ s^{-1} – 1.4 \times 10^7\ s^{-1}$ were measured in pure liquid disordered (L_d) membranes. In ternary mixtures containing saturated and unsaturated phospholipids and cholesterol, liquid ordered (L_o) domains segregated from the L_d phase at 23°C. The lateral mobility of lipids in L_o domains was ~ 8-fold lower compared to the L_d phase while the rotational mobility decreased by a factor of 1.5. Burst integrated steady state anisotropy histograms as well as anisotropy imaging were used to visualize the rotational mobility of lipid probes in phase separated bilayers. These experiments and FCS measurements at different focal diameter indicated a heterogeneous microenvironment in the L_o phase. Finally, the potential of the opto-electro setup to study the influence of lipid domains on the electrophysiological properties of ion channels was tested. It was found that the electrophysiological activity of gramicidin A (gA), a well characterized ion channel forming peptide, was related to lipid domain partitioning. During liquid-liquid phase separation, gA was largely excluded from L_o domains. Simultaneously, the number of electrically active gA dimers increased, due to the increased surface density of gA in the L_d phase.

2.2 Introduction

The lipid composition of biological membranes, its spatial organization and its temporal dynamics become more and more acknowledged to be fundamental for function and regulation of integral- and membrane-associated proteins [16, 2]. Data obtained by various labs with different techniques provide growing evidence that cell membranes are organized in separated, spatially confined and dynamic domains [3-15]. Many details of these domains such as their molecular characteristics or their size distribution, which is somewhere below the resolution limit of conventional light microscopy, remain to be clarified. Two fundamental determinants for the origin of membrane compartmentalization have been

found. At first the lateral mobility in a cell membrane seems to be bounded by protein/lipid interactions with the cytoskeleton meshwork. Secondly, phase separation of lipid components and cholesterol into liquid ordered (L_o) and disordered (L_d) domains may cause sorting of membrane components according to their affinity for different lipid phases.

The nature of lipid phase separation has been studied in detail using model membranes like giant unilamellar vesicles and supported lipid bilayers [12-17]. The biologically interesting regimes where L_o and L_d phases coexist have been mapped in phase diagrams [13, 18-21]. To study the dynamics of lipids and proteins in coexisting L_o and L_d phases techniques such as fluorescence recovery after photo-bleaching, fluorescence resonance energy transfer, single particle tracking and fluorescence correlation spectroscopy (FCS) have been deployed. In this context FCS [49, 23] and its recent advancements [7, 15, 56, 25] have been proven to be a particularly valuable tool. Using FCS, the concentration and the lateral diffusion of single dye labeled (lipid and proteins) probes can be evaluated with high statistical accuracy. Additionally, free versus hindered diffusion can be discriminated at the nanometer scale [7, 15]. Another fluorescence method which is sensitive to dynamics of lipid-probes is time resolved anisotropy (TRA) [26, 27]. However, in contrast to FCS, which detects lateral movements in the micro to millisecond range, TRA is used to measure rotational dynamics occurring during the fluorescence lifetime of the probe. The rotational correlation times and respectively the limiting anisotropy of lipid probes revealed by TRA report the short range interactions within the very local environment of studied probe which can be related to the order of the acyl chains of lipids [28, 29].

One key function of a biological membrane is its electrical excitability which is the basis of signaling as well as energy conserving processes in cells [33]. Yet, most model systems, which are used to study lipid phase separation processes lack a controlled accession of this important parameter of a lipid membrane. In this study, electrically addressable, horizontal planar bilayers separating two water bulk phases, are used in combination with a polarization sensitive FCS setup. The setup permits electrical recordings simultaneous to the evaluation of the lateral (FCS) and rotational diffusion (TRA) of fluorescently labeled probes. BLMs have been traditionally employed in electrophysiology to record single channel currents of purified reconstituted membrane proteins [31-33], but they have also been used in combination with fluorescence microscopy and FCS [40-43]. However, to our knowledge, only in one study BLMs were used as a model system to analyze lipid phase separation. Samsonov et al. showed qualitatively that large scale L_o and L_d domains coexist in BLMs when ternary lipid compositions are cooled below the phase transition temperature (T_m) [37]. The BLMs bear some advantages over other model systems such as supported lipid bilayers. First, the lipid phase separation is not disturbed by any surface interaction. Second, this system allows for an easy exchange of the surrounding solution. Finally, the opto-electrical setup permits the application of membrane potentials and measurement of the according membrane currents.

Here, the HLBs are characterized with respect to temperature dependent dynamics of lipid motion and domain formation at the single molecule level. As a test case for electro-optical measurements labeled gramicidin A (gA), a simple and well characterized peptide ion channel [43, 38] was used. Our results indicate that lipid diffusion and phase separation is partially dependent on the preparation (solvent) of the bilayer. However, the basic characteristics of coexisting L_o and L_d domains are the same as for other model systems. Heterogeneity in anisotropy and FCS measurements at different focal diameter indicate the existence of domains in the L_o phase smaller than the resolution limit of the microscope. When a ternary BLM containing gA is cooled below the T_m, gA is excluded from the L_o domains and simultaneously the number of open channels increases. The increased electrophysiological activity can be mainly attributed to an increased concentration of the peptide in the L_d and to a lesser extend to a decreased bilayer thickness in the L_d phase which stabilizes the ion conducting dimer conformation.

2.3 Material and methods

2.3.1 Chemicals

2-Dioleoyl-sn-glycero-3-phosphocholine (DOPC) was purchased from Avanti Polar Lipids (Alabaster, AL). Distereoyl-sn-glycero-3-phosphocoline (DSPC), cholesterol (CO), n-decane, n-hexane, squalene and gramicidin A were purchased from Sigma Aldrich (Munich, Germany). Cholesteryl-BODIPY FL C_{12} (CO-BDY) was purchased from Molecular Probes (Eugene, OR). The organic dye Atto647N (fluorescence excitation and emission maxima of 645 and 670 nm, respectively; Atto-Tec, Siegen, Germany) labeled phosphoethanolamine lipid Atto647N-1,2-dihexdecanoyl-sn-glycero-3-phosphatidyl-ethanolamine (DPPE647), the Atto647N labeled sphingomyelin lipid Atto647N-Sphingomyelin (SM647), and the Atto647N labeled Atto647N-Ceramide (CER647) were prepared by Atto-Tec and were previously applied in live-cell studies. The structures of Atto647N and the labeled lipids are depicted in the supplement of [15]. While DPPE647 is labeled at the head group, i.e., in the water phase, SM647 and CER647 are labeled at the water-lipid interface, by replacing the native long acyl chain with a short acyl chain carrying the dye.

Lipids were stored in methanol/chloroform (1:1) under nitrogen at -20°C. For bilayer preparation lipids were mixed accordingly, dried under vacuum and dissolved in hydrocarbons to a final concentration of 50 mg/ml. To yield an appropriate label concentration in the bilayer for fluorescence fluctuation analysis the molar ratio of lipids / labeled lipids was adjusted to 50,000 : 1.

2.3.2 Horizontal lipid bilayers

The horizontal bilayer chip is made of Polytetrafluoroethylene (PTFE) with drilled holes for *Cis* and *Trans* compartments and electrode access. A 25 µm thin PTFE sheet with a round

~100 µm small aperture is sandwiched between a coverslide and the chamber body using double side adhesive film (Fig. 2.1*A*).

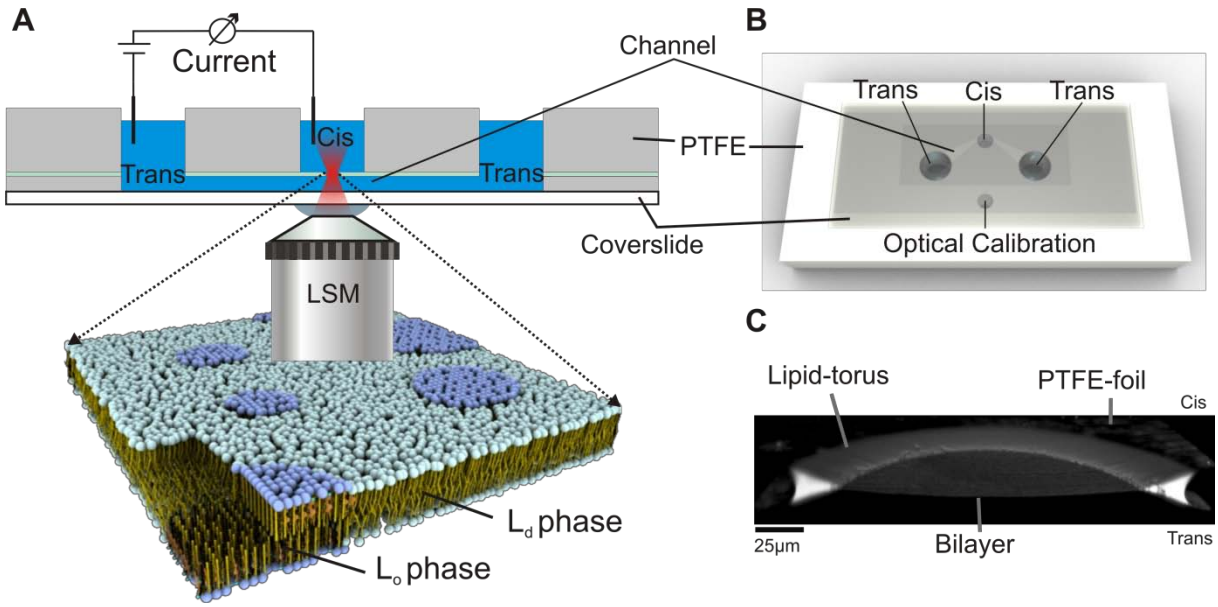

FIGURE 2.1 Setup of the horizontal bilayer chamber. (*A*) Schematic view of the setup. The chamber contains two compartments (*Cis* and *Trans*) which are separated by a thin PTFE film. The film is perforated by a 100 µm hole which is the only connection between the *Trans* and *Cis* compartment. When a lipid solution is painted over the hole a bilayer forms spontaneously. The distance from the bilayer to the coverslide is 100 µm. Thus membrane is accessible by a high numerical aperture water objective. Electrodes in *Cis* and *Trans* allow electrophysiological recordings of the bilayer. (*B*) Bottom view of the chamber. The *Cis* and *Trans* compartments have a buffer volume of 100 µl. (*C*) Side-cut of a 3D reconstruction (LSM *YZ*-stack) of the bilayer. The membrane spans the aperture in the PTFE film. The interface of the film and the bilayer is bridged by the torus which contains the bulk solvent and lipids.

The lower adhesive film contains a laser edged channel structure to connect the *Trans* compartments (Fig. 2.1*B*). The exclusive connection between the *Cis* and *Trans* compartment is the aperture in the PTFE sheet. After assembly of the chamber and filling with 100 mM KCl, 10 mM Mops/Tris pH 7 buffer the bilayer was "painted" over the aperture using a 90° bended Hamilton syringe (Bonaduz, Switzerland). Bilayer formation was monitored optically and electrically. The distance between the coverslide and the planar bilayer is 100 µm which allows optical access by high numerical aperture water objectives required for fluorescence fluctuation analysis (Fig. 2.1*A*). For electrical measurements silver/silver chloride electrodes embedded in agarose were connected to the *Cis* and *Trans* compartments. Electrical recordings were made using a CV-5-1GU headstage connected to a GeneClamp 500B amplifier from Axon Instruments (Sunnyvale, CA). Data were digitalized with a Digidata 1322A and monitored with the software Clampex 9 (Axon Instruments). After each measurement session the coverslide with the adhesives was removed and the chamber body was cleaned in ethanol before re-usage. For preparation of pure L_d bilayers

DOPC was used as the only lipid component. Ternary mixtures of DOPC/DSPC/Cholesterol in a molar ratio of 2-1/1/1 were used for phase separation studies, according to the phase diagram in [20].

2.3.3 Confocal microscopy

Confocal imaging and fluorescence fluctuation recordings were performed on an Insight Cell 3D microscope from Evotec technologies (Hamburg, Germany, now Perkin Elmer), equipped with a 543 nm continuous-wave HeNe and a 635 nm pulsed diode laser (~80 ps pulse width, PicoQuant, Berlin, Germany), a 40x water immersion objective (UApo340 40x, NA 1.15, Olympus, Tokyo, Japan) and avalanche photo diode detectors (SPCM-AQR-13-FC, Perkin Elmer Optoelectronics, Fremont, CA). Fluorescence excitation was performed with linear polarized light and the laser power was adjusted to 5- 20 µW. The emission light was split according to polarization and detected on two channels each equipped with a detector. The signal from each detector was split up on the correlator and the imaging unit of the Insight and on a PHR 800 router in combination with a PicoHarp 300 counting module (PicoQuant). The PicoHarp 300 allowed for an interactive analysis such as the recording of raw photon traces and online FCS and lifetime analysis. The repetition rate of the laser was set to 40 MHz and the resolution of the PicoHarp 300 to 16 ps. Fluorescence images were obtained by scanning the sample by a rotating beam-scanner along the lateral *XY* and by an objective lens positioning system along the axial *Z*-direction. After bilayer preparation an *XZ*-scan was performed and the confocal spot was positioned a few hundred nanometers underneath the membrane. For a *Z*-scan, the focus was moved in 100 nm steps through the membrane and 20 s photon traces were recorded at each position. If the count rate was stable over the measurement period, the traces were analyzed to determine rotational (TRA) and lateral (FCS) diffusion times using the software SymphoTime and FluoFit (PicoQuant).

2.3.4 Time resolved anisotropy (TRA)

Rotational diffusion times were evaluated by globally fitting the parallel $I_{||}$ and perpendicular $I\perp$fluorescence decay according to the following model [39]:

$$I_{\parallel}(t) = G\int_{-\infty}^{t} IRF_{\parallel}(t')\frac{1}{3}\alpha e^{-\frac{t-t'}{\tau_{FL}}}\left[1 + 2\left(R_{INF} + \beta e^{\frac{t-t'}{\phi}}\right)\right]dt' \qquad (2.1)$$

$$I_{\perp}(t) = G\int_{-\infty}^{t} IRF_{\perp}(t')\frac{1}{3}\alpha e^{-\frac{t-t'}{\tau_{FL}}}\left[1 - \left(R_{INF} + \beta e^{\frac{t-t'}{\phi}}\right)\right]dt' \qquad (2.2)$$

where G accounts for the different detection sensitivities in the two detection channels, $IRF_{||}(t)$ and $IRF\perp(t)$ are the time-resolved instrument response functions of the microscope, τ_{FL}

and α are the characteristic decay time (fluorescence lifetime) and amplitude of the fluorescence lifetime component, respectively, R_{INF} is the residual anisotropy (for $t \rightarrow \infty$), and Φ and β are the characteristic decay time (rotational correlation time) and the initial anisotropy, respectively. The value of $G = 0.95$ was determined by tail-matching the parallel and vertically polarized decays of a fast rotating dye (Atto647N in aqueous buffer). The instrument response function (IRF) of the microscope was recorded using reflected laser light at the cover slip interface. R_{INF} was zero in all of our fits. Depolarization due to the focusing optics has not been corrected for in this model. The quality of the fit was judged by X^2 (1-1.5) and the residuals. The rotational diffusion coefficient was calculated according to $D_{rot} = 1 / (6\,\Phi)$

2.3.5 Fluorescence correlation spectroscopy (FCS)

The translational diffusion time τ_D was evaluated using cross-correlation between the parallel and perpendicular polarized photon traces. The correlation curves were fitted by a two dimensional diffusion model including a triplet term [40].

$$G(\tau) = \frac{1}{N}\frac{1}{\left(1 + {}^{t}/_{\tau_D}\right)}\left(1 + \frac{T}{1-T}e^{\frac{-t}{\tau_T}}\right) \tag{2.3}$$

N is the mean number of particles in the confocal volume. T is the average fraction of molecules which are in the triplet state and τ_T the triplet correlation time, which depends on the sum of the population and depopulation rates of the triplet system. $\tau_D = w_0^2 / (4D_{lat})$ is the average molecular diffusion time through the Gaussian-assumed focal intensity profile and characterized by the lateral diffusion coefficients D_{lat} and the focal radius w_0 (defined as the radius at which the Gaussian-assumed focal intensity profile has dropped to $1/e^2$ of its maximum value). w_0 was estimated from FCS measurements on the dye Atto655-maleimid in aqueous buffer with the known diffusion coefficient of $D_{lat} = 407\ \mu m^2/s$ [41]. A good estimate of the lateral lipid membrane mobility D_{lat} was obtained from the shortest diffusion time τ_D determined for the correlation curves recorded from a Z-scan over the bilayer.

More exact values of D_{lat} and w_0 were determined by using Z-scan FCS [57]. The diffusion times $\tau_D(\Delta z)$ determined from correlation data recorded at different Z-position Δz of the focus relative to the BLM were fitted to

$$\tau_D = \frac{{w_0}^2}{4D_{lat}}\left(1 + \frac{\lambda^2 \Delta z^2}{\pi^2 n^2 {w_0}^4}\right) \tag{2.4}$$

where λ is the excitation wavelength and n the refractive index of the buffer.

As a control the waist size of the confocal volume was determined by scanning single gold beads with diameter of Ø = 40 nm (Fig. 2.2). Since the beads are much smaller than the

waist size of the laser focus the resulting image corresponds to the effective point spread function of the microscope. The fitted w_0 = 320 nm compares well with the w_0 = 330 nm determined by Z-Scan FCS.

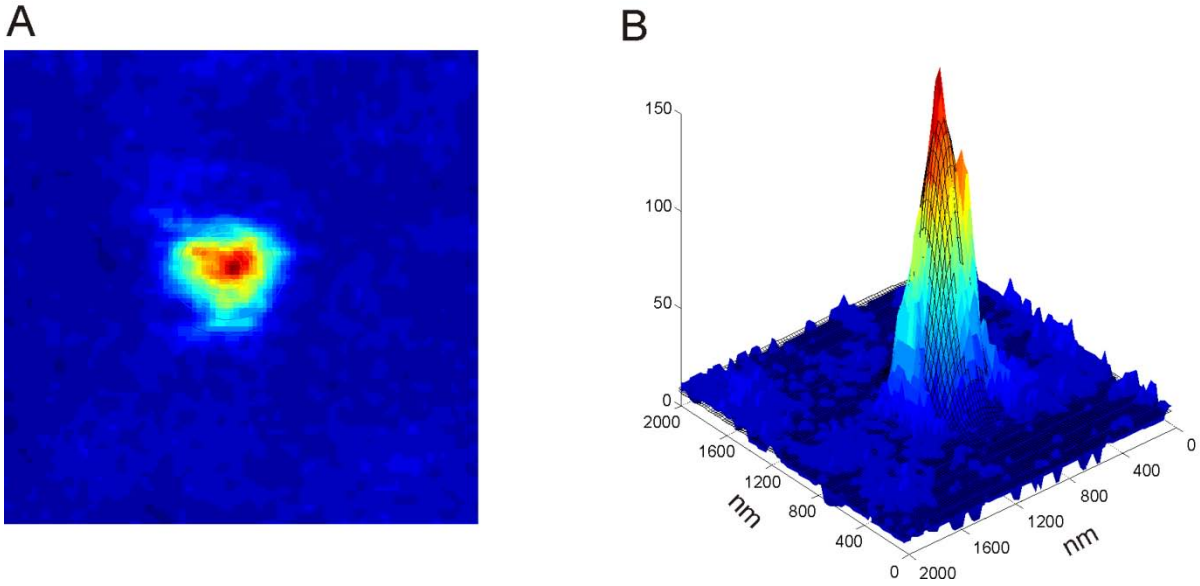

FIGURE 2.2 Determination of the minimal waist size of the laser focus. (A) LSM-image of a 10 nm Quantum-Dot excited with λ = 470 nm and detected at λ >645 nm . (B) 2D gauss fit of the point spread function resulting in an estimate of $w_0 \approx$ 280 nm for the 470 nm laser focus.

2.3.6 Steady state anisotropy

The steady state anisotropy *r* was calculated from the average signal count rates $I_{||}$ and $I_{\perp}$ in the parallel and perpendicular detection channel, respectively, and from the *G*-factor defined in equations (1) and (2).

$$\bar{r} = \frac{I_{\parallel} - GI_{\perp}}{I_{\parallel} + 2GI_{\perp}} \tag{2.5}$$

Either scanning anisotropy images were calculated pixel-wise using equation 5 with the software ImageJ (http://rsbweb.nih.gov/ij/), or the steady state anisotropy *r* was determined on a single-molecule level [43]. For this, photon traces recorded for a very diluted sample (far less than one fluorescent molecule per laser spot) were binned with 1 ms resolution, fluorescence bursts due to single-molecule transits selected by introducing a threshold to distinguish the photon burst from background, and the single-molecule steady state anisotropy calculated from all the photons selected from a single burst using the software SymphoTime from PicoQuant.

2.3.7 Temperature Control

The temperature in the horizontal bilayer chamber was adjusted by two water cooled peltier elements (41 W each) which were controlled by a temperature sensor feedback. The actual temperature directly at the bilayer was checked by a filament temperature sensor. The peltier elements were connected to the top of the bilayer chamber by a copper interface protruding inside the PEEK body to accelerate heat exchange. A temperature range between 15°C and 45°C was settable with this equipment.

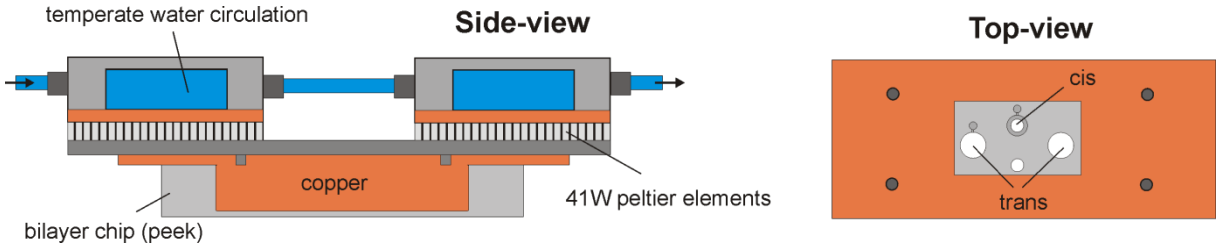

FIGURE 2.3 Setup of the temperature control. A copper interface protruding into the bilayer chip facilitates the heat exchange. The detachable top part, including peltier elements and water circulation, was used to adjust the temperature in measurement compartments.

2.3.8 Bilayer viscosity determination

From the size dependence of the lateral diffusion coefficient the membrane viscosity can be estimated using the Saffman-Delbrück approximation [44],

$$D_{lat} = \frac{kT}{4\pi\eta h}\left(ln\frac{\eta h}{\mu_w a} - \gamma\right) \tag{2.5}$$

and the Petrov-Schwille approximation [45],

$$D_{lat} = \frac{kT}{4\pi\eta h}\left[\ln\left(\frac{2}{\varepsilon}\right) - \gamma + \frac{4\varepsilon}{\pi} - \left(\frac{\varepsilon^2}{2}\right)\ln\left(\frac{2}{\varepsilon}\right)\right]$$
$$\times\left[1 - \left(\frac{\varepsilon^3}{\pi}\right)\left(\ln\left(\frac{2}{\varepsilon}\right) + 0.73761\varepsilon^{2.74819}/(1 + 0.52119\varepsilon^{0.61465}\right)\right] \tag{2.6}$$

with $\varepsilon = 2a\mu_w/\eta$. The lateral diffusion coefficient D_{lat} is dependent on the surface viscosity η, the membrane thickness h, the viscosity of the surrounding aqueous medium μ_w and the radius of the diffusing particle a. γ is the Euler constant.

2.3.9 L_o domain tracking

Horizontal planar bilayers made of 2:1:1 (DOPC/DSOC/CO) containing DPPE-Atto532 were prepared as described above. Domains were imaged on an Olympus IX81 using

mercury lamp excitation and camera detection (F-View). The frame rate was adjusted to 1 s^{-1}. The domain trajectories were tracked using the Matlab routine Poly-Particle-Tracker [46]. Size dependent diffusion coefficients were evaluated from the trajectories using linear fits of the time dependent mean square displacement of the domains.

2.3.10 Gramicidin A labeling and electrophysiological activity

C-terminal labeling of gA with Atto637-NHS (Atto-Tec, Siegen, Germany) was conducted as described in [43]. Briefly, a primary amino group was added to the peptide by coupling ethylenediamine to the hydroxyl group of the C-terminal end. In a second reaction the NHS-ester group of Atto637 reacted with the primary amine to result in the product gA-637. The labeled peptide was purified from excess dye by dilution with water and subsequent centrifugation. The hydrophobic peptide was recovered from the pellet. This procedure was repeated until no free dye was detectable in the supernatant. Finally, the pellet was dissolved in methanol and the solution was stored at -20°C. The degree of labeling determined by spectroscopy (A_{280} and A_{637}) was 0.5. The mean single channel conductance of unmodified gA and gA-637 were ≈ 18 pS in a DOPC bilayer suspended in 1M NaCl.
The dimerization constant of gA-637 was determined according to [41]:

$$K = \frac{G_2}{4G_2^2 - 4G_2 * G_0 + G_0^2} \tag{2.7}$$

With G_o as the total surface density of gA in the bilayer and G_2 as the dimer surface density. Since only the dimeric peptides form an active channel, G_2 was determined electrically by using the mean single channel conductance to calculate the number of open channels from the total current amplitude. G_2 was divided by the total surface area of the bilayer, which was determined from laser scanning images. G_o was determined by FCS. The surface density of the fluorescent gA was directly calculated from the number of particles and the waist radius of the confocal spot. G_o was corrected by the degree of labeling.

2.4 Results

2.4.1 Effect of hydrocarbon solvents on lipid mobility in horizontal bilayers

Three different solvents with increasing chain length (decane, hexadecane and squalene) were used for BLM preparation to study the influence of hydrocarbon solvents on the mobilities of lipid molecules in the free standing horizontal bilayer membrane. The bilayers were prepared with the painting technique [31] from DOPC dissolved in the respective solvent.

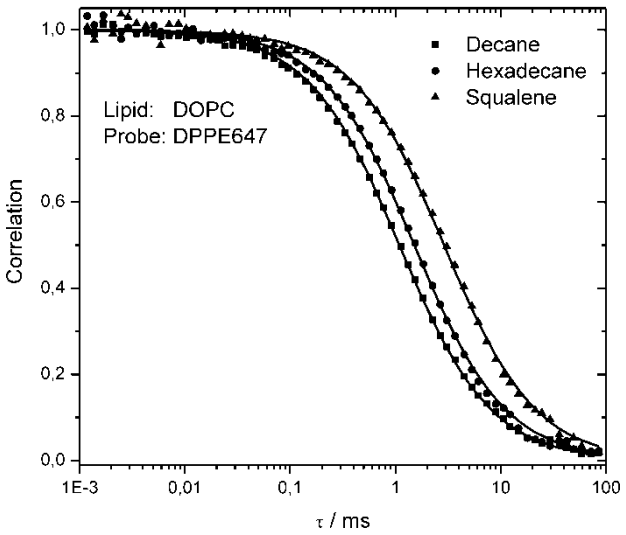

FIGURE 2.4 Influence of hydrocarbon solvents on the lateral diffusion of lipids in pure DOPC bilayers at 23°C. FCS results are shown for bilayers prepared with the indicated solvents. The diffusion coefficients of the probe DPPE647 were D_{lat} = 25 ± 2 µm^2/s, 16 ± 2 µm^2/s and 9 ± 1 µm^2/s in bilayers prepared with decane, hexadecane and squalene, respectively.

In this way, the bilayer formed only a single, liquid disordered (L_d) phase. The mobilities were investigated by the fluorescent lipid analog DPPE647, a phosphoglycero-lipid labeled with the organic dye Atto647N, which was incorporated into the bilayer at a very low concentration resulting in 1-10 fluorescent molecules in the confocal volume. After a bilayer had formed, which was observed by capacitance increase and torus formation, the system was allowed to equilibrate for 10 minutes before the first measurements were performed. Two different techniques were applied to determine the lipid mobility of the DOPC bilayer: fluorescence correlation spectroscopy (FCS) for the lateral and time resolved anisotropy (TRA) for the rotational diffusion of the lipid probe. Representative results of the FCS measurements for the bilayers in the different solvents are depicted in Fig. 2.4. The lateral mobility of the lipids in the bilayer was significantly reduced when longer hydrocarbon solvents compared to n-decane were used. The translational diffusion time through the laser focus increased and consequently the lateral diffusion coefficient decreased from τ_D = 1.1 ms and D_{lat} = 25 µm^2/s (decane) over τ_D = 1.5 ms and D_{lat} = 16 µm^2/s (hexadecane) to τ_D = 2.8 ms and D_{lat} = 9 µm^2/s (squalene), respectively. The lipid diffusion coefficient

determined in the presence of squalene is comparable to values of $D_{lat} = 4 – 7$ µm^2/s as reported for solvent free L_d membranes [25, 29, 49, 50]. The rotational mobility determined by TRA also increased significantly when the short alkanes were used with rotational correlation times and diffusion coefficients of Φ = 14.9 ns and $D_{rot} = 1.1 \times 10^7$ s^{-1} (squalene), Φ = 12.4 ns and $D_{rot} = 1.3 \times 10^7$ s^{-1} (hexadecane), and $\Phi = 6.4$ ns and $D_{rot} = 2.6 \times 10^7$ s^{-1} (decane), respectively. Decane was chosen as the solvent in the following experiments, because the stability and lifetime of the bilayers were significantly higher compared to membranes prepared with longer hydrocarbon solvents.

2.4.2 Phase separation

Horizontal bilayers made of DOPC/DSPC/CO (2:1:1) exhibited large scale phase separation into L_d and L_o domains at room temperature (Fig. 2.5*A*). Segregated domains had circular shape and were highly dynamic, i.e., they showed fusion to larger also circular domains. This is in agreement with the phase behavior of ternary lipid bilayers reported in [37] and indicates that both phases were in a fluid like state. Domain formation was visualized by fluorescence emission of Atto647N-lipids: phosphoethanolamine (DPPE647), sphingomyelin (SM647) and ceramide (CER647). All of the labeled lipids showed a similar partitioning pattern (Fig. 2.5*A*). The bright regions were identified to be the L_d phase by co-localization of fluorescently (Bodipy) labeled cholesterol CO-BDY, which has been shown to preferentially partition into the L_d phase [25]. CO-BDY had a partitioning coefficient at 23°C (L_o/L_d) of $\gamma = 0.26$ which is similar to the distribution of this probe in solvent free bilayers [25]. In contrast to native SM and CER, the Atto647N labeled lipids partitioned predominantly into the L_d phase. The partitioning coefficient was $\gamma \approx 0.1$ for CER647, SM647 and DPPE647 (table 2.1). However, this has been observed for the majority of other lipid-dye combinations, as well. The native partitioning of lipids has been found to be disturbed after labeling with a photo stable, but bulky fluophore [51, 52]. Nevertheless, these fluorescent sphingo-lipid analogs (SM647, CER647) have been found to form transient molecular complexes in the plasma membrane of living cells independent of the dye position or even the nature of the head group [15].

2.4.3 Lateral mobility of lipid probes in L_o and L_d phase

Next, the mobility of lipids in the L_d and L_o phases was compared. For an exact determination of the diffusion coefficients, *Z*-scan FCS was applied [57]. The focus was moved incrementally in *Z*-direction through the bilayer plane. The correlation data and the corresponding diffusion times $\tau_D(\Delta z)$ were determined (equation 2.3) for the different *Z*-positions Δz. The dependence of τ_D on Δz allowed for an exact determination of the lateral diffusion coefficients (equation 2.4). First, the lateral mobility of DPPE647, SM647 and CER647 in DOPC was measured in pure L_d phase bilayers at 23°C. All probes had comparable mobilities between $D_{lat} \approx 20 – 24$ µm^2/s (table 2.1). Upon addition of 20 mol %

cholesterol to the DOPC bilayer lateral mobilities of the probes did not change significantly (data not shown). In other studies lipid diffusion in the L_d phase was found to be slightly decreased upon addition of 20 mol% cholesterol [13]. In case of domain formation in the ternary lipid mixtures (DOPC/DSPC/CO, 2:1:1, Fig. 2.5*A*) the recorded photon traces were used to differentiate between mobilities in bright (L_d) and dark (L_o) domains (Fig. 2.5*B*). Because the lateral diffusion in the L_d domains ($D_{lat} \approx 18 – 25$ μm^2/s, table 2.1) was similar to that determined for the pure DOPC L_d phase bilayers, it can be concluded that the additional, saturated lipid DSPC mostly partitioned in the L_o phase at 23°C. In contrast, lipid diffusion in the L_o domains was 7 to 12-fold slower ($D_{lat} \approx 2 – 3$ μm^2/s) (Fig. 2.5*C*, table 2.1).

2.4.4 Rotational diffusion in the L_d and L_o phase

The same photon traces that were the basis of the FCS analysis were utilized for the time resolved anisotropy (TRA) analysis. The time resolved fluorescence decays recorded for parallel and perpendicular polarization (Fig. 2.5*D*) were analyzed (equations 1 and, 2) to obtain the rotational diffusion coefficient D_{rot} and the fluorescence lifetime τ_{FL} of the fluorescent lipid analogs CER647, SM647 and DPPE647 in both phases. A single anisotropic decay component and a single fluorescence lifetime were sufficient to yield statistically reliable fits. In pure DOPC (L_d) membranes the rotational diffusion coefficient was $D_{rot} \approx 2.4 \times 10^7$ s^{-1} for all three lipids (table 2.2). This value is in the same range as rotational diffusion coefficients of comparable lipid probes in an L_d membrane measured with single molecule anisotropy imaging [53]. Under phase separating conditions lipid rotation occurred with $D_{rot} \approx 1.4 \times 10^7$ s^{-1} in the L_d phase and between $D_{rot} \approx 1.0 \times 10^7$ s^{-1} to 0.8×10^7 s^{-1} in the L_o phase (table 2.2). The decreased rotational mobility in the L_o domains is in line with the characteristic higher lipid order and a condensed packing in the L_o phase. The reduced rotational motion in the L_d phase under phase separating conditions compared to pure L_d bilayers indicates that also the L_d phase changes its micro viscosity. However, this change does not significantly affect the lateral diffusion constant (see above). Since the addition of 30 mol % cholesterol to a pure L_d bilayer does not change rotational motion (data not shown) of the lipid probes, it can be concluded that residual amounts DSPC are present in the L_d phase under phase separating conditions.

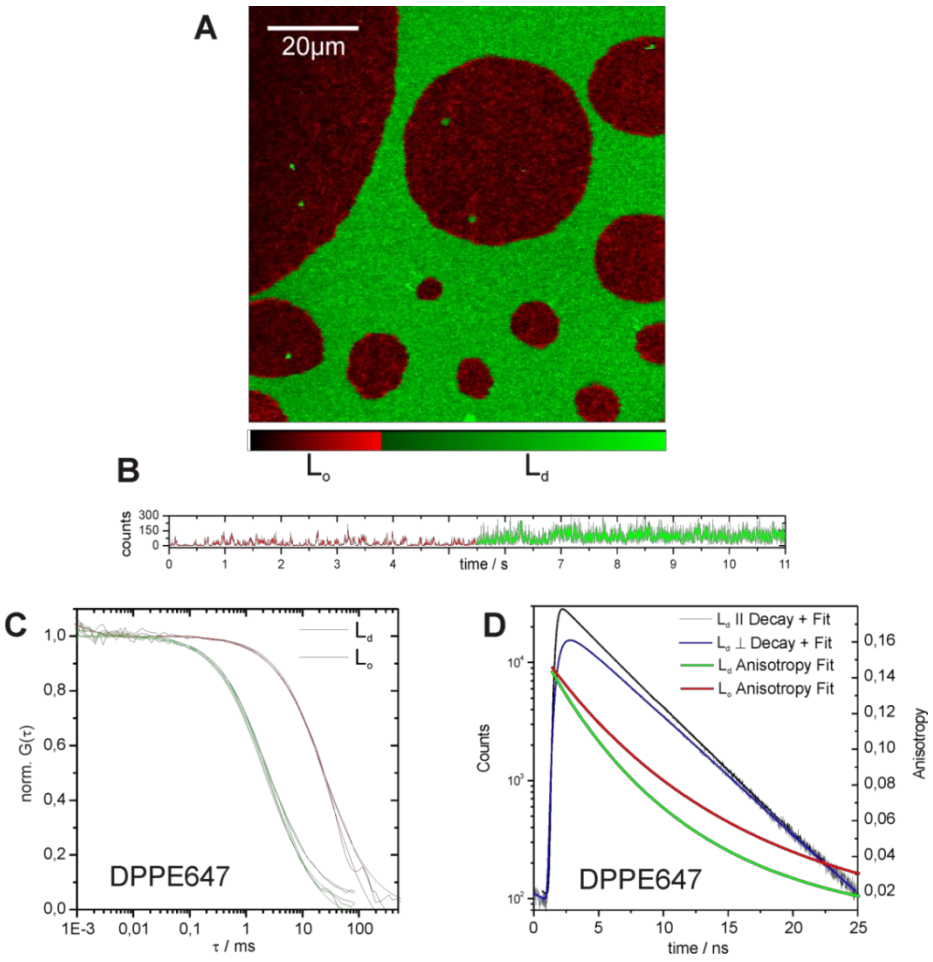

Probe	L_o µm²/s	L_d µm²/s	c (L_o)/c (L_d)
CO-BDY	**3.6** ± 0.1	**25.6** ± 2.9	**0.26** ± 0.08
DPPE647	**2.0** ± 0.4	**24.3** ± 2.4	**0.10** ± 0.01
SM647	**2.7** ± 0.5	**18.4** ± 2.1	**0.11** ± 0.07
CER647	**3.2** ± 0.5	**18.9** ± 3.9	**0.07** ± 0.04

	L_o		L_d		τ_{FL}
Probe	Φ / ns	β	Φ / ns	β	/ ns
DPPE647	**16.5** ± 1.3	0.15	**12.1** ± 0.2	0.15	4.1
SM647	**20.3** ± 2.3	0.11	**13.2** ± 2.0	0.14	4.1
CER647	**21.5** ± 1.3	0.12	**9.2** ± 0.2	0.12	4.0

FIGURE 2.5 Lateral and rotational mobility in DOPC/DSPC/CO (2:1:1) bilayers at 23°C. (*A*) Intensity image of a phase separated membrane (*XY*-plane). A look up table was used to emphasize the partitioning of the probe DPPE647. The L_d phase appears brighter than the L_o phase. (*B*) Fluctuating photon count time trace binned at 1 ms resolution from a single point measurement in the membrane plane. Count rates from the L_d phase are larger than from the L_o phase. Due to the fluid nature of the system, both phases crossed the confocal volume, revealed by the jump in count rate at ~ 5.5 s. (*C*) FCS data obtained from fluctuations in the L_d and L_o. The correlation curve is shifted to longer times for L_o, indicating the decrease in mobility. (*D*) Fluorescence intensity decay for parallel and perpendicular polarized emission after pulsed excitation of DPPE647 in the L_d phase. The fits yield the lifetime and the rotational correlation time of the probe. The anisotropy decay in the L_d (green) and L_o (red) which results from the fits are shown for comparison. The anisotropy decays slower in the L_o, indicating a lowered rotational mobility. The resulting lateral and rotational diffusion coefficients are listed in tables 1 (left) and 2(right).

2.4.5 Dipole-orientation of Atto647N-Lipids

The anisotropy decay of a membrane probe is strongly influenced by the position and the orientation of the dipole with respect to the acyl chains of lipids [60]. The Atto647N dye was either attached to the head group (DPPE647) or replacing the acyl chain (SM647, CER647) of the lipid, see supplement in [15]. For both positions the anisotropy and fluorescence decay in the bilayer were similar (table 2.2). The dipoles of the Atto647N-probes were found to be aligned parallel to the membrane plane at the hydrophilic / hydrophobic interface between the lipid head groups and the acyl chains. This orientation was determined by anisotropy imaging of giant unilamellar vesicles (GUVs) containing the respective probes (Fig. 2.6). The fluorescence intensity was significantly increased at membrane positions that were oriented parallel to the polarized excitation light.

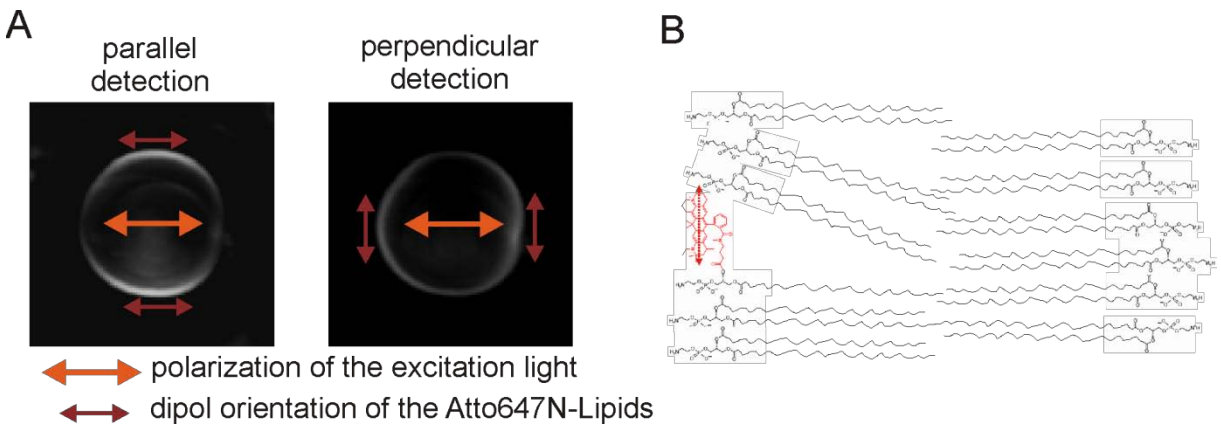

FIGURE 2.6 Dipole-orientation of Atto647N-Lipids. (A) The equatorial plane of a GUV made of DOPC containing DPPE-647N is depicted. The excitation polarization vector is shown in orange. The emission was split according to parallel and perpendicular polarized light onto two detectors. The intensity distribution on the GUV equator clearly indicates that the Attto647N dipole is oriented parallel to the membrane plane. (B) 2D cartoon of a bilayer of PC-lipids containing one DPPE-647 molecule. The dipole-orientation is shown with a red arrow.

While a parallel dipole orientation to the membrane is favorable for excitation of the dye in the horizontal bilayer setup, the sensitivity for lipid order is reduced due to the position and the rotation axes. Consequently, the observed rotational motion of the probe was not notably restricted as found for hydrophobic probes which intercalate parallel to the lipid acyl chains [60]. Further, the fluorescence lifetime of the fluorescent label did not change between phases, indicating no phase dependence of molecular parameters (such as inter-molecular quenching) other than of mobility.

The phase partitioning data of the Atto647N lipid analogues show that all labeled lipids are greatly excluded from the liquid ordered phase. This phenomenon has also been reported for the majority of other fluorescent lipid analogues [51]. Interestingly, lipid analogues which are able to partition into the ordered phases seem to adopt a perpendicular dipole orientation

to membrane plane (see [51] Fig. 7). In Fig. 2.6*B* a possible consequence of the parallel membrane orientation of the Atto647N dipole is depicted. The fluorescent dye may cause (in some way) a steric mismatch between neighboring lipids which will introduce some disorder in the membrane acyl chains. Hence, the Atto647N lipid analogues will be excluded ("squeezed out") from ordered regions due to their energetically unfavorable conformation.

2.4.6 Steady state anisotropy

To visualize the steady state anisotropy in the bilayer anisotropy images were calculated pixel by pixel from the signal intensity in the parallel and perpendicular detection channel (equation 2.5). Fig. 2.7 shows the intensity and the anisotropy image of a DOPC/DSPC/CO mixture at 23°C. As before (Fig. 2.5*A*), the partitioning of the probe is evident in the intensity image (Fig. 2.7*A*), where the dark domains correspond to the L_o phase. The anisotropy image (Fig. 2.7*B*) depicts slightly larger anisotropy values in the L_o phase, which is in line with a decreased rotational diffusion coefficient. However, in contrast to the L_d phase, where the values are narrow distributed around 0.1, a wide range of anisotropy values is observed for the L_o phase, ranging from ~0.1 to 0.3-0.4, with the higher values indicating very slow rotational motion.

To get further insight into this strong heterogeneity, steady state anisotropy values were reordered on a single-molecule level. For determination of the steady state anisotropy from single molecules, the laser spot was positioned on different positions in the L_d and L_o phases of the bilayer and photon traces were recorded over time. The concentration of DPPE647 was reduced such that less than one fluorescent molecule was present per laser spot per time. The fluorescence bursts indicating single molecule transits (Fig. 2.7*C*) were used to calculate the steady state anisotropy (equation 2.5). Selection of more than 2000 single molecule fluorescence bursts resulted in a histogram of anisotropy values for the L_d and L_o phase (Fig. 2.7*D*).The distribution of anisotropy values of the L_o phase peaks at much higher values ($\bar{r} \approx 0.16$) and is much broader than the distribution of values for the L_d phase ($\bar{r} \approx 0.1$), tailing off to very high values $\bar{r} > 0.3$, confirming the heterogeneity in anisotropy as previously observed using anisotropy imaging. It seems that the L_o phase itself contains a sub-population where lipid rotation is significantly reduced. Unfortunately, the ability to resolve additional, very slow rotational components in the L_o phase is limited by the fluorescence lifetime (4 ns) of the lipid analogue. Thus, the resolution of our time-resolved anisotropy data was not good enough to reliably determine very slow rotational components.

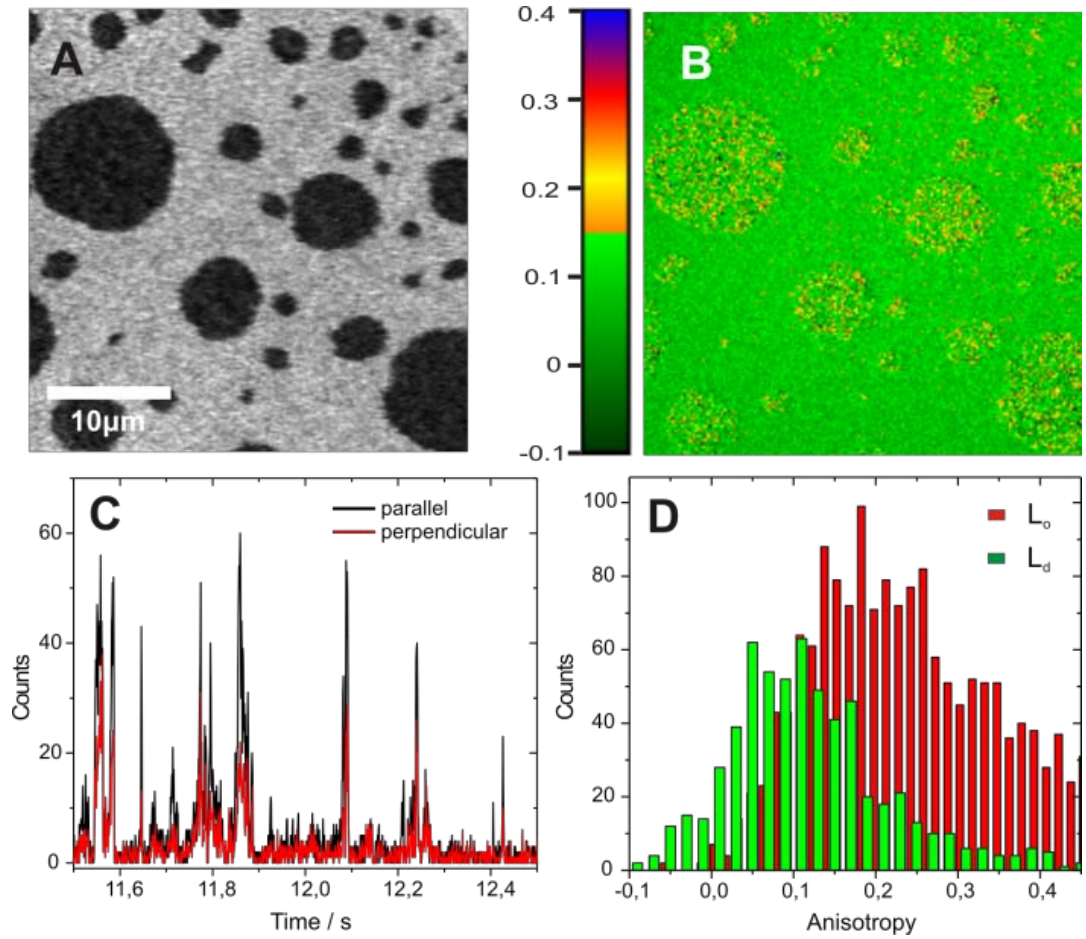

FIGURE 2.7 Steady state anisotropy and FCS diffusion laws in DOPC/DSPC/CO (2:1:1) bilayers, probe DPPE647. (*A*) Intensity image of a bilayer with L_o (dark) and L_d (bright) domains. (*B*) Pixel by pixel calculated anisotropy from parallel and perpendicular images. The anisotropy was larger and more heterogeneous in the L_o-domains. (*C*) Section of a photon trace recorded by a point measurement in the L_o phase (1 ms binning). Single molecule transits are visible as photon bursts. For each transit the anisotropy was calculated by burst integration of the parallel and perpendicular detection channel and application of equation 5. (*D*) Single molecule anisotropy histograms calculated from as described in (*C*) in the L_d and L_o phase of the membrane, with peaks at around 0.1 and 0.16, respectively. The distribution in the L_o phase is shifted to higher anisotropy values and is much broader, confirming the lowered rotational mobility as well as indicating a heterogeneous lipid environment in the L_o phase.

2.4.7 FCS diffusion laws in lipid domains and temperature dependence

Since large scale phase separation of lipids is found only at temperatures which are significantly below physiological temperatures of cell membranes [16], lipid diffusion was compared at temperatures which are above (37°C) and below (23°C) the transition between phase separation ($L_o \leftrightarrow L_d$) and an apparently homogenous L_d membrane. In Fig. 2.8*A* the temperature dependent mixing of the L_d phase (green) and the L_o phase (red) is depicted. At temperatures above 35°C the lipid mixing seemed to be homogenous. Obviously, phase separation degraded above 35°C. To determine the diffusion constants and the mode of diffusion at different temperatures Z-Scan FCS was applied.

The diffusion time data obtained at multiple *Z*-positions was used to determine the principal mechanism of diffusion at 23°C where lipids largely phase separate and at 37°C where the ternary mixture seems to be homogeneous [7, 8, 58]. Provided the diffusion of the probe is not hindered by membrane heterogeneities smaller than the optical resolution, the relation between diffusion time and focus area is expected to be linear with a slope of four times the diffusion coefficient (free diffusion). During a *Z*-scan, the membrane area probed by the laser focus increases as the focus is moved out of the plane of the bilayer. The size of the focal area was determined relative to minimal waist radius w_0 and the particle number N_{min} at the minimum waist: $A_{\mathrm{focus}} = w_0^2 \times N / N_{\mathrm{min}}$ [59] (the particle numbers N were determined from the inverse of the correlation function's amplitude $N = 1 / G(0)$). This relation is valid as long as the surface density of lipid probes is independent from the probed area which we can assume is true for a homogenous membrane and also for domains on the order much smaller and much larger than the confocal spot. From the slope of fits (Fig. 2.8*E*) the lateral diffusion coefficient was determined to be $D_{\mathrm{lat}} \approx 4\ \mu m^2/s$ in the L_o phase and $D_{\mathrm{lat}} \approx 25\ \mu m^2/s$ in the L_d phase at 23°C, which confirms the previous measurements. At 37°C the lateral diffusion constant was $D_{\mathrm{lat}} \approx 32\ \mu m^2/s$ which follows from the increased mobility at higher temperatures. Most importantly, the results show that the diffusion data in the L_d phase at 23°C and at 37°C can be well fitted with a linear regression intersecting at the origin which is an indication for free diffusion. In contrast to this, a positive intersection is observed when the diffusion data of the L_o phase at 23°C is linearly fitted (Fig. 2.8*E*). By FCS simulations on lipid/protein diffusion in membranes, it was shown that a positive intersection is an indication for hindered diffusion due to partitioning into nano-domains [7, 8].

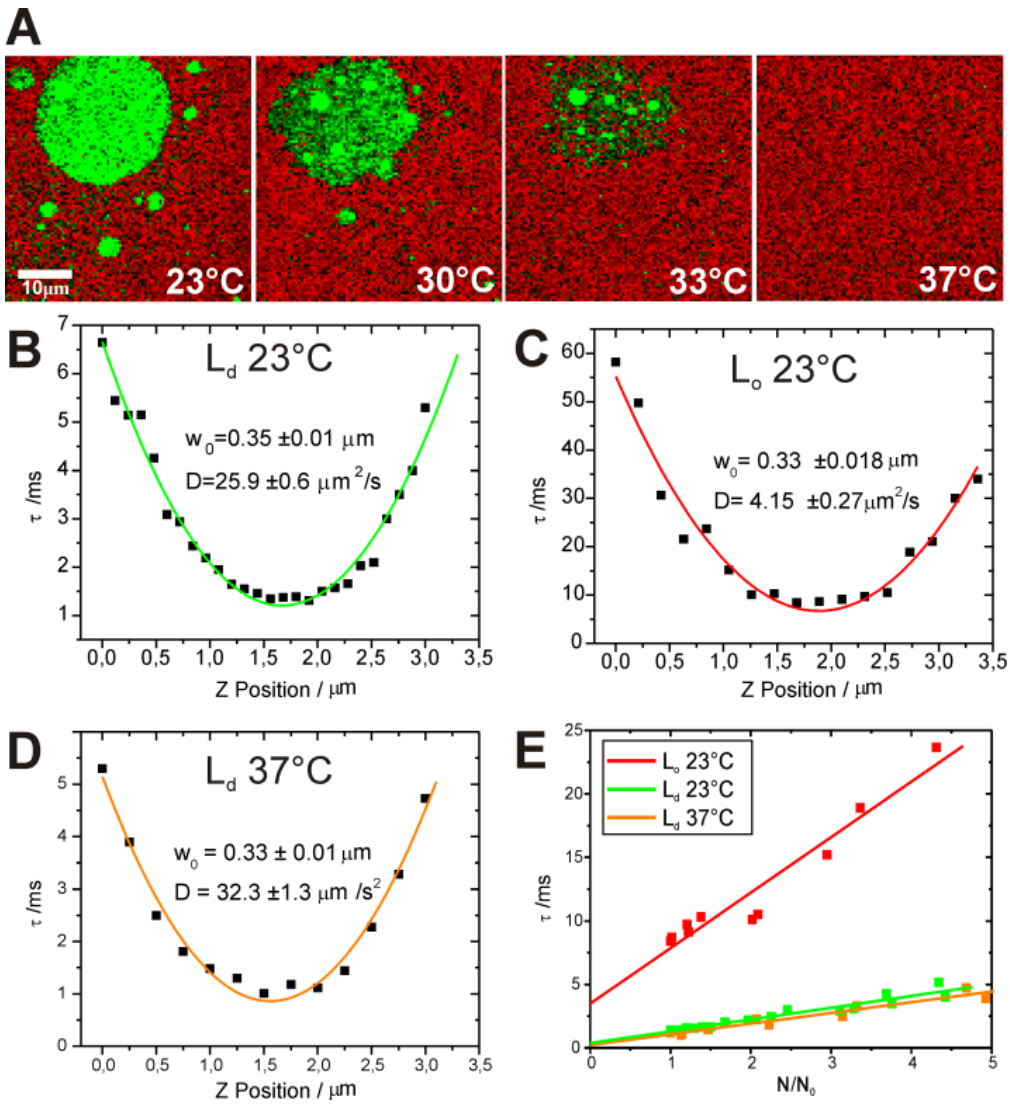

FIGURE 2.8 Temperature dependent diffusion of the lipid probe SM647 in DOPC/DSPC/CO (1:1:1) bilayers. (*A*) The separated L_d and L_o phases started to mix with increasing temperatures to a homogeneous membrane at ≈ 35°C (colors as in fig. 4*A*). (*B-D*) Lateral diffusion coefficients D_{lat} and the beam waist w_0 of the laser determined with *Z*-scan FCS in the L_d and L_o phase at 23°C and 37°C, showing an increase in mobility with increasing temperature [57]. At 23°C two diffusion constants are found, representing the L_d and L_o, respectively. At 37°C a single diffusion constant was sufficient to fit the FCS data. (*E*) Diffusion laws in the L_o and L_d phase at 23°C and 37°C [7]. The dependence of diffusion time vs. area (N/N_{min}) is linear intersecting at the origin if the diffusion is free which is the case in the L_d phase at 23°C and at 37°C [59]. In the L_o phase at 23°C the intersection is clearly positive which indicates hindered diffusion due to, for example, solid ordered nano-domains.

2.4.8 Hydrodynamic viscosity of planar bilayers in the L_d phase

The hydrodynamic viscosity of a membrane is a measure of how strongly lipids (and proteins) in the bilayer interact. The most widely used hydrodynamic model in biophysics, describing the relation between membrane inclusion radius, lateral diffusion coefficient and membrane viscosity, is the Saffman-Delbrück-Approximation (SD) [44]. Unfortunately, the

SD model has a limited applicable range of inclusion sizes (small proteins) to predict correct results.

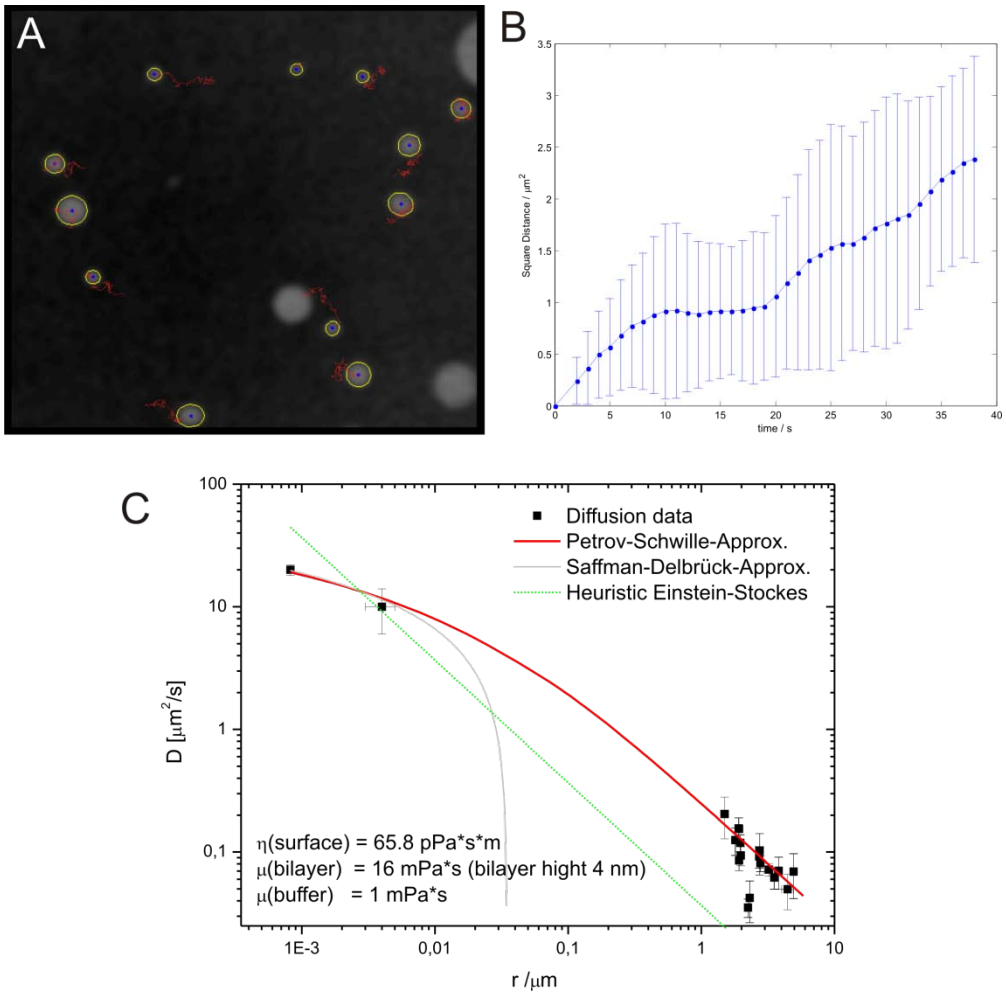

FIGURE 2.9 Hydrodynamic viscosity of HLBs. (A) Movies of L_o (bright) domains diffusing in the L_d bilayer (dark) were recorded with 1s time resolution using epi-fluorescence excitation and a fluoview camera. The diffusion trajectories were evaluated with the program poly-particle-tracker[46]. (B) Mean square displacement over time of a single L_o domain. A linear fit ($x^2 = 4Dt$) results in the lateral diffusion constant D of the specific domain. (C) Double log plot of the diffusion coefficients against the membrane inclusion radius. Diffusion of single lipids $r \approx 0.8$ nm (left data point) and the trimeric beta-barrel protein PorB $r \approx 4$ nm was determined by FCS. The tracking results of L_o domains are on the order of r = 1-8 µm. A fit of the data with the Petrov-Schwille-Approximation yields the surface viscosity and the bulk viscosity of the bilayer in the L_d phase. Buffer viscosity was taken as 1 mPa*s.

Additionally, Gambin et al. challenged the validity of SD approximation even for membrane proteins and found that a heuristic Einstein-Stokes model (ES) fitted their diffusion data best [57]. An exact numeric solution of the hydrodynamic viscosity problem, developed by Hughes, Pailthorpe and White (HPW), is applicable to arbitrary inclusions sizes. However, an easy application of this model is impeded by its great computational effort. Recently, an

analytical approximation of the HPW model was proposed by Petrov and Schwille (PS) to reduce the computational effort [45].

To determine the viscosity of the HLBs the size dependent lateral diffusion coefficients of L_o domains with radii between 1-8 µm were measured using a particle tracking technique. Additionally, diffusion data of lipids and one membrane-protein (PorB) obtained by FCS were used. The results are shown in Fig. 2.9. Unfortunately, the range of inclusion sizes between 5 nm and 1 µm could not be probed, because it was not feasible to include appropriate molecules in the bilayer in that specific size range. The data were fitted using the SD, the ES and the PS approximations Fig. 2.9*C*. As expected the SD approximation fitted the data only to inclusion radii smaller than ≈ 10 nm, before the model approached an asymptotic barrier. The ES model did not result in a reasonable fit, while the PS approximation fitted the data nicely over complete size range. The fitted surface viscosity (PS) of the bilayer in the L_d phase at 23°C was $\eta = 66 \pm 20$ pPa·s·m. With a bilayer thickness (DOPC) of h ≈ 4 nm [58] we yield a membrane viscosity of $\mu = 16.5 \pm 5$ mPa·s. Values reported for solvent free pure lipid bilayers range between 60.8 mPa·s [59]. Thus, our planar bilayers prepared with n-decane are ≈ 4-fold more fluid compared to solvent free membranes.

2.4.9 Electrical resistance of binary and ternary lipid mixtures

In a number of studies ion channel like activity has been observed in pure phospholipid bilayers when the temperature of the membrane was near the T_m of the used lipid [60, 61]. Accordingly, the permeability of liposomes was found to be increased at the T_m[62, 63]. This phenomenon is suggested to be the result of the increased area fluctuations near the T_m which lead to formation of transient lipid pores [61]. The opto-electrical setup was applied to test whether such current fluctuations also occur at the transition between coexisting L_d and L_o domains and a homogeneous L_d membrane. Therefore, electrophysiological recordings were performed in parallel to the optical measurements in a temperature range of 15°C to 45°C with the binary mixture DPPC/DOPC (3:1) (Fig. 2.10*A*) and the ternary lipid mixture DOPC/DSPC/CO (1:1:1). The bilayer was painted at 55°C. After equilibration the temperature was lowered to 15°C with 1°C/min. A holding potential of 100 mV was applied to probe the membrane resistance and current fluctuations. The mean current was calculated for every °C/min. As a control the phase transition temperature of the binary lipid mixture was determined by measuring the vertical polarized fluorescence intensity of cholesterol-BODIPY in liposomes. The phase transition of the binary mixture falls between 41°C-30°C (fig. 8*A* red trace). Discrete current fluctuations similar to ion channel gating events occurred in the same temperature range as lipids started to phase separate (Fig. 2.10*A*). In many cases the bilayer ruptured at the 36°C during the temperature scan, which is an additional indication for instabilities in the membrane structure during phase separation. When a ternary mixture containing cholesterol was studied no current fluctuation within the

experimental error were observed. This was also true when L_o domains started to segregate from the L_d phase at ~35°C. The specific resistance of the ternary membrane decreased linearly from $5 \times 10^7\ \Omega cm^2$ at 20°C to $3.5 \times 10^7\ \Omega cm^2$ at 40°C (Fig. 2.10*B*). It can be concluded that the bilayer becomes electrical unstable (leaky) at the main phase transition ($L_d \leftrightarrow S_o$), whereas the membrane remains electrically sealed at the transition from the L_o to the L_d phase.

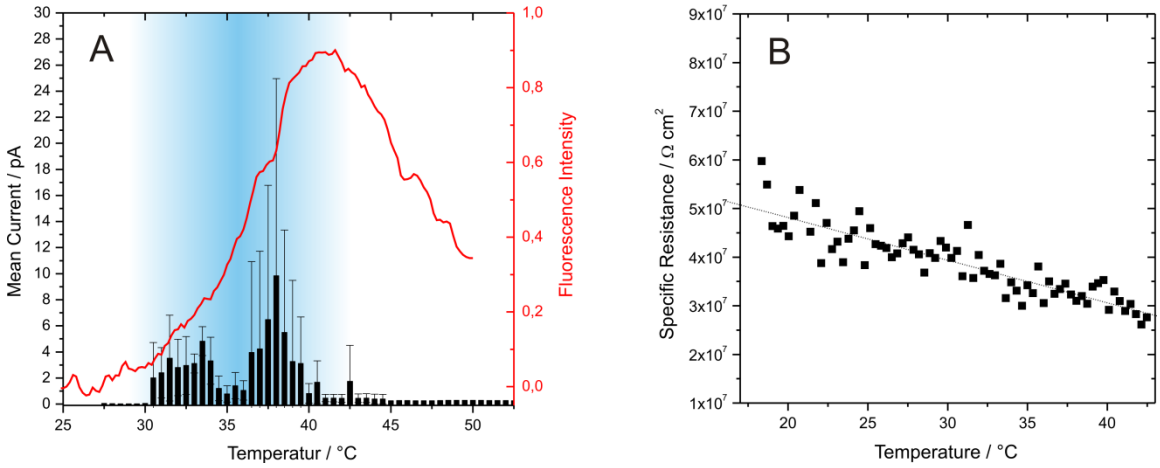

FIGURE 2.10 Conductance of BLMs at the phase transition (A) Current fluctuations in the phase transition range (blue) of the binary mixture DPPC/DOPC (3:1). The mean currents of one minute intervals with an applied HP of 100 mV were plotted versus temperature. The phase transition of the binary mixture was probed by polarized fluorescence measurement of cholesterol-BODIPY in liposomes (red trace). (B) Specific resistance of the ternary mixture DOPC/DSPC/CO (2:1:1) in a temperature range of 20°C to 40°C. The resistance was linearly dependent on the temperature. No current fluctuations were observed in the probed temperature range.

2.4.10 Partitioning and electrical activity of gramicidin A in lipid domains

The short antibiotic peptide gA is one of the best characterized ion channels to date [38, 64]. It is able to form a 2.8nm long trans-membrane beta helix with an aqueous pore diameter of 0.4nm. This cation conducting conformation was found to be the result of an N- to N-terminal dimerization of two gA monomers [41]. The structure of the trans-membrane gA dimer itself seems to be unaffected by the lipid composition of the membrane [65, 66]. However, the dimerization constant is dependent on the hydrophobic thickness and the lipid composition of the bilayer as well as the membrane potential [41, 64, 67].

Here a functional, C-terminal, Atto637-labeled derivate of gA was used to study the effect of liquid-liquid phase separation on the activity and partitioning of gA. The peptide was added directly to the lipid solution (DOPC/DSPC/CO 1/1/1) in a molar ratio of (1/50000). The bilayer was prepared at 39°C to ensure a homogeneous mixing of lipid species (Fig. 2.11*A*). The gA concentration in the membrane was determined by FCS (fig. 9*C*), and the active dimer concentration was determined by electrical conductance measurements (Fig. 2.11*B*).

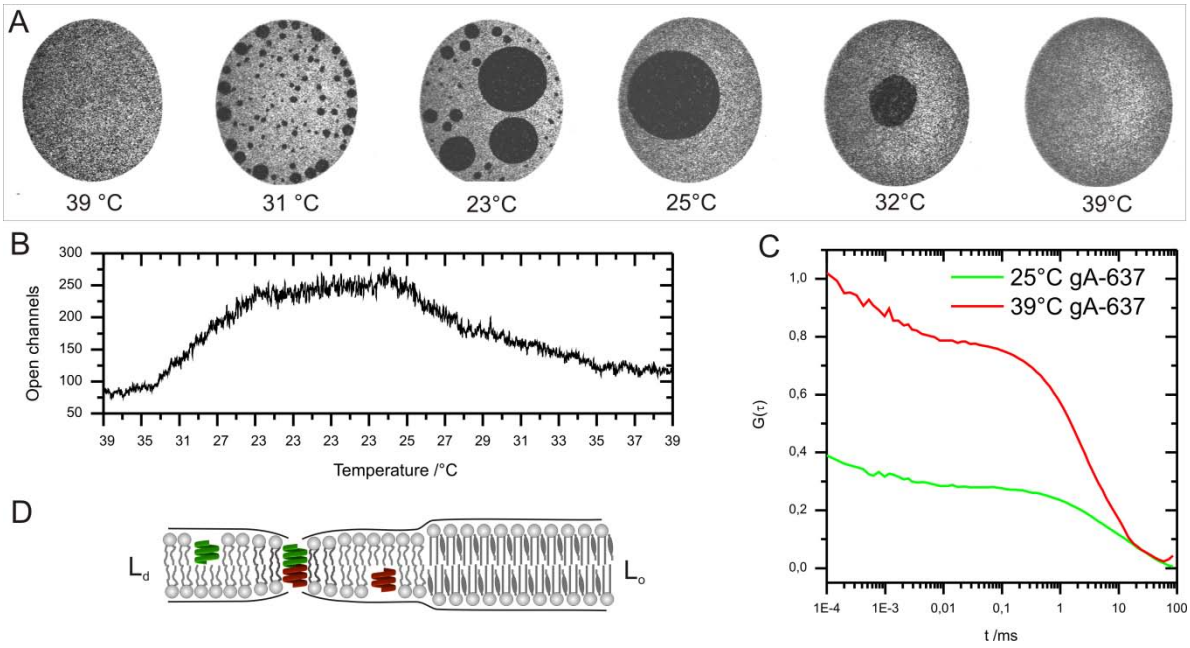

FIGURE 2.11 Phase partitioning and electrical activity of gramicidin A. (*A*) Lipid phase separation in a DOPC/DSPC/CO (1:1:1) membrane (Ø = 100 µm) containing gA-637 was induced by cooling the bilayer from 39°C to 23°C. gA-637 was largely excluded from the L_o domains (dark). (*B*) Simultaneously the electrical activity of gA-637 was monitored via conductance measurements of the bilayer. The number of open gA channels increased 3.3 fold as the lipids phase separated. (*C*) FCS measurement at 39°C and 23°C revealed that the surface density in the L_d phase at 23°C was 2.2 fold increased compared to the homogenous membrane at 39°C. The dimerization constant determined from the number of open channel and the total number of gA-637 (FCS) changed during phase separation from $K_{39°C} = 3.3 \times 10^{11}$ cm^2/mol to $K_{23°C} = 4.1 \times 10^{11}$ cm^2/mol. (*D*) Scheme of gA monomers forming an active dimer in the L_d phase. The peptide is energetically excluded from the thicker and ordered, cholesterol enriched L_o phase. The thinner membrane in the L_d phase results in a higher dimerization constant of gA. However, the increased electrical activity of gA in the L_d phase can be mainly attributed to the increased surface density due to exclusion from the L_o domains.

As the membrane was cooled to 23°C, large scale L_o domains segregated from the L_d phase. gA was found to be largely excluded from the L_o domains (Fig. 2.11*A*). Simultaneously, the number of electrically active dimers increased 3.3 fold as the lipids phase separated. Accordingly, the surface density of gA in the L_d phase, determined by FCS, increased 2.2 fold at 23°C. Interestingly, the dimerization constant K (equation 2.6), did not change significantly between 39°C and 23°C with values of 3.3×10^{11} cm^2/mol (39°C) and 4.1×10^{11} cm^2/mol (23°C). Thus, the increased electrical activity at 23°C was mainly caused by the higher surface density of gA due to exclusion from the L_o domains and not by a change of hydrophobic thickness of the membrane. When the temperature was raised back to 39°C lipid domains mixed again to a single phase. As expected the number of active gA dimers decreased again. The results show that the electrophysiological activity of gA can be simply regulated by phase partitioning in lipid domains.

2.5 Discussion

The aim of this study was to characterize the diffusion and electrical properties of horizontal black lipid bilayers containing biological relevant ternary lipid mixtures and compare the results with other established membrane model systems. Additionally, the potential of the setup to relate electrical activity of ion channels to partitioning behavior in lipid domains was explored using the ion channel gA.

In contrast to supported bilayers or GUVs, for any black lipid membrane preparation the use of a hydrocarbon solvent is essential, because the actual bilayer is thinned out from a bulk region of a solvent lipid mixture (Torus). This raises the problem that the solvent may also partition inside the actual bilayer, which may cause changes in the natural properties of the membrane. To address this the influence of three different solvents on lipid diffusion was determined. The results show that the lateral and rotational diffusion constants depend on the nature of the hydrocarbon solvents used for bilayer preparation. Since the lateral and rotational mobility increased with decreasing chain length of the solvents it can be concluded that shorter alkanes (< C16) partially reside in the bilayer membrane after equilibration of the horizontal bilayer system. This causes a more fluid membrane and a depressed T_m compared to solvent free bilayers. In other studies on BLMs, solvent partitioning was also found to increase the bilayer thickness, probably by intercalation of the solvent molecules between the inner and outer leaflet [40, 68, 69]. However, during the measurements on phase separation in ternary HLBs, domain formation always extended through both leaflets of the membrane regardless of the solvent used (Fig. 2.5*A*). Thus, the coupling between the opposing leaflets is not affected by the presence of decane, hexane or squalene.

Apart from solvent partitioning effects, large scale domain segregation in ternary horizontal bilayers occurred in accordance to the established phase diagrams which were derived using GUVs [18-21]. Moreover, the basic characteristics of liquid-liquid domain formation can be reconstituted in horizontal bilayers: Lateral and rotational diffusion is significantly reduced and the lipid order is higher in the L_o domains compared to L_d domains. A ~8-fold decrease in lateral diffusion (L_d/L_o) was found. Similar differences between lateral diffusion in L_o and L_d domains of 3- to 20-fold have been reported for other model membranes [12, 25, 49].

A detailed analysis of lipid anisotropy, which reports the very local environment of the probe, and of the lateral diffusion on various length scales revealed that the anisotropy is homogeneous and lateral diffusion is free in the L_d phase. Interestingly, both the anisotropy values as well as the lateral diffusion law indicate a heterogeneous lipid distribution in the L_o phase at 23°C. The origin of the heterogeneities is not clear, but could be due to a non-ideal segregation of the lipid species such that nano L_d domains remain in the L_o phase. Another possibility may be the formation of nano S_o domains in regions of the L_o phase where cholesterol content is low. Further details on potential nano-domains in the L_o phase

may be elaborated by combining FCS (or TRA) and stimulated emission depletion (STED) nanoscopy [70] a microscopy approach featuring a spatial resolution far below that of conventional microscopy, i.e., in the range of the nano-domains' sizes [15, 71].
To explore the full potential of the horizontal bilayer technique the influence of lipid phase partitioning on the electrophysiological activity of the ion channel gA was studied. It was found that the monomeric as well as the dimeric gA were largely excluded from the L_o phase. The sorting of the peptide to the L_d phase resulted in an increased electrophysiological activity monitored by an increase in detected membrane current. The activity of gA was found to be simply modulated by the surface density in the lipid domains. This is consistent with the results of Boheim et al. [72] who found indications for lipid domain partitioning effects of gA and alamethicin: Near the transition temperature of SMPC bilayers the electrical activity of the peptides was significantly higher. However, in that study the setup allowed only for electrical recordings. Thus, the authors could only speculate about domain partitioning effects of the peptides. In the present study we could directly relate the sorting of gA, due to phase partitioning, to its electrophysiological activity. The results show that the presented setup can be used to study quantitatively the relation of ion channel function and lipid phase separation in a defined system. The technique could now be applied to more complex proteins which are thought to be regulated by lipid domains [64, 73].

2.6 References

1. Fielding, C. J., editor. 2005. Lipid Rafts and Caveolae. Wiley-VCH.

2. van Meer, G., D. R. Voelker, and G. W. Feigenson. 2008. Membrane lipids: where they are and how they behave. *Nat Rev Mol Cell Biol*. 9:112–124.

3. Simons, K., and G. van Meer. 1988. Lipid sorting in epithelial cells. *Biochemistry*. 27:6197–6202.

4. Sako, Y., and A. Kusumi. 1994. Compartmentalized structure of the plasma membrane for receptor movements as revealed by a nanometer-level motion analysis. *J Cell Biol*. 125:1251–1264.

5. Simons, K., and E. Ikonen. 1997. Functional rafts in cell membranes. *Nature*. 387:569–572.

6. Gaus, K., E. Gratton, E. P. W. Kable, A. S. Jones, I. Gelissen, L. Kritharides, and W. Jessup. 2003. Visualizing lipid structure and raft domains in living cells with two-photon microscopy. *Proc Natl Acad Sci U S A*. 100:15554–15559.

7. Wawrezinieck, L., H. Rigneault, D. Marguet, and P.-F. Lenne. 2005. Fluorescence correlation spectroscopy diffusion laws to probe the submicron cell membrane organization. *Biophys J*. 89:4029–4042.

8. Lenne, P.-F., L. Wawrezinieck, F. Conchonaud, O. Wurtz, A. Boned, X.-J. Guo, H. Rigneault, H.-T. He, and D. Marguet. 2006. Dynamic molecular confinement in the plasma membrane by microdomains and the cytoskeleton meshwork. *EMBO J*. 25:3245–3256.

9. Wenger, J., F. Conchonaud, J. Dintinger, L. Wawrezinieck, T. W. Ebbesen, H. Rigneault, D. Marguet, and P.-F. Lenne. 2007. Diffusion analysis within single nanometric apertures reveals the ultrafine cell membrane organization. *Biophys J*. 92:913–919.

10. Lingwood, D., J. Ries, P. Schwille, and K. Simons. 2008. Plasma membranes are poised for activation of raft phase coalescence at physiological temperature. *Proc Natl Acad Sci U S A*. 105:10005–10010.

11. Eggeling, C., C. Ringemann, R. Medda, G. Schwarzmann, K. Sandhoff, S. Polyakova, V. N. Belov, B. Hein, C. von Middendorff, A. Schönle, and S. W. Hell. 2009. Direct observation of the nanoscale dynamics of membrane lipids in a living cell. *Nature*. 457:1159–1162.

12. Dietrich, C., L. A. Bagatolli, Z. N. Volovyk, N. L. Thompson, M. Levi, K. Jacobson, and E. Gratton. 2001. Lipid rafts reconstituted in model membranes. *Biophys J*. 80:1417–1428.

13. Scherfeld, D., N. Kahya, and P. Schwille. 2003. Lipid dynamics and domain formation in model membranes composed of ternary mixtures of unsaturated and saturated phosphatidylcholines and cholesterol. *Biophys J*. 85:3758–3768.

14. Crane, J. M., and L. K. Tamm. 2004. Role of cholesterol in the formation and nature of lipid rafts in planar and spherical model membranes. *Biophys J*. 86:2965–2979.

15. Kiessling, V., J. M. Crane, and L. K. Tamm. 2006. Trans bilayer effects of raft-like lipid domains in asymmetric planar bilayers measured by single molecule tracking. *Biophys J*. 91:3313–3326.

16. Baumgart, T., A. T. Hammond, P. Sengupta, S. T. Hess, D. A. Holowka, B. A. Baird, and W. W. Webb. 2007. Large-scale fluid/fluid phase separation of proteins and lipids in giant plasma membrane vesicles. *Proc Natl Acad Sci U S A*. 104:3165–3170.

17. Feigenson, G. W. 2007. Phase boundaries and biological membranes. *Annu Rev Biophys Biomol Struct*. 36:63–77.

18. Feigenson, G. W., and J. T. Buboltz. 2001. Ternary phase diagram of dipalmitoyl-PC/dilauroyl-PC/cholesterol: nanoscopic domain formation driven by cholesterol. *Biophys J*. 80:2775–2788.

19. de Almeida, R. F. M., A. Fedorov, and M. Prieto. 2003. Sphingomyelin/Phosphatidylcholine/Cholesterol phase diagram: boundaries and composition of lipid rafts. *Biophys J*. 85:2406–2416.

20. Feigenson, G. W. 2006. Phase behavior of lipid mixtures. *Nat Chem Biol*. 2:560–563.

21. Goni, F. M., A. Alonso, L. A. Bagatolli, R. E. Brown, D. Marsh, M. Prieto, and J. L. Thewalt. 2008. Phase diagrams of lipid mixtures relevant to the study of membrane rafts. *Biochim Biophys Acta*. 1781:665–684.

22. Magde, D., E. Elson, and W. W. Webb. 1972. Thermodynamic fluctuations in a reacting system–measurement by fluorescence correlation spectroscopy. *Physical Review Letters*. 29:705.

23. Chiantia, S., J. Ries, and P. Schwille. 2008. Fluorescence correlation spectroscopy in membrane structure elucidation. *Biochim Biophys Acta*. .

24. Dertinger, T., V. Pacheco, I. von der Hocht, R. Hartmann, I. Gregor, and J. Enderlein. 2007. Two-focus fluorescence correlation spectroscopy: a new tool for accurate and absolute diffusion measurements. *Chemphyschem*. 8:433–443.

25. Ries, J., S. Chiantia, and P. Schwille. 2009. Accurate determination of membrane dynamics with line-scan FCS. *Biophys J*. 96:1999–2008.

26. Jähnig, F. 1979. Structural order of lipids and proteins in membranes: evaluation of fluorescence anisotropy data. *Proc Natl Acad Sci U S A*. 76:6361–6365.

27. Goswami, D., K. Gowrishankar, S. Bilgrami, S. Ghosh, R. Raghupathy, R. Chadda, R. Vishwakarma, M. Rao, and S. Mayor. 2008. Nanoclusters of GPI-anchored proteins are formed by cortical Actin-driven activity. *Cell*. 135:1085–1097.

28. Gidwani, A., D. Holowka, and B. Baird. 2001. Fluorescence anisotropy measurements of lipid order in plasma membranes and lipid rafts from Rbll-2h3 mast cells. *Biochemistry*. 40:12422–12429.

29. Ariola, F. S., Z. Li, C. Cornejo, R. Bittman, and A. A. Heikal. 2009. Membrane fluidity and lipid order in ternary giant unilamellar vesicles using a new bodipy-cholesterol derivative. *Biophys J*. 96:2696–2708.

30. Hille, B. 2001. Ion Channels of Excitable Membranes. Sinauer Associates, Inc.

31. Mueller, P., and D. O. Rudin. 1963. Induced excitability in reconstituted cell membrane structure. *J Theor Biol*. 4:268–280.

32. Hladky, S. B., and D. A. Haydon. 1970. Discreteness of conductance change in bimolecular lipid membranes in the presence of certain antibiotics. *Nature*. 225:451–453.

33. Hill, K., K. Model, M. T. Ryan, K. Dietmeier, F. Martin, R. Wagner, and N. Pfanner. 1998. Tom40 forms the hydrophilic channel of the mitochondrial import pore for preproteins [. *Nature*. 395:516–521.

34. Fahey, P. F., D. E. Koppel, L. S. Barak, D. E. Wolf, E. L. Elson, and W. W. Webb. 1977. Lateral diffusion in planar lipid bilayers. *Science*. 195:305–306.

35. Ide, T., and T. Yanagida. 1999. An artificial lipid bilayer formed on an agarose-coated glass for simultaneous electrical and optical measurement of single ion channels. *Biochemical and Biophysical Research Communications*. 265:595–599.

36. Borisenko, V., T. Lougheed, J. Hesse, E. Füreder-Kitzmüller, N. Fertig, J. C. Behrends, G. A. Woolley, and G. J. Schütz. 2003. Simultaneous optical and electrical recording of single gramicidin channels. *Biophys J*. 84:612–622.

37. Samsonov, A. V., I. Mihalyov, and F. S. Cohen. 2001. Characterization of cholesterol-sphingomyelin domains and their dynamics in bilayer membranes. *Biophys J*. 81:1486–1500.

38. Andersen, O. S., R. E. Koeppe, and B. Roux. 2005. Gramicidin channels. *IEEE Trans Nanobioscience*. 4:10–20.

39. Eggeling, C., K. Gall, K. Palo, P. Kask, and L. Brand. 2003. Confocal fluorescence techniques in industrial application. SPIE:101–109.

40. Widengren, J., U. Mets, and R. Rigler. 1995. Fluorescence correlation spectroscopy of triplet states in solution: a theoretical and experimental study. *The Journal of Physical Chemistry*. 99:13368–13379.

41. Müller, C. B., A. Loman, V. Pacheco, F. Koberling, D. Willbold, W. Richtering, and J. Enderlein. 2008. Precise measurement of diffusion by multi-color dual-focus fluorescence correlation spectroscopy. *EPL (Europhysics Letters)*. 83:46001.

42. Benda, A., M. Bene, V. Mareczek, A. Lhotsk, W. T. Hermens, and M. Hof. 2003. How to determine diffusion coefficients in planar phospholipid systems by confocal fluorescence correlation spectroscopy. *Langmuir*. 19 (10):4120–4126.

43. Schaffer, J., A. Volkmer, C. Eggeling, V. Subramaniam, G. Striker, and C. A. M. Seidel. 1999. Identification of single molecules in aqueous solution by time-resolved fluorescence anisotropy. *The Journal of Physical Chemistry A*. 103:331–336.

44. Saffman, P. G., and M. Delbrück. 1975. Brownian motion in biological membranes. *Proc Natl Acad Sci U S A*. 72:3111–3113.

45. Petrov, E. P., and P. Schwille. 2008. Translational diffusion in lipid membranes beyond the Saffman-Delbrück approximation. *Biophys J*. 94:L41–L43.

46. Rogers, S. S., T. A. Waigh, X. Zhao, and J. R. Lu. 2007. Precise particle tracking against a complicated background: polynomial fitting with gaussian weight. *Phys Biol*. 4:220–227.

47. Veatch, W. R., R. Mathies, M. Eisenberg, and L. Stryer. 1975. Simultaneous fluorescence and conductance studies of planar bilayer membranes containing a highly active and fluorescent analog of gramicidin A. *J Mol Biol*. 99:75–92.

48. Mueller, P., D. O. Rudin, H. T. Tien, and W. C. Wescott. 1962. Reconstitution of cell membrane structure in vitro and its transformation into an excitable system. *Nature*. 194:979–980.

49. Bacia, K., D. Scherfeld, N. Kahya, and P. Schwille. 2004. Fluorescence correlation spectroscopy relates rafts in model and native membranes. *Biophys J*. 87:1034–1043.

50. Korlach, J., P. Schwille, W. W. Webb, and G. W. Feigenson. 1999. Characterization of lipid bilayer phases by confocal microscopy and fluorescence correlation spectroscopy. *Proc Natl Acad Sci U S A*. 96:8461–8466.

51. Baumgart, T., G. Hunt, E. R. Farkas, W. W. Webb, and G. W. Feigenson. 2007. Fluorescence probe partitioning between Lo/Ld phases in lipid membranes. *Biochim Biophys Acta*. 1768:2182–2194.

52. Shaw, J. E., R. F. Epand, R. M. Epand, Z. Li, R. Bittman, and C. M. Yip. 2006. Correlated fluorescence-atomic force microscopy of membrane domains: structure of fluorescence probes determines lipid localization. *Biophys J*. 90:2170–2178.

53. Harms, Sonnleitner, Schutz, Gruber, and Schmidt. 1999. Single-molecule anisotropy imaging. *Biophys J*. 77:2864–2870.

54. Lakowicz, J. 2006. Principles of Fluorescence Spectroscopy. Springer, Singapore.

55. Humpolickova, J., E. Gielen, A. Benda, V. Fagulova, J. Vercammen, M. Vandeven, M. Hof, M. Ameloot, and Y. Engelborghs. 2006. Probing diffusion laws within cellular membranes by Z-scan fluorescence correlation spectroscopy. *Biophys J*. 91:L23–L25.

56. Gudmand, M., M. Fidorra, T. Bjørnholm, and T. Heimburg. 2009. Diffusion and partitioning of fluorescent lipid probes in phospholipid monolayers. *Biophys J*. 96:4598–4609.

57. Gambin, Y., R. Lopez-Esparza, M. Reffay, E. Sierecki, N. S. Gov, M. Genest, R. S. Hodges, and W. Urbach. 2006. Lateral mobility of proteins in liquid membranes revisited. *Proc Natl Acad Sci U S A*. 103:2098–2102.

58. Uhrikova, D., N. Kucerka, A. Islamov, A. Kuklin, V. Gordeliy, and P. Balgavy. 2003. Small-angle neutron scattering study of the lipid bilayer thickness in unilamellar dioleoylphosphatidylcholine vesicles prepared by the cholate dilution method: n-decane effect. *Biochim Biophys Acta*. 1611:31–34.

59. Peters, R., and R. J. Cherry. 1982. Lateral and rotational diffusion of bacteriorhodopsin in lipid bilayers: experimental test of the Saffman-Delbrück equations. *Proc Natl Acad Sci U S A*. 79:4317–4321.

60. Antonov, V. F., V. V. Petrov, A. A. Molnar, D. A. Predvoditelev, and A. S. Ivanov. 1980. The appearance of single-ion channels in unmodified lipid bilayer membranes at the phase transition temperature. *Nature*. 283:585–586.

61. Wunderlich, B., C. Leirer, A.-L. Idzko, U. F. Keyser, A. Wixforth, V. M. Myles, T. Heimburg, and M. F. Schneider. 2009. Phase-state dependent current fluctuations in pure lipid membranes. *Biophys J*. 96:4592–4597.

62. Blicher, A., K. Wodzinska, M. Fidorra, M. Winterhalter, and T. Heimburg. 2009. The temperature dependence of lipid membrane permeability, its quantized nature, and the influence of anesthetics. *Biophys J*. 96:4581–4591.

63. Papahadjopoulos, D., K. Jacobson, S. Nir, and T. Isac. 1973. Phase transitions in phospholipid vesicles. Fluorescence polarization and permeability measurements concerning the effect of temperature and cholesterol. *Biochim Biophys Acta*. 311:330–348.

64. Lundbaek, J. A., S. A. Collingwood, H. I. Ingolfsson, R. Kapoor, and O. S. Andersen. 2010. Lipid bilayer regulation of membrane protein function: gramicidin channels as molecular force probes. *J R Soc Interface*. 7:373–395.

65. Allen, T. W., O. S. Andersen, and B. Roux. 2003. Structure of gramicidin A in a lipid bilayer environment determined using molecular dynamics simulations and solid-state NMR data. *J Am Chem Soc*. 125:9868–9877.

66. Ketchem, R., B. Roux, and T. Cross. 1997. High-resolution polypeptide structure in a lamellar phase lipid environment from solid state NMR derived orientational constraints. *Structure*. 5:1655–1669.

67. Sandblom, J., J. Galvanovskis, and B. Jilderos. 2001. Voltage-dependent formation of gramicidin channels in lipid bilayers. *Biophys J*. 81:827–837.

68. White, and Thompson. 1973. Capacitance, area, and thickness variation in thin lipid films. *Biochim Biophys Acta*. 323(1):7–22.

69. White, S. H. 1976. The lipid bilayer as a "solvent" for small hydrophobic molecules. *Nature*. 262:421–422.

70. Hell, S. W., and J. Wichmann. 1994. Breaking the diffraction resolution limit by stimulated emission: stimulated-emission-depletion fluorescence microscopy. *Opt Lett*. 19:780–782.

71. Ringemann, C., B. Harke, C. v. Middendorff, R. Medda, A. Honigmann, R. Wagner, M. Leutenegger, A. Schonle, S. W. Hell, and C. Eggeling. 2009. Exploring single-molecule dynamics with fluorescence nanoscopy. *New Journal of Physics*. 11:103054.

72. Boheim, G., W. Hanke, and H. Eibl. 1980. Lipid phase transition in planar bilayer membrane and its effect on carrier- and pore-mediated ion transport. *Proc Natl Acad Sci U S A*. 77:3403–3407.

73. Martens, J. R., K. O'Connell, and M. Tamkun. 2004. Targeting of ion channels to membrane microdomains: localization of KV channels to lipid rafts. *Trends Pharmacol Sci*. 25:16–21.

3. Membrane binding and channel formation of Colicin A studied with an electro-optical approach

3.1 Abstract

Colicin A (ColA) is a water soluble protein that is toxic for sensitive *E. coli* cells. Its toxic action is to short-circuit the electro-chemical potential of the plasma membrane by forming a voltage dependent ion channel. An important feature of ColA is the transition from a water soluble conformation to an integral membrane protein. This transition seems to be a general step in the formation of the active ion-conduction conformation of pore-forming toxins. Here the membrane binding and subsequent channel opening of ColA is studied using horizontal artificial bilayers and liposomes. It was found that acidic pH dramatically enhances membrane binding, while at neutral pH binding is negligible. An applied membrane potential does not affect the binding to artificial bilayers. However, a trans-membrane potential of > 60 mV is required to activate the open channel confirmation of ColA. Using the environment sensitive fluorescent probe NBD the membrane immersion of multiple helices of ColA was determined. All tested sites resided at the membrane water interface which is compatible with the penknife model of the membrane bound conformation of ColA. The ion permeability of the open state, probed by electrophysiology, was low with a single channel conductance of $\Lambda \approx 20$ pS. The bulky dye calcein was released from liposomes incubated with ColA. No evidence for oligomerization during channel formation was found, when FRET pairs of ColA monomers were studied with fluorescence lifetime and fluorescence cross correlation analysis.

3.2 Introduction

Pore-forming toxins are secreted by many pathological bacteria as a weapon against host cells or against competing bacteria [1, 2]. The mechanism of action generally involves the secretion of the monomeric toxin in a water soluble conformation. Upon contact of the toxin with the target cell-membrane a conformational change is triggered which induces membrane insertion and in most cases an oligomerization process. Examples of pore-forming toxins are colicins, diphtheria toxin, tetanus toxin, equinatoxin and aerolysin. Colicins are a plasmid-encoded class of bacteriocines which are secreted by various *E. coli* strains under environmental stress conditions and are directed against other *E .coli* strains [1, 3]. Over 30 different types of colicins have been identified. The toxic action of colicins is either nuclease activity in the cytosol or ion-channel formation in the plasma membrane of the target *E. coli* cells. The crystal structures of the water-soluble conformation revealed that all pore-forming colicins are arranged in three domains [4, 5] (Fig. 3.1). The domains were named according to their specific function: the receptor binding domain, the translocation domain and the channel-forming domain. The first two domains are responsible for the

binding to and the translocation of the protein through the outer membrane into the periplasm of the target *E. coli* cells [3, 6]. At the plasma membrane the pore-forming domain inserts into the bilayer and forms a voltage-dependent ion channel which short circuits the vital electro-chemical gradient of the target cell [7, 8]. The crystal structure of the pore-forming domain of ColA obtained in an aqueous environment, shows a ten-helix bundle containing a central hydrophobic helical hairpin [4] (Fig. 3.1). The structural similarities between colicins and also other pore forming toxins suggest that a conserved mechanism of pore-formation is at work. Although the procedure of pore formation is far from being understood some steps of the mechanism have been established.

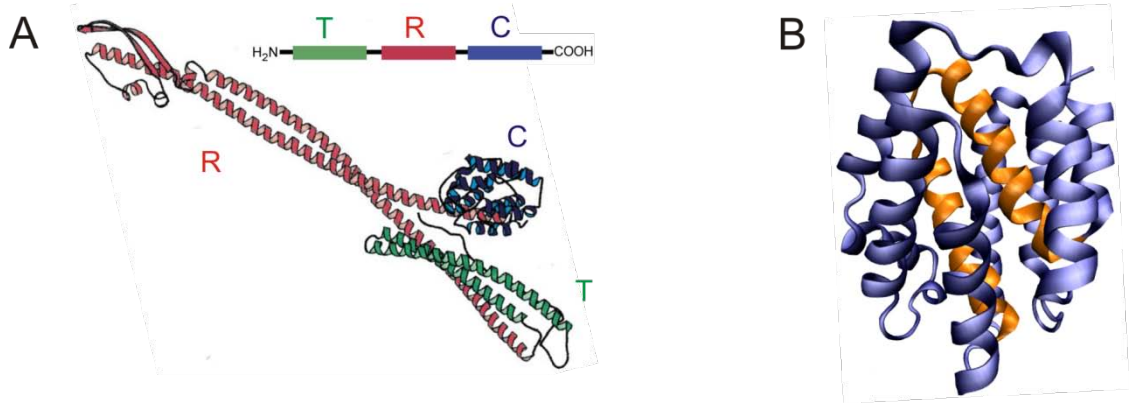

FIGURE 3.1 Ribbon representations of (A) Colicin Ia [5, 9], and (B) the pore-forming domain of Colicin A [4], derived from X-ray diffraction analysis of 3-D crystals. (A) The complete structure of Colicin is arranged in three domains: the translocation domain (green) the receptor binding domain (red) and the channel-forming domain (blue). (B) The water-soluble conformation of the pore-forming domain of ColA is a ten helix bundle with central hydrophobic hairpin (orange).

The binding of the pore-forming domain to the bilayer is promoted by electro static interactions between negatively charged lipids and positively charged amino acids of the protein [10, 11]. Additionally, acidic pH has been found to enhance membrane binding and insertion in vitro [12, 13]. As an intermediate step during acidic membrane binding ColA was found to form a molten globule state *in vitro* [14-16]. For the membrane bound conformation of ColA two models have been proposed. The umbrella model suggests that during binding the hydrophobic hairpin of the pore-forming domain is inserted into the bilayer core, while the aliphatic helices lie at the membrane water interface [17, 18]. According to the penknife model all ten helices of ColA remain at the bilayer water interface with helices one and two hinged away from the rest of the protein [19, 20].

For the transition from the membrane bound state to the ion conduction conformation a trans-membrane potential of more than + 60 mV on the ColA side is required [7, 8]. Until now, the conformation of the ion conduction channel has not been resolved. However, it has been shown by electrophysiological experiments that a substantial amount (helices 2-5) of the 10 helices of the pore-forming domain is translocated to the *Trans* side of the bilayer

upon opening of the channel [21, 22]. Some contradicting properties of the open channel have greatly complicated the establishment of an appropriate structural model: The ion conductivity of the open conformation is very low, but large ions and even proteins can be translocated by ColA [23, 24]. Additionally, the ColA channel seems to be not very selective for mono-valent anions or cations, but has remarkably high proton selectivity [25]. Both properties, conductivity and selectivity, indicate on the one hand a very narrow pore (low conductance and high proton selectivity) one the other hand the low selectivity for other ions and the translocation of large ions and proteins argues in favor of a channel with a diameter of at least 1 nm. Actually, it has been shown that even whole proteins with a size of 2.5 nm can be translocated through a bilayer by ColA [22]. To make the picture even more complicated most studies point to a monomeric pore, but from structural considerations the amount of protein in monomeric channel seems to be too low to constitute a large translocation pore.

In this study an electro-optical approach is used to characterize the membrane binding of ColA and the subsequent channel opening upon application of a trans-membrane potential. The electro-optical setup is comprised of a horizontal lipid bilayer chip, which is a modified version of the planar lipid bilayer technique, and a confocal laser scanning microscope equipped with single photon detection unit. This setup allows for single channel conductance- (voltage clamp), diffusion- (FCS), environment- (fluorescence lifetime) and oligomerization- (FRET) measurements, simultaneously. Accessing these parameters simultaneously is promising in the context of ColA, because to study the open channel conformation a controllable and stable membrane potential is required which was lacking in previous studies on colicins.

3.3 Material and Methods

3.3.1 Chemicals

E. coli polar lipid extract was purchased from Avanti Polar Lipids (Alabaster,AL). N-decane and Tris(2-carboxyethyl)phosphine hydrochloride (TCEP) were purchased from Sigma Aldrich (Munich, Germany). N,N-dimethyl-N-(iodoacetyl)-N-(7-nitrobenz-2-oxa-1,3-diazol-4-yl) ethylenediame (NBD amide) was purchased from Molecular Probes (Eugene, OR). The organic dyes Atto488-maleimide and Atto647N-maleimide were purchased from Atto-Tec, Siegen, Germany. Lipids were stored in methanol/chloroform (1:1) under nitrogen at -20°C. For bilayer preparation lipids were mixed accordingly, dried under vacuum and dissolved in n-decane to a final concentration of 50 mg/ml.

3.3.2 Mutagenesis, preparation and purification of ColA

ColA mutagenesis, expression and purification were conducted in the group of Prof. Steinhoff (University Osnabrueck, Department of Physics) by Dr. Pulagam V. L. Padmavathi. The plasmid pLR1, which encodes the wild-type ColA, was used as template to replace different residues within the ColA sequence with a cystein. To introduce Cys codons into *E. coli* ColA open reading frame site directed mutagenesis was performed using the Quick-Change method from Stratagene (La Jolla, CA). Plasmid DNA was purified using the HiSpeed Plasmid Purification kit from Qiagen (Hilden, Germany). *E.coli* K-12 C600 mutants were grown in LB medium (Luria-Bertani medium: 10 g /l peptone, 5 g/l yeast extract, 10 g/l NaCl) until an OD600 of 0.7, and expression was induced by mitomycin C (300 ng/l). After 4 hours of expression at 37 °C, cells were harvested by centrifugation, the supernatant was collected and the proteins were precipitated with ammonium sulphate (243 g/l) at 4 °C. After 1 hour, the suspension was centrifuged and the pellet was dissolved in 10 mM sodium phosphate buffer (pH 6.8) containing 1 mM EDTA. The solution was then dialyzed overnight against 10 l of 10 mM sodium phosphate buffer, pH 6.8 (+1 mM EDTA), to remove the remaining ammonium sulphate and centrifuged at 15 000 rpm for 45 minutes.

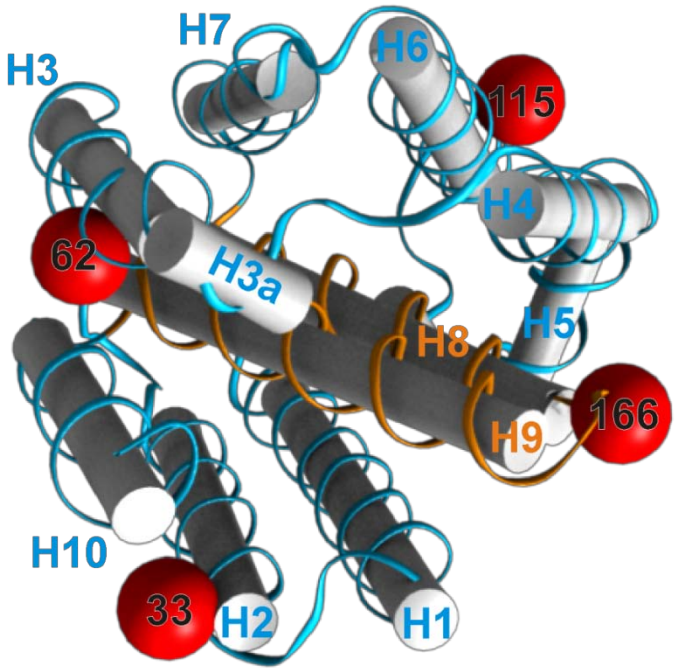

FIGURE 3.2 Labeling sites of ColA: Single cystein mutations were introduced at positions 33 (helix 2), 62 (helix 3), 115 (helix 6) and 166 (loop between helix 8 and 9). The fluorescent dye NBD (400 Da) was covalently bound to the cystein residues.

The supernatant was applied to a Hitrap SP HP (GE Healthcare, Sweden) column using an FPLC system (Pharmacia). The protein that bound to the column was eluted by a 0–400 mM NaCl gradient. The purity of collected fractions was assessed to be > 90% based on SDS

PAGE electrophoresis. The biological activity of the ColA mutants was assayed by their effect on wild type *E. coli* cells. All double mutants exhibited full biological activity, i.e. being lethal for the wild type cells.

3.3.3 Fluorescence labeling of single cysteine ColA mutants

ColA-NBD was synthesized by allowing reduced, single cysteine ColA (5mg/ml) to react with IANBD amide (20-fold molar excess over ColA) in aqueous solution adjusted to pH 7.3 for 12h (see protocol for thiol-reactive probes at molecular probes). ColA-488 and ColA-647N were produced using the reactive maleimide group of the dyes Atto488 and Atto647N. A 20-fold molar excess of dye was incubated with reduced (2mM TCEP) ColA in phosphate buffer adjusted to pH 6.8 for 12h. The products ColA-X were purified from non-reacted dyes by size exclusion chromatography using NAP-5 columns (GE-Healthcare). The degree of labeling (DOL) was determined by absorption spectroscopy. The protein concentration was estimated from A_{280} (corrected by the dye absorption at 280 nm) with a calculated ε of XXX (Expasy ProtParam). The dye concentration was estimated using the absorption at the respective dye absorption maximum. The resulted DOLs varied between 0.6 and 0.9.

3.3.4 Horizontal lipid bilayers and electrophysiology

The horizontal bilayer chip is made of Polytetrafluoroethylene (PTFE) with drilled holes for *Cis* and *Trans* compartments and electrode access. A 25 µm thin PTFE sheet with a round ≈ 100 µm small aperture is sandwiched between a coverslide and the chamber body using double side adhesive film. The lower adhesive film contains a laser edged channel structure to connect the *Trans* compartments. The exclusive connection between the *Cis* and *Trans* compartment is the aperture in the PTFE sheet. After assembly of the chamber and filling with 1 M KCl, 10 mM Mops/Tris pH 7 or pH 4 buffer the bilayer was “painted” over the aperture using a 90° bended Hamilton syringe (Bonaduz, Switzerland). Bilayer formation was monitored optically and electrically. The distance between the coverslide and the planar bilayer is 100 µm which allows optical access by high numerical aperture water objectives required for fluorescence fluctuation analysis. For electrical measurements silver/silver chloride electrodes embedded in agarose were connected to the *Cis* and *Trans* compartments. Electrical recordings were made using a CV-5-1GU headstage connected to a GeneClamp 500B amplifier from Axon Instruments (Sunnyvale, CA). Data were digitalized with a Digidata 1322A and monitored with the software Clampex 9 (Axon Instruments). After each measurement session the coverslide with the adhesives was removed and the chamber body was cleaned in ethanol before re-usage.

3.3.5 Confocal microscopy setup

Confocal imaging and fluorescence fluctuation recordings were performed on a modified Insight Cell 3D microscope from Evotec technologies (Hamburg, Germany, now Perkin

Elmer), equipped with a 470 nm and a 635 nm pulsed diode laser (80 ps pulse width, PicoQuant, Berlin, Germany), a 40x water immersion objective (UApo340 40x, NA 1.15, Olympus, Tokyo, Japan) and avalanche photo diode detectors (SPCM-AQR-13-FC, Perkin Elmer Optoelectronics, Fremont, CA). The laser powers were adjusted to 5 - 20 µW. The emission light was split according to the wavelength and detected on two channels. The signal from each detector was split up on the correlator and the imaging unit of the Insight and on a PHR 800 router in combination with a PicoHarp 300 counting module (PicoQuant). The repetition rate of the laser was set to 40 MHz and the resolution of the PicoHarp 300 to 16 ps. Fluorescence images were obtained by scanning the sample by a rotating beam-scanner along the lateral *XY* and by an objective lens positioning system along the axial *Z*-direction.

3.3.6 Fluorescence correlation spectroscopy (FCS)

The translational diffusion time τ_D was evaluated using auto-correlation the respective photon traces. The correlation curves were fitted by a three (solution) or two dimensional (membrane) diffusion model including a triplet term [40].

$$G(\tau) = \frac{1}{N}\frac{1}{\left(1 + {}^{\tau}/_{\tau_D}\right)}\left(1 + \frac{T}{1-T}e^{\frac{-t}{\tau_T}}\right) \tag{3.1}$$

N is the mean number of particles in the confocal volume. *T* is the fraction of molecules which are in the triplet state and τ_T the triplet correlation time. $\tau_D = w_0^2 / (4D_{lat})$ is the average molecular diffusion time through the Gaussian-assumed focal intensity profile and characterized by the lateral diffusion coefficients D_{lat} and the focal radius w_0 (defined as the radius at which the Gaussian-assumed focal intensity profile has dropped to $1/e^2$ of its maximum value). w_0 was estimated from FCS measurements on the dye Atto655-maleimid in aqueous buffer with the known diffusion coefficient of D_{lat} = 407 µm^2/s [41].

3.3.7 Fluorescence cross-correlation spectroscopy (FCCS)

FCCS is used among other things to study binding reactions of molecules which are labeled with appropriate fluorescent dyes. The main read out parameter of FCCS is the concentration of the bound complex in comparison to the free binding partners. Here, we use a two color setup with overlapping foci of 470 nm and 635 nm. The fluorescence signals from the two potential binding partners (ColA-488 and ColA-647) were recorded independently on two detectors. Each photon trace was auto-correlated and additionally the two detectors were cross-correlated. The three correlation-curves were fitted according to:

$$G_{red}(\tau) = \frac{c_{red} \cdot Diff_{red} + c_{red-green} \cdot Diff_{red-green}}{V \cdot (c_{red} + c_{red-green})^2} \tag{3.2}$$

$$G_{green}(\tau) = \frac{c_{green} \cdot Diff_{green} + c_{red-green} \cdot Diff_{red-green}}{V \cdot (c_{green} + c_{red-green})^2} \quad (3.3)$$

$$K(\tau) = \frac{c_{red-green} \cdot Diff_{red-green}}{V \cdot (c_{red} + c_{red-green}) \cdot (c_{green} + c_{red-green})} \quad (3.4)$$

$$Diff = \frac{1}{\left(1 + {}^{\tau}/_{\tau_D}\right)} \quad and \;\; V = (\pi/2)^{2/3} \cdot {\omega_0}^2 \cdot z_0 \quad (3.5, 3.6)$$

$$N_{coinc} = \frac{(K(0) - 1)}{(G_{red}(0) - 1)(G_{green}(0) - 1)} = N_{red} \cdot N_{green} \cdot (K(0) - 1) \quad (3.7)$$

The auto-correlation and cross-correlation function of the red and green channel are G_{red} , G_{green} and K with c as the average concentration, which is related to the average number of molecules in the confocal volume by $N = c \cdot V$, $Diff$ is the diffusion term of the 2D diffusion model shown in equation 1 and V is volume of the confocal spot.

3.3.8 Confocal fluorescence lifetime measurements

The confocal fluorescence lifetime was determined from the same photon traces used for FCS evaluation. The repetition rate of the pulsed lasers excitation was set to 40 MHz. Using the PicoHarp300 equipment and the software SymphoTime (PicoQuant) fluorescence decay histograms were recorded with a bin width of 16 ps. The instrument response function (IRF) of the respective laser / detector combination was recorded using reflected laser light at the cover slide interface. The fluorescence lifetime was determined by fitting the fluorescence decay histograms to a reconvolution model including the IRF using the software SymphoTime.

3.3.9 Steady state fluorescence measurements

Steady state fluorescence measurements were performed with a Jasco FP 6500 fluorimeter (Jasco, Gross-Umstadt, Germany). The excitation and emission slits were set to a width of 5 nm. NBD was excited at 470 nm. Calcein was excited at 490 nm. Atto488 and Atto637N were excited at 480 nm and 620 nm, respectively. Samples were continuously stirred in a Hellma quartz-suprasil cell (QS 10 mm) (Hellma GmbH & Co. Kg, Müllheim, Germany).

3.3.10 Calcein efflux from liposomes incubated with ColA

A 100 mM calcein solution was prepared either in 100 mM KCl, 100mM MOPS/TRIS pH 7 or in 100 mM KCl, 100mM acetat pH 4. 15 mg of *e.coli* polar lipids extract was prepared by evaporating the solvent chloroform under vacuum. The dried lipids were dissolved in 1 ml of the 100 mM calcein solution and were then sonicated for 5 min on ice. The resulting

LUVs had a mean diameter of $Ø \approx 200$ nm which was determined with dynamic light scattering (data not shown). The free calcein was removed from the liposomes with the trapped calcein by size exclusion chromatography using NAP5 columns (GE-Healthcare).
The actual calcein efflux measurements were conducted according to table 1. The fluorescence emission of calcein was monitored at 515 nm to detect calcein release from liposomes after ColA addition. As long as the calcein concentration inside the liposomes is ≈ 100 mM the fluorescence is the largely quenched. When calcein is released from the liposomes the fluorescence will increase, due to the now un-quenched emission of calcein.

3.4 Results

3.4.1 Membrane binding of ColA is pH dependent

After the translocation of ColA across the outer membrane of the *E. coli* target cell, the pore-forming domain has to be inserted into the plasma membrane. The first step in pore-formation is binding of ColA to the plasma membrane. The *in vitro* binding of ColA to membranes made of natural *E. coli* lipids was studied using horizontal lipid bilayers as well as large uni-lammellar vesicles. ColA was labeled either with the fluorescent dye NBD to probe a change in hydrophobicity upon membrane binding or with Atto488 to measure the diffusion properties in aqueous solution and at the bilayer.

In Fig. 3.3 a typical horizontal bilayer binding experiment is depicted. After preparation of the HLB from 50 mg/ml *E. coli* lipids dissolved in n-decane, the membrane was imaged by scanning the *X*-*Z* plane. Since no fluorescent label was present, the bilayer itself is not visible on the image (Fig. 3.3*A*). Only the auto-fluorescence of the PTFE foil and the lipid torus are observable. After a stable bilayer was formed, ColA-488 was added to the *Trans* compartment of the bilayer chip in a concentration of ≈ 10 nM. On the scanned image the fluorescence of ColA-488 is clearly visible on the *Trans* side of the bilayer. The bilayer is indirectly visible, since it acts as a barrier to the *Cis* side for ColA-488.The system was then allowed to equilibrate for 5 minutes. Afterwards, the bilayer was scanned again to detect binding of ColA-488 at the bilayer. The binding to bilayer was studied at pH 7 (Fig. 3.3*A*) and pH 4 (Fig. 3.3*B*), respectively. The ionic strength was chosen to be high (1 M KCl), mainly because the electrical signal of single ColA-488 channels would be too small to be resolved by the setup under physiological salt conditions. Additionally, the high ionic strength also prevents unspecific electro-static binding of ColA-488 to the bilayer. The results show, that at neutral pH no significant accumulation of ColA-488 at the bilayer was detectably (Fig. 3.3*A*). The intensity directly at the membrane was the same as in the *Trans* solution after 5 min incubation time. In contrast to this, under acidic pH conditions binding to the bilayer was observable directly after addition of ColA-488 (Fig. 3.3*B*). After 5 min incubation time the concentration of ColA-488 in the *Trans* compartment was decreased due to significant accumulation of ColA-488 at the bilayer. Additionally, the bright spots in the *Trans* solution indicate that the protein tended to aggregate at low pH (Fig. 3.3*B*).

It is known that ColA relies on a trans-membrane potential to form an active ion-channel in artificial bilayers. Therefore, it was tested whether an applied membrane potential already affects membrane binding of ColA. When a holding potential of + 100 mV (positive on the ColA side of the bilayer) was applied during incubation of ColA-488 no significant increase of binding was detectable compared to a membrane without a potential (data not shown). It can be concluded that an applied membrane potential does not affect membrane binding of ColA.

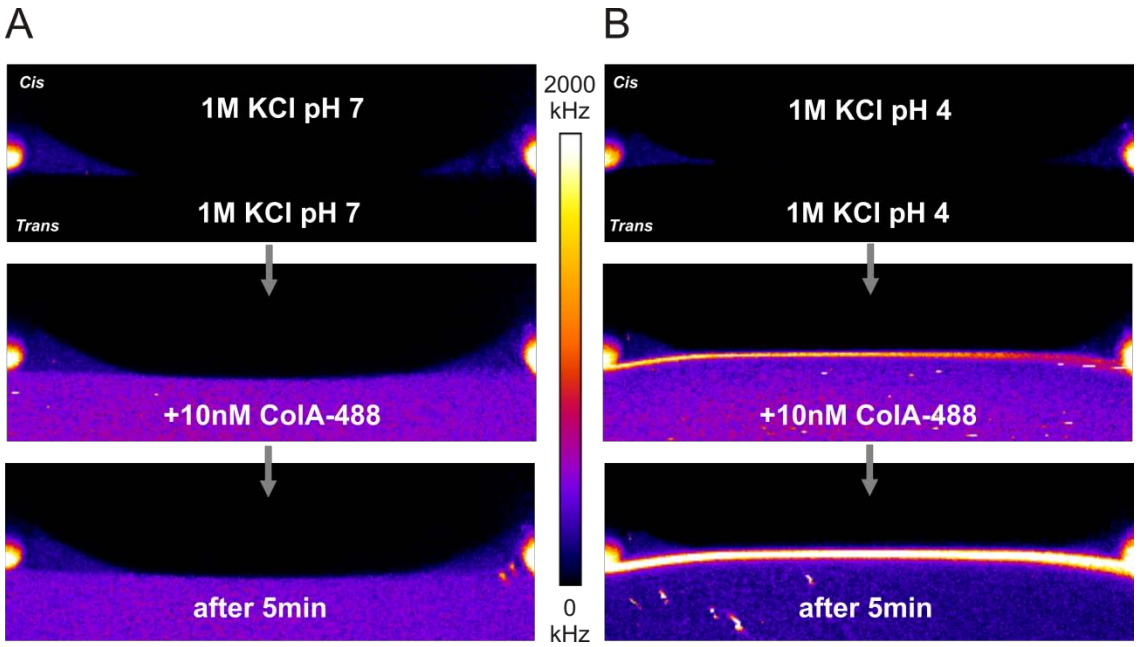

FIGURE 3.3 pH dependent binding of ColA to lipid membranes. (A) Horizontal lipid bilayers were prepared in 1M KCl pH 7 buffer. The actual bilayer appeared black in the *X-Z* image because no fluorescent label was present in the membrane. After addition of 10 nM fluorescently labeled ColA-488 to the *Trans* compartment, the lipid bilayer was indirectly visibly as the barrier between *Cis* and *Trans*. After 5 minutes incubation, membrane binding of ColA-488 was negligible at pH 7. (B) When the pH of the buffer was lowered to 4 the same amount of ColA-488 added to the *Trans* side resulted in a distinct membrane staining. After 5 minutes incubation the concentration of ColA488 was drastically increased at the bilayer, showing an efficient membrane binding of ColA at pH 4.

The same pH dependent membrane binding of ColA seen on horizontal bilayers was observed when ColA-NBD was incubated with LUVs prepared from *E. coli* lipids. The NBD emission intensity as well as the emission wavelength are strongly dependent on the dielectric constant of local environment of the probe [61]. The more hydrophobic the environment is the higher is the emission intensity and the maximum emission wavelength is blue-shifted. This property of NBD was used to probe the change in hydrophobicity upon membrane binding of ColA-NBD. Freshly sonicated vesicles (Ø ≈ 200 nm) were incubated with ColA-NBD in a 500 µl cuvette in 0.2 M NaCl pH 7. The fluorescence emission of ColA-NBD was observed at 514nm after excitation at 480 nm. In Fig. 3.4 a typical time course of the fluorescence intensity of ColA-NBD upon incubation with liposomes is depicted. After addition of ColA-NBD to the liposome solution at pH 7 the fluorescence raised to a stable low intensity plateau, indicating that NBD was mostly exposed to an aqueous environment. With the addition of acetat the proton concentration of the buffer was raised to pH 4.

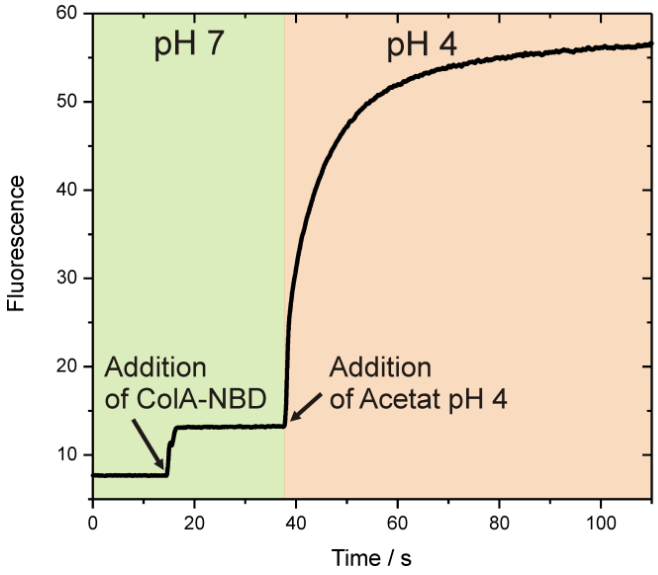

FIGURE 3.4 The environment sensitive fluorescent probe NBD was used to study pH dependent binding of ColA-NBD to liposomes. 0.1mg/ml liposomes were incubated in 200 mM NaCl pH 7 buffer. After the addition of 50 nM ColA-NBD, fluorescence at 518 nm increased to a low level corresponding to ColA-NBD exposed to water. When the bulk pH in the cuvette was lowered to 4 by addition of acetat, NBD fluorescence increased 5 fold which indicates that ColA-NBD subsequently bound to the surface of the liposomes.

Immediately the fluorescence intensity of ColA-NBD increased, due to a more hydrophobic environment of NBD, which is an indication for binding of ColA-NBD to the liposomes. ColA-NBD emission in the absence of liposome stayed constant after acidification of the buffer (data not shown). The binding curve of ColA-NBD to *E. coli* liposomes resembled a simple saturation curve with a half saturation time of ≈ 5 s under the applied conditions. The results confirm that membrane binding of ColA is strongly dependent on the proton concentration of the membrane surrounding aqueous solution.

3.4.2 Electrophysiological properties of single ColA channels

To characterize the electrophysiological single channel properties of ColA, the protein was added to the *Cis* side of a freshly prepared bilayer made of *E. coli* lipids. The concentration of ColA which was sufficient to result in single channel activities was dependent on the proton concentration of the applied buffer, which follows from the increased binding at pH 4 as seen in Fig. 3.3 and Fig. 3.4. For the analysis of the single channel conductance of ColA a trans-membrane potential of 80 mV to 100 mV was applied to induce the open channel conformation. In Fig. 3.5*A* a typical current trace of a single channel at pH 7 is depicted. The conformational changes between the open and closed channel are visible as current steps (gating events) in the current trace. The mean single channel conductance was calculated from over 500 individual gating events according to Ohms law (Fig. 3.5*B*). The resulting conductance histograms show peak values of Λ = 18 pS at pH 7 and Λ = 8 pS at pH 4, respectively. Interestingly, the mean single channel conductance at pH 4 was

significantly lower (2 fold) compared to pH 7, which could be an indication for a reduced pore diameter and / or a change in the electrical charge in the lumen of the pore due to protonation of amino acid residues at pH 4.

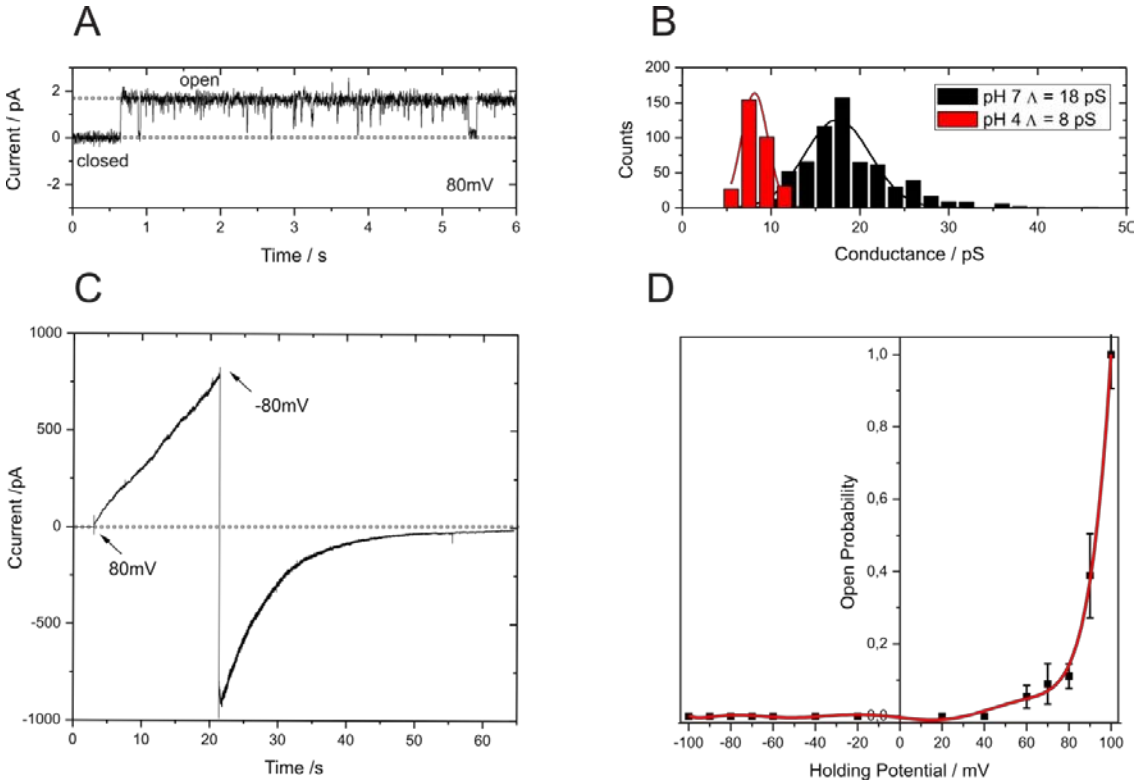

FIGURE 3.5 Electrophysiological characteristics of ColA in lipid bilayers. (A) Single channel gating of ColA at 80 mV in 1 M KCl pH 7 indicated one distinct open state. (B) The conductance histogram derived from more than 500 gating events shows a narrow distribution with a mean conductance of 18 pS at pH 7 and 8 pS at pH 4. (D) A positive holding potential on the side of ColA addition was essential for channel opening. The current increased linearly at +80 mV due to subsequent channel openings. After the direction of the electrical field was reversed to - 80mV, ColA channels closed again with a fast and a slow time constant. (B) Open probability of ColA at different holding potentials. The open channel confirmation was populated at potentials > 60 mV. Efficient opening was found at HP > 90 mV

The dependence of channel formation on the electrical field applied on the bilayer was tested using multiple channel experiments. ColA was added to the *Cis* side of bilayer in an increased concentration compared to single molecule experiments to allow multiple channel incorporations. A trans-membrane potential of 80 mV was applied for 15 s, which resulted in a linear increase of current due to steady opening of ColA channels (Fig. 3.5*C*). When the direction of the applied potential was abruptly inverted, the number of open channels decreased with two velocity constants to zero. The majority of open channels closed as quickly as the channels opened at + 80mV. A second less abundant fraction closed with significantly slower time constant. The results show that ColA channel opening is strictly dependent on the right orientation of a trans-membrane potential. Channel opening is

reversible by inverting the membrane potential. To open ColA channels the potential has to oriented such that is positive on the side of ColA binding, as it is the case *in vivo*, where ColA binds from the periplasmic side to the plasma membrane in *E. coli*.

The strength of membrane potential which is necessary to induce the open channel conformation was determined by open probability experiments. After addition of ColA to the bilayer a certain membrane potential was applied for two minutes. For every potential the mean ColA current was calculated and the resulting U/I plot was normalized (Fig. 3.5*D*). It is obvious that channel opening requires at least a potential of +60 mV. However, efficient opening of ColA channels occurs at potentials of > 90 mV in planar lipid bilayers. For comparison the membrane potential of the *E. coli* plasma membrane ranges between +85 mV at pH 5 and +145 mV at pH 8 (positive on the periplasmic side of the membrane) [29]. Hence, the membrane potential values for efficient channel incorporation (+ 90 mV) determined *in vitro* would be sufficient for channel incorporation in the *E. coli* plasma membrane (≈ + 120 mV) *in vivo*, as well.

3.4.3 Oligomerization measurements of ColA

To study oligomerization a FRET pair of ColA monomers was prepared by labeling single cystein mutants with a donor dye (ColA-488) and an acceptor dye (ColA-647).

As a first approach we applied steady state FRET measurements using soluble and liposome reconstituted mixtures of ColA-488 and ColA-647.

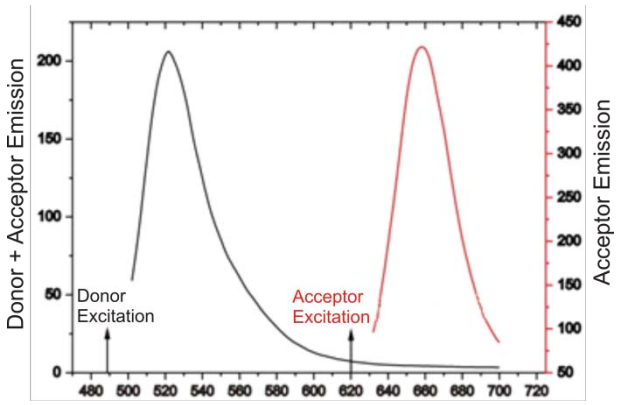

FIGURE 3.6 Steady state FRET measurements of the FRET-pair ColA-488 and ColA-647. 200nM donor and acceptor were incubated with ≈ 0.2 mg/ml LUVs in pH 4 buffer for 3 hours. To detect FRET the donor was excited at 488 nm and the donor as well as the acceptor emission was recorded. No acceptor fluorescence was observable when the donor was excited. However, direct excitation of the acceptor resulted in distinct donor emission. Thus no significant energy transfer between ColA-488 and ColA-647 was found under the applied conditions.

The Förster-distance of the applied FRET pair was 5 nm which should be sufficient to detect oligomerization regardless in which positions the monomers (Ø = 3.3nm) would be arranged. A 1:1 mixture of ColA-488 + ColA-647 was studied in a concentration range from

5 nM to 500 nM in aqueous solution as well as in the presence of liposomes under neutral and acidic pH conditions.

No significant FRET from ColA-488 to ColA-647 was detectable under any of the applied conditions. Typical emission spectra are depicted in Fig. 3.6. The excitation of the donor in the presence of the acceptor resulted in donor fluorescence exclusively. Only after direct excitation at 620 nm the acceptor fluorescence became visible. Overnight incubation of the FRET preparations and an increased acceptor concentration produced the same negative FRET results.

As a second approach confocal fluorescence lifetime measurements were applied with the same ColA FRET pairs described above, but this time using the horizontal lipid bilayer setup. The fluorescence lifetime of a donor dye is dependent on the energy transfer efficiency from the donor to the acceptor dye according to: $E_{FRET} = 1 - (\tau_{DA}/\tau_D)$. In practice the determination of the donor lifetime is the most reliable readout to detect FRET, because the fluorescence lifetime can be measured independently from concentration effects with high precision. After horizontal bilayer preparation a 1:1 nano-molar concentration of ColA-488 and Col-647 was added to the *Trans* compartment of the bilayer-chip (Fig. 3.7*A*). The laser focus was placed in the *Trans* solution and the donor lifetime was determined. ColA was then allowed to bind to the bilayer for five minutes. Finally, the excess protein was washed out by perfusion of the *Trans* compartment. The laser focus was placed directly on the bilayer containing the bound ColA and the donor lifetime was determined again (Fig. 3.7*A*). As a control the lifetime of donor was determined in absence of the acceptor under the same conditions. Besides the lifetime information also the FCS-data were evaluated to estimate the binding of ColA to the bilayer (Fig. 3.7*B*). The lateral diffusion time of the donor ColA-488 was 0.2 ms in the *Trans* solution. After accumulation of ColA-488 at the bilayer the diffusion time decreased significantly to 2.2 ms, which indicates stable binding of the toxin to the bilayer. For comparison, the lateral diffusion time of a fluorescently labeled lipid in the horizontal bilayer under the same conditions was determined to be ≈ 1 ms. The fluorescence lifetime of the donor ColA-488 in solution was 3.6 ns. The lifetime of ColA-488 did not change significantly after the protein was bound to the bilayer. Most importantly the lifetime of the donor did not change when the acceptor ColA-647 was present in a 1:1 molar ratio. Since no evidence for FRET under the applied conditions was found, it can be concluded that ColA did not oligomerize after binding to the bilayer. Application of a trans-membrane potential of 100 mV resulted in channel openings of ColA. However, the donor lifetime stayed constant, also under these conditions.

For the improbable case that no FRET occurred even though oligomerization took place, which could be due to unfavorable dipole orientations of the donor and acceptor, fluorescence cross correlation spectroscopy was applied to determine whether ColA-488 and ColA-647 diffused as a bound complex.

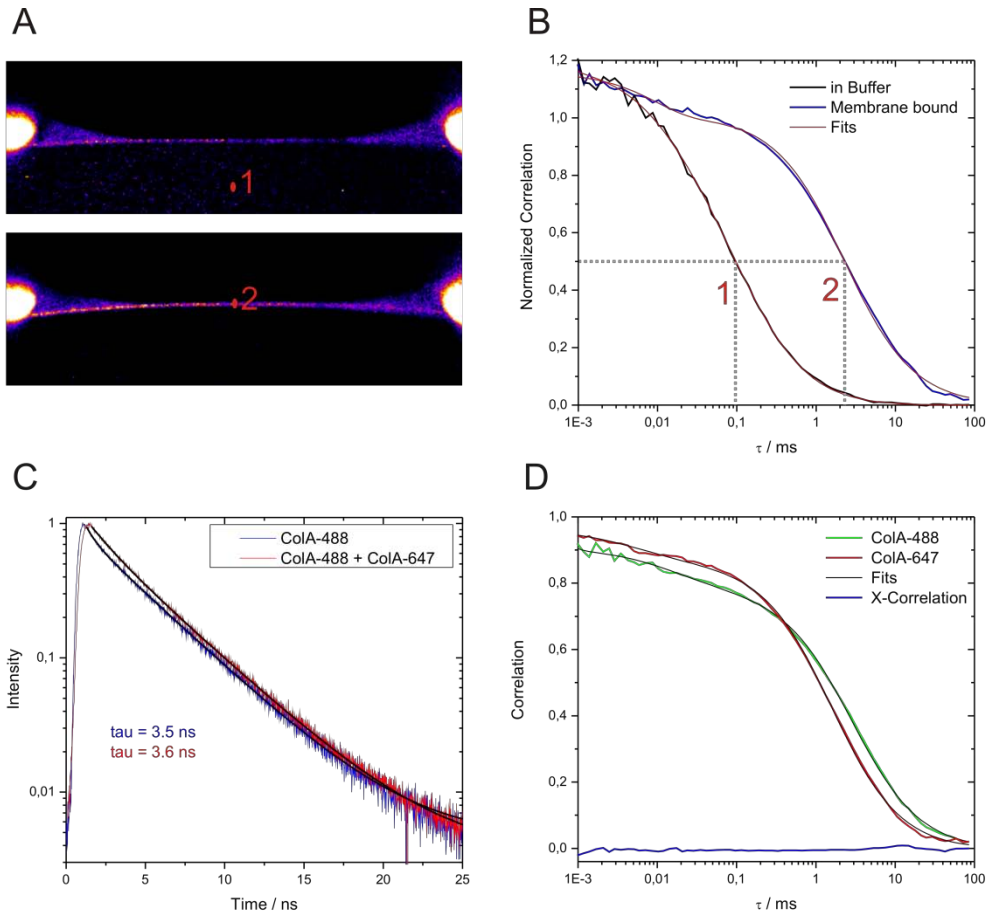

FIGURE 3.7 Oligomerization measurements of ColA in HLBs (A) ColA-488 was added to *Trans* in a concentration of < 1 nM (position 1) to ensure a low surface density in the bilayer (position 2) after perfusion of *Trans.* (B) FCS measurements at position 1 and 2 indicate a reduction of diffusive mobility of ColA-488 upon membrane binding from 0.1ms in solution to 2.5 ms at the bilayer. The reduced mobility indicates a constant binding of ColA-488 to lipid molecules of the bilayer. (C) The fluorescence lifetime of the donor (ColA-488) bound to the bilayer was 3.6ns. When the acceptor was present in a 1:1 molar ratio the lifetime of the donor did not change significantly. (D) Cross-correlation between the donor (green) and acceptor (red)signals showed no correlation amplitude (blue trace) which indicates that the donor and acceptor molecules diffused independently from each other.

The same conditions as described in Fig. 3.7*A* were used except that the ColA-488 and ColA-647 were excited simultaneously using overlapping confocal laser spots with 470 nm and 635 nm wavelength. The emitted photons were recorded independently on two detectors, and the resulting photon traces were cross-correlated to determine the amount of oligomerized ColA-488 and ColA-647. The results show that the diffusion times of ColA-488 and ColA-647 at the bilayer indicating constant binding of both binding partners (Fig. 3.7*D*). However, the cross-correlation amplitude was zero, which implies that no binding between ColA-488 and ColA-647 occurred under the applied conditions.

3.4.4 ColA induces calcein efflux from liposomes at acidic pH

A fluorescence assay based on self-quenching was used to probe the translocation of the bulky dye calcein through ColA pores formed in liposomes. Liposomes containing a self quenching concentration ≈ 100 mM of calcein were prepared by sonication and subsequent size exclusion purification. The proton concentration inside the liposomes was either adjusted to pH 7 or to pH 4. The calcein liposomes were added to an excess volume (1:200) of buffer adjusted to pH 7 or pH 4, to start the experiment. Using this preparation four pH configurations were produced, which were permutation of inside and outside pH of 4 and 7 (see Fig. 3.8*B* legend). After 200 s equilibration time, ColA was added to the liposome solution (Fig. 3.8*B*). For two of the four pH configurations a rapid increase of fluorescence emission was detected upon addition of ColA, indicating calcein release from the liposomes.

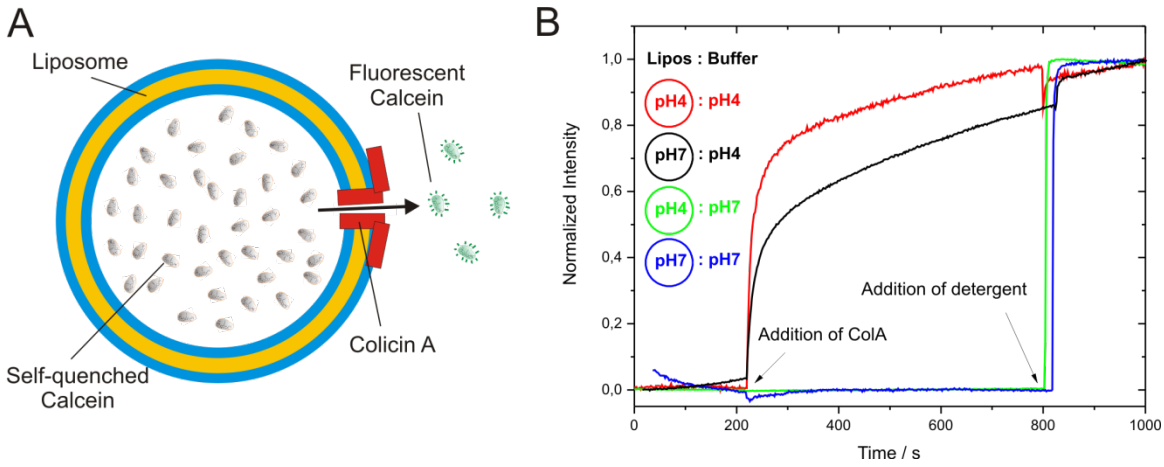

FIGURE 3.8 Calcein release from liposome incubated with ColA. (A) A schematic representation of the experimental design is depicted. Calcein is trapped in a self-quenching concentration of > 80 mM inside LUVs. When calcein can permeate through open ColA channels the fluorescence emission will increase. (B) Time course measurements of liposome trapped calcein using four different pH configurations. ColA was added to the cuvette after 200 s, respectively. In case of pH 4 in the outside solution the fluorescence increased rapidly after ColA addition, which indicates that calcein was released from the liposomes (red and black trace). In case of pH 7 in the outside solution no increase was observed (green and blue trace). All calcein was released from the liposomes after 800 s by addition of detergent.

In both cases the proton concentration of the outside solution was adjusted to pH 4. When the proton concentration outside the liposomes was lowered to pH 7 no calcein release was detected after addition of ColA. The results are surprising in two ways. In the first place, ColA should not be able to produce open ion channels in liposomes without an applied membrane potential at all. Secondly, if the calcein-efflux is due to pore-formation of ColA the open diameter of channel has to exceed 1 nm.

3.4.5 The membrane bound state of ColA

To determine conformational changes of ColA during membrane binding and channel opening the environmental sensitive fluorescence probe NBD was used. NDB was

covalently bound cystein residues, which were introduced at specific sites of ColA to probe the membrane immersion depth of the respective region (see Fig. 3.2).

Calibration of the NBD fluorescence lifetime dependence on the dielectric constant of its environment was achieved by determining the lifetime in six different environments (Fig. 3.9*A+B*). The lifetime of NBD rose non-linearly from 0.5 ns in water to 7.3 ns in n-decane, with the most drastic increase towards lower dielectric constants.

Binding of ColA-NBD to the horizontal bilayer was determined by laser scanning the X-Z plane of the bilayer as depicted in Fig. 3.3. After perfusion of excess protein the laser focus was positioned on the membrane and the fluorescence lifetime of NBD was determined. Subsequently a trans-membrane potential of 100 mV was applied to induce the open channel conformation of ColA. Channel opening was detected by monitoring the membrane conductance (Fig. 3.9*C*). After channel opening the NBD lifetime was determined again to detect a possible membrane insertion of a specific labeling site. For comparison, the lifetime of all ColA-NBD mutants was determined in aqueous solution without membranes. The lifetime results show that, after membrane binding of ColA, all probed labeling sites were exposed to a more hydrophobic environment compared to the conformation in aqueous solution (Fig. 3.9*D*). Comparison with the calibration curve of the NBD lifetime dependence on hydrophobicity (Fig. 3.9*B*) indicates that all probed labeling sites were located at the membrane water interface. Mutant 115 which is located at helix 6 seemed to be most deeply immersed in the membrane. Surprisingly, mutant 166, which is located at the loop between the hydrophobic helices 8 and 9 and which was shown (by ESR spectroscopy) to be insert in the bilayer [18], was exposed to a hydrophilic environment in the HLB binding experiments. To induce the open channel conformation of ColA a membrane potential of 100 mV was applied. The number of open ColA channels first increased slowly, but with proceeding time the opening rate increased (Fig. 3.9*C*). The lifetime of ColA-NBD mutants was determined 10 min and 20 min after the membrane potential was applied. No significant differences between the lifetime, determined at zero potential and 10-20 min after application of 100 mV were detected (Fig. 3.9*D*).

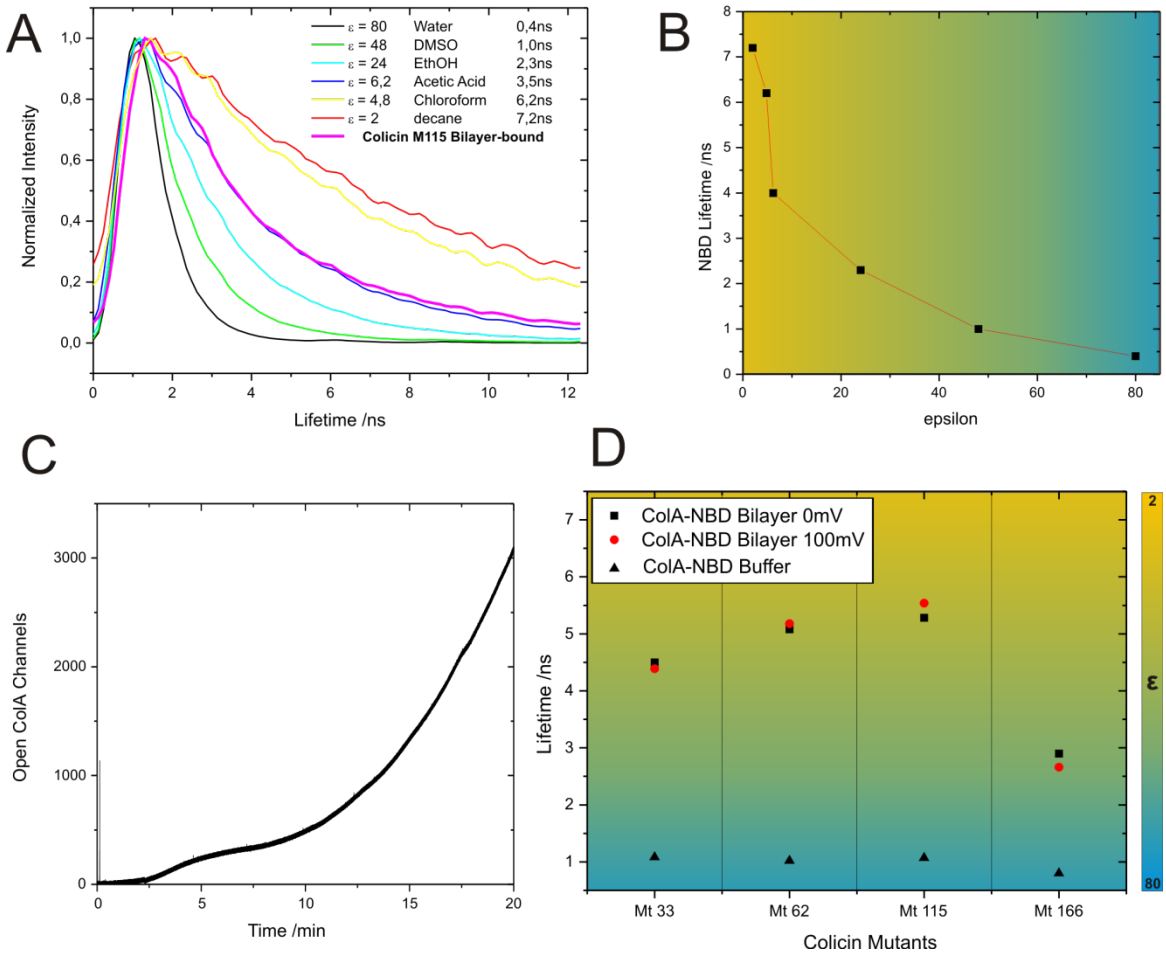

FIGURE 3.9 Fluorescence lifetime of ColA-NBD mutants. (A) Calibration of the environment sensitive probe NBD. The dielectric constant was step-wise changed from ε = 80 (water) to ε = 2 (n-decane). The fluorescence lifetime of NBD is clearly dependent on the polarity of the surrounding medium. (B) The dependence of the NBD lifetime on the dielectric constant of the medium is depicted. The lifetime increases from 0.7 ns in water to 7 ns in the apolar solvent n-decane, which corresponds to the environment in the middle of the bilayer. (C) ColA-NBD mutants were added to the Trans compartment (pH 4) of the HLB-chamber as described in Fig 2. After membrane binding the excess of ColA-NBD was wash out. A membrane potential of 100 mV was applied to open ColA channels. After 15 min ≈ 1000 ColA channels had opened. (D) The lifetime of ColA-mutants was

A comparison between the total concentration of membrane bound ColA and the number of open channels showed that less than 1% of the total ColA population switch to the open channel conformation after incubation at 100 mV for 20 min. Hence, an analysis of the open channel conformation using FFS was not feasible under the applied conditions.

3.5 Discussion

Despite the long history of Colicin research some crucial aspects of the pore-formation process are still not understood. The main difficulty in obtaining structural information seems to be that the open channel conformation requires not only membrane binding / reconstitution of ColA but also a correctly oriented trans-membrane potential. In this study a combined electro-optical approach was sued to characterize the membrane binding and channel-formation of ColA. As the horizontal bilayer set-up allows accessing electrical and optical parameters simultaneously, an analysis of the open-channel conformation was aspired.

3.5.1 pH dependence of membrane binding

The membrane binding of ColA was found to be strongly dependent on an acidic proton concentration of the buffer. The acidic pH mediated binding of pore-forming Colicins to membranes has been reported before [12, 14, 30]. Positively charged residues of the protein interact with negatively charged lipid head groups of the bilayer. Additionally, at acidic pH glutamate residues in the pore-forming domain will be protonated, which results in a favorable conformation of the amphipatic helices for binding to the bilayer [12]. Some experimental data indicate that the pore-forming domain of ColA forms a molten globule at acidic pH [14]. In this conformation the tertiary structure of the protein is opened or completely lost, while the secondary structure is retained. Hence, the molten globule with the central hydrophobic hairpin exposed would increase the affinity of ColA for membranes. Interestingly, to our knowledge, all studies on the pH dependence of Colicin membrane binding have been done *in vitro*. The question arises how Colicins bind to the plasma membrane of *E. coli* cells in vivo when the proton concentration in the periplasm is not necessarily acidic. Since the pH in the periplasm is essentially the same as in the extra cellular space, the data obtained *in vitro* would imply that pore-forming Colicins would be lethal to *E. coli* cells only under acidic conditions of the outside medium. *In vivo* Colicins are expressed as a response to environmental stress conditions to eliminate competing *E. coli* cells. One stress factor under conditions, where competition is relevant, is the acidification of the outside medium due to the mixed acid fermentation metabolism of *E. coli* in the absence of oxygen. This scenario would be in line with pH dependence of pore-formation measured *in vitro*. However, a closer look at the membrane potential of the *E. coli* plasma membrane under different pH conditions may suggest also another mechanism: At acidic pH the plasma-membrane potential of *E .coli* drops significantly from 140 mV at pH 8 to ≈ 60 mV at pH 4 [29]. Since the membrane potential is the driving force for channel formation, we would have two limiting factors, which are opposing each other. The membrane binding is increased at low pH while the channel-formation is increased at high pH, due to the high membrane potential. Thus, the channel-formation rate at neutral pH

may be limited by weak membrane binding of Colicins but is facilitated by the high membrane potential, whereas at acidic pH the situation is reversed. Additionally, the ion conductance of the open channel is 2-fold reduced at acidic pH compared to neutral pH (Fig. 3.5), which would require 2-times more open channels at pH 4 to result in the same solute efflux from the cytosol compared to pH 7. To address this consideration a detailed study of Colicin binding and toxicity in living *E. coli* cell would be required.

3.5.2 Electrophysiological properties of the ColA-channel

Channel openings of ColA could be observed under neutral and acidic pH when a trans-membrane potential of > + 60 mV was applied on the ColA side. The channel conductance at neutral pH was 18 pS in 1 M KCl, which agrees well with what has been reported before [8]. The ion conductance of the ColA channel is low compared to other narrow sized ion-channels. For example, the well known potassium channel KcsA with a pore diameter of ≈ 0.2 - 0.6 nm [31, 32], which allows only for single file motion of potassium ions, has a ≈ 5-fold higher conductance value under the same conditions [33]. The ion conductance of ColA is comparable to the simple pore-forming peptide gramicidin A, which has a pore diameter of 0.15 nm [34]. ColA channels have been found to exhibit high proton selectivity over other mono-valent ions, which is a feature that has been observed only in the narrowest known pores [25].

Surprisingly, the lumen of Colicin pores, determined by polymer accession experiments, has been estimated to be quite large (Ø = 1 nm). Moreover, the pore forming domain has been shown to translocate major parts of the upstream Colicin polypeptide across the bilayer. Even artificially attached proteins of up to a size of 2.6 nm have been found to be translocated across the membrane [21, 22, 38]. Additionally, the ColA-channel has been shown to be permeable for large ions [21, 22], which contradicts the low ion-conductance values, if we assume a conventional pore-formation mechanism. In this study indications for permeation of a large molecule (Calcein, Ø = 1 nm) through ColA-pores were found, which will be discussed below. A pore-formation model, which could reconcile the opposing properties of the channel, implies that lipid molecules are involved in constituting the active channel [36, 37]. The properties of a partly lipidic pore could be a flexible pore-size, and at the same time a low ion conductance due to relatively hydrophobic pore interior.

3.5.3 ColA induced Calcein efflux from liposomes

The low ion conductance values of the active ColA pore determined by electrophysiological measurements imply a small diameter of the pore. Using a fluorescence assay based on quenching of the dye Calcein, it was found that Calcein release from liposomes was induced by addition of ColA to liposome solution under acidic buffer conditions. Under neutral pH conditions no Calcein release was detected. Interpretation of the results is not straight forward, since content release from liposomes can be induced by pore-formation and / or by protein induced liposome fusion. Since the liposome solution became turbid after addition of

ColA at acidic pH, it can be concluded that ColA induced liposome aggregation / fusion. In one other study ColA has been shown to induce liposome fusion [12], as well. In this study liposome fusion required also acidic pH conditions. Interestingly, the non-pore-forming domains of ColA were found to be important to induce membrane fusion. Whether the calcein efflux in the presented experiments is exclusively caused by liposome leakage due to the fusion process or translocation of calcein through open ColA channels is involved, as well, remains open.

The finding of ColA induced membrane fusion may be artificial, because the ColA toxin will not come in contact with liposomes under *in vivo* conditions. However, the results could be interpreted in favor of the mentioned lipidic pore model, because the perturbation of the lipid bilayer structure, which is one basic step in membrane fusion, could be important in pore-formation of ColA at plasma membrane *in vivo*, as well.

3.5.4 ColA is a monomer in aqueous solution as well as in a membrane environment

It is known that most pore-forming toxins oligomerize in the target membrane to form an active ion channel [2, 39]. In case of ColA contradictory results have been published. Some studies indicate that ColA is secreted as a monomeric protein which is able to form an ion channel without oligomerization in vitro [40]. However, in a recent cryo-electron microscopy study oligomeric rings of membrane reconstituted Col-Ia were detected [41, 42]. Here three approaches were applied to determine the oligomeric state of ColA after binding to the bilayer. Steady state FRET of liposome reconstituted ColA and lifetime FRET of ColA bound to horizontal lipid bilayers indicated that ColA remains monomeric after binding to the bilayer. Additionally, fluorescence cross-correlation spectroscopy of the FRET pair reconstituted in HLBs resulted in independent diffusion of the monomers. It can be concluded that the majority of the ColA population is monomeric after membrane binding at pH 4. However, it cannot be excluded that a small fraction of the membrane bound ColA population oligomerizes, because the small signal from the oligomers would be superimposed by the large monomer signal.

The main difference between the conditions for membrane reconstitution of ColA in the present study and the oligomeric rings of Col-Ia observed in [42] is the protein to lipid ratio. Obviously, at very high protein content of Col-Ia stable oligomers form in the membrane. Whether this oligomeric structures represent the natively active conformation of the toxin remains to be shown.

3.5.5 The membrane bound conformation of ColA

The fluorescence lifetime of NBD was used to probe the membrane immersion depth of four specific labeling sites in the pore-forming domain of ColA. So far two conformations have been reported for the membrane bound ColA. In the penknife conformation all helices of the pore-forming domain are located at the membrane water interface. In the umbrella model the

hydrophobic helices 8 and 9 are inserted in the bilayer while the rest stays at the membrane water interface (Fig. 3.10).

The presented results indicate that, after membrane binding, all tested sites were exposed to an environment which was moderately hydrophobic. It can be concluded that all tested regions were oriented at the membrane water interface. This conformation would be in line with the penknife model (Fig. 3.10*B*) [19, 20]. The essential difference between the penknife model and the umbrella model is the orientation of the hydrophobic helices 8 and 9. In the umbrella model the hydrophobic hairpin is inserted in the bilayer while it stays at the membrane interface in the penknife model. In the present measurements residue 166, which is located at the loop between H8+9, showed the most hydrophilic exposition. However, in other studies residue 166 has been found to be inserted in the bilayer core [17, 18]. The difference in the results could be caused by several factors: (1) The polarity of the NBD dye may impede the insertion of the hydrophobic hairpin in the bilayer. However, NBD has been used in many other studies to probe membrane insertion. (2) The hairpin insertion may be facilitated in SUVs by the curvature stress of the lipids in liposomes, whereas in our case the insertion in a planar bilayer may be energetically more costly. (3) Since the NBD label is located at the loop in the hydrophobic hairpin, there is a chance that is exposed to the aqueous buffer on the *Trans*-side of the bilayer (Fig. 3.10*A*). This conformation would be in line with the umbrella model. However, additional measurement would be required to determine a *Trans* exposition of residue 166. For example a membrane impermeable fluorescence quencher could be used to determine the side of exposition of residue 166.

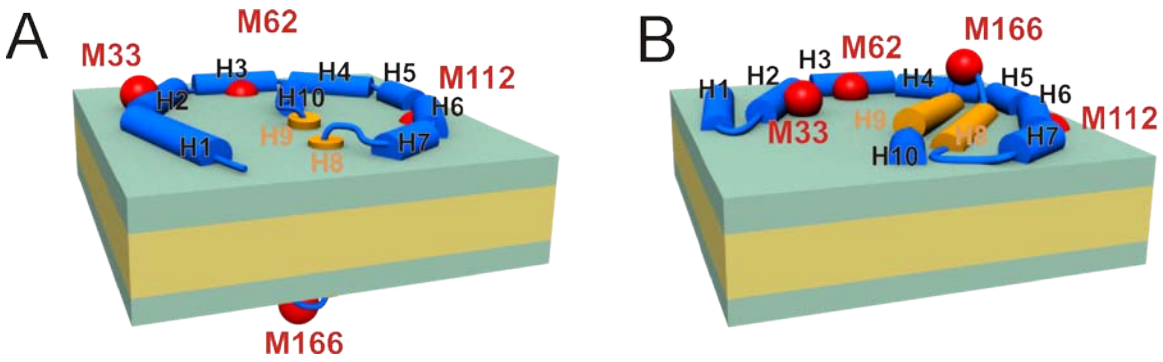

FIGURE 3.10 Conformation of the pore-forming domain of ColA. (A) In the umbrella helices 8+9 (orange) are inserted in the bilayer. All other helices are oriented at the membrane water interface. Residue 166 could be exposed to the bilayer core or to the *Trans* side of membrane. (B) In the penknife model all helices are oriented at the membrane interface.

3.5.6 The open channel conformation of ColA

The open channel conformation was induced by applying a trans-membrane potential of 100 mV after membrane binding of ColA. Channel activity was observed electrically. The membrane immersion of all tested residues did not significantly change after application of a membrane potential. This could mean that none of the tested sites is involved in the conformational changes during channel opening. However, this possibility seems unlikely because rather severe conformation changes are expected to produce an open channel from the membrane bound conformation. The most obvious reason why no changes in the membrane immersion depth were detected by lifetime measurements is that even after 20 min of constant application of a membrane potential (100 mV) less than 1 % of the total membrane bound ColA converted to the open channel conformation. Hence, in the lifetime determination the signal from the membrane bound conformation greatly outweighed the changes in lifetime due to channel opening. Unfortunately, the fraction of closed to open channels could not be changed. Application of higher membrane potentials (> 100 mV) led to membrane rupture after a few hundred channels openings. Since no significant differences between the electrical activity of wild type ColA and the NBD-labeled mutants were found, it can be concluded that the partition coefficient between the closed and open channel conformation under the applied conditions was not influenced by the mutations or by the fluorescent dye. Thus, with this unfavorable partition coefficient it is impossible to study the open channel conformation using ensemble techniques. Even application of single molecule techniques will be extremely challenging. Other labeling approaches would be required to sort out fluorescence signals from the open channel configuration compared to high background of closed channel configurations. For example, intra molecular FRET may be useful, if the FRET signal was significantly increased during channel opening.

3.6 References

1. Goot, F. G. v. d. 2001. Pore-forming toxins, Springer

2. Gilbert, R. J. C. 2002. Pore-forming toxins. *Cell Mol Life Sci*. 59:832–844.

3. Cascales, E., S. K. Buchanan, D. Duche, C. Kleanthous, R. Lloubes, K. Postle, M. Riley, S. Slatin, and D. Cavard. 2007. Colicin biology. *Microbiol Mol Biol Rev*. 71:158–229.

4. Parker, M. W., J. P. Postma, F. Pattus, A. D. Tucker, and D. Tsernoglou. 1992. Refined structure of the pore-forming domain of Colicin A at 2.4 a resolution. *J Mol Biol.* 224:639–657.

5. Wiener, M., D. Freymann, P. Ghosh, and R. M. Stroud. 1997. Crystal structure of Colicin Ia. *Nature*. 385:461–464.

6. Lazzaroni, J.-C., J.-F. Dubuisson, and A. Vianney. 2002. The Tol proteins of *Escherichia Coli* and their involvement in the translocation of group A Colicins. *Biochimie*. 84:391–397.

7. Schein, S. J., B. L. Kagan, and A. Finkelstein. 1978. Colicin K acts by forming voltage-dependent channels in phospholipid bilayer membranes. *Nature*. 276:159–163.

8. Martinez, M. C., C. Lazdunski, and F. Pattus. 1983. Isolation, molecular and functional properties of the C-terminal domain of colicin A. *EMBO J*. 2:1501–1507.

9. Zakharov, S. D., and W. A. Cramer. 2002. Colicin crystal structures: pathways and mechanisms for Colicin insertion into membranes. *Biochim Biophys Acta*. 1565:333–346.

10. Parker, M. W., A. D. Tucker, D. Tsernoglou, and F. Pattus. 1990. Insights into membrane insertion based on studies of colicins. *Trends Biochem Sci*. 15:126–129.

11. Lakey, J. H., M. W. Parker, J. M. Gonzalez-Manas, D. Duche, G. Vriend, D. Baty, and F. Pattus. 1994. The role of electrostatic charge in the membrane insertion of Colicin A. Calculation and mutation. Eur *J Biochem*. 220:155–163.

12. Davidson, V. L., W. A. Cramer, L. J. Bishop, and K. R. Brunden. 1984. Dependence of the activity of Colicin E1 in artificial membrane vesicles on pH, membrane potential, and vesicle size. *J Biol Chem*. 259:594–600.

13. Musse, A. A., and A. R. Merrill. 2003. The molecular basis for the pH-activation mechanism in the channel-forming bacterial Colicin E1. *J Biol Chem*. 278:24491–24499.

14. van der Goot, F. G., J. M. Gonzalez-Manas, J. H. Lakey, and F. Pattus. 1991. A 'molten-globule' membrane-insertion intermediate of the pore-forming domain of Colicin A. *Nature*. 354:408–410.

15. Gonzalez-Manas, J. M., J. H. Lakey, and F. Pattus. 1992. Brominated phospholipids as a tool for monitoring the membrane insertion of Colicin A. *Biochemistry*. 31:7294–7300.

16. van der Goot, F. G., J. H. Lakey, and F. Pattus. 1992. The molten globule intermediate for protein insertion or translocation through membranes. *Trends Cell Biol*. 2:343–348.

17. Lakey, J. H., D. Baty, and F. Pattus. 1991. Fluorescence energy transfer distance measurements using site-directed single cysteine mutants. The membrane insertion of Colicin A. *J Mol Biol*. 218:639–653.

18. Padmavathi, P. V. L., and H.-J. Steinhoff. 2008. Conformation of the closed channel state of Colicin A in proteoliposomes: An umbrella model. *J Mol Biol*. 378:204–214.

19. Lakey, J. H., D. Duche, J. M. Gonzalez-Manas, D. Baty, and F. Pattus. 1993. Fluorescence energy transfer distance measurements. The hydrophobic helical hairpin of Colicin A in the membrane bound state. *J Mol Biol*. 230:1055–1067.

20. Duche, D., M. W. Parker, J. M. Gonzalez-Manas, F. Pattus, and D. Baty. 1994. Uncoupled steps of the Colicin A pore formation demonstrated by disulfide bond engineering. *J Biol Chem*. 269:6332–6339.

21. Qiu, X. Q., K. S. Jakes, P. K. Kienker, A. Finkelstein, and S. L. Slatin. 1996. Major transmembrane movement associated with Colicin Ia channel gating. *J Gen Physiol*. 107:313–328.

22. Slatin, S. L., A. Nardi, K. S. Jakes, D. Baty, and D. Duche. 2002. Translocation of a functional protein by a voltage-dependent ion channel. *Proc Natl Acad Sci U S A*. 99:1286–1291.

23. Raymond, L., S. L. Slatin, and A. Finkelstein. 1985. Channels formed by Colicin E1 in planar lipid bilayers are large and exhibit ph-dependent ion selectivity. *J Membr Biol*. 84:173–181.

24. Bullock, J. O., E. R. Kolen, and J. L. Shear. 1992. Ion selectivity of Colicin E1: Ii. Permeability to organic cations. *J Membr Biol*. 128:1–16.

25. Slatin, S. L., A. Finkelstein, and P. K. Kienker. 2008. Anomalous proton selectivity in a large channel: Colicin A. *Biochemistry*. 47:1778–1788.

26. Widengren, J., U. Mets, and R. Rigler. 1995. Fluorescence correlation spectroscopy of triplet states in solution: a theoretical and experimental study. *The Journal of Physical Chemistry*. 99:13368–13379.

27. Müller, C. B., A. Loman, V. Pacheco, F. Koberling, D. Willbold, W. Richtering, and J. Enderlein. 2008. Precise measurement of diffusion by multi-color dual-focus fluorescence correlation spectroscopy. *EPL (Europhysics Letters)*. 83:46001.

28. Johnson, A. E. 2005. Fluorescence approaches for determining protein conformations, interactions and mechanisms at membranes. T*raffic*. 6:1078–1092.

29. Felle, H., J. S. Porter, C. L. Slayman, and H. R. Kaback. 1980. Quantitative measurements of membrane potential in *escherichia coli*. *Biochemistry*. 19:3585–3590.

30. Geli, V., M. C. Koorengevel, R. A. Demel, C. Lazdunski, and J. A. Killian. 1992. Acidic interaction of the Colicin A pore-forming domain with model membranes of *Escherichia Coli* lipids results in a large perturbation of acyl chain order and stabilization of the bilayer. *Biochemistry*. 31:11089–11094.

31. Doyle, D. A., J. M. Cabral, R. A. Pfuetzner, A. Kuo, J. M. Gulbis, S. L. Cohen, B. T. Chait, and R. MacKinnon. 1998. The structure of the potassium channel: molecular basis of K^+ conduction and selectivity. *Science*. 280:69–77.

32. Meuser, D., H. Splitt, R. Wagner, and H. Schrempf. 1999. Exploring the open pore of the potassium channel from *Streptomyces lividans*. *FEBS Lett*. 462:447–452.

33. Schrempf, H., O. Schmidt, R. Kümmerlen, S. Hinnah, D. Müller, M. Betzler, T. Steinkamp, and R. Wagner. 1995. A prokaryotic potassium ion channel with two predicted transmembrane segments from *Streptomyces lividans*. *EMBO J*. 14:5170–5178.

34. Smart, O. S., J. Breed, G. R. Smith, and M. S. Sansom. 1997. A novel method for structure-based prediction of ion channel conductance properties. *Biophys J*. 72:1109–1126.

35. Hille, B. 2001. Ion Channels of Excitable Membranes. Sinauer Associates, Inc.

36. Slatin, S. L. 1988. Colicin E1 in planar lipid bilayers. *Int J Biochem*. 20:737–744.

37. Zakharov, S. D., E. A. Kotova, Y. N. Antonenko, and W. A. Cramer. 2004. On the role of lipid in Colicin pore formation. *Biochim Biophys Acta*. 1666:239–249.

38. Kienker, P. K., K. S. Jakes, R. O. Blaustein, C. Miller, and A. Finkelstein. 2003. Sizing the protein translocation pathway of Colicin Ia channels. *J Gen Physiol*. 122:161–176.

39. Strong, P. 2004. Cellular and molecular mechanisms of toxic action–pore-forming peptides and protein toxins. *International Journal of Toxicology*. 23:73–75.

40. Wu, Z., K. S. Jakes, B. S. Samelson-Jones, B. Lai, G. Zhao, E. London, and A. Finkelstein. 2006. Protein translocation by bacterial toxin channels: a comparison of Diphtheria toxin and Colicin Ia. *Biophys J*. 91:3249–3256.

41. Cavard, D., P. Sauve, F. Heitz, F. Pattus, C. Martinez, R. Dijkman, and C. Lazdunski. 1988. Hydrodynamic properties of colicin A. Existence of a high-affinity lipid-binding site and oligomerization at acid pH. *Eur J Biochem*. 172:507–512.

42. Greig, S. L., M. Radjainia, and A. K. Mitra. 2009. Oligomeric structure of Colicin Ia channel in lipid bilayer membranes. *J Biol Chem*. 284:16126–16134.

4. Conclusion

In this thesis electrical addressable, horizontal lipid bilayers were combined with fluorescence fluctuation spectroscopy. The basic characterization of lipid dynamics in HLBs indicated that the bilayer properties are comparable to other model membrane systems like GUVs and SLBs. It was found that lateral and rotational diffusion of fluorescent lipid probes are slightly increased in the HLB setup compared to solvent free model membranes. This is most probably due to residual hydrocarbon solvent remaining in the bilayer. The stability and electrical properties of HLBs are essentially the same of conventional BLMs.

Using ternary lipid mixtures mimicking the plasma membrane of eukaryotic cells, large scale lipid phase separation could be conveniently induced in a temperature controlled manner in HLBs. The diffusion properties of the lipid phases were found to be in accordance to the published results for GUVs and SLBs. The electrical properties of the HLB during lipid phase separation indicated that the bilayer remains electrically sealed during liquid-liquid phase separation. However, unspecific membrane leaks were found to be induced by liquid-solid phase separation. Since the seal of biological membranes needs to be tightly regulated, the electrically instabilities during liquid-solid phase separation found in HLBs argue against a comparable mechanism in biological membranes. Probably the cholesterol content in eukaryotic membranes inhibits the formation of the solid ordered phase.

To demonstrate the capabilities of the HLB-setup to correlate optical with electrical signals, the effects of liquid phase separation on the electrical activity of the ion channel forming peptide gramicidin A (gA) was studied. It was found that gA was excluded from the L_o domains in the bilayer during phase separation. As a consequence, the concentration of gA was enhanced in the remaining L_d phase. Since channel formation of gA is a dimerization process of gA monomers that depends on the concentration of gA monomers, the number of open channels increased as the lipids phase separated. The results show that the general concept of lipid domain mediated sorting and function regulation of ion channel proteins can be studied with the presented setup.

In a second study the electro-optical setup was used to characterize membrane binding and channel formation of Colicin A (ColA), which is a toxin secreted by *E. coli*. ColA is an interesting target for an electro-optical study, because the protein depends on a trans-membrane potential of more than 60 mV to produce open ion channels in a lipid membrane. While ColA has been studied for more than 30 years, the mechanism of channel formation remains unknown. It was aimed to follow membrane insertion of specific sites of ColA during channel opening. While the pH-dependent membrane binding and voltage dependent single channel opening could be determined, the vast majority of the ColA population resided in the membrane bound conformation when a membrane potential was applied. Even though a fraction of the ColA population converted in the open channel conformation, the

associated fluorescence signal could not be distinguished from the high membrane bound signal. Therefore the structural rearrangements during channel opening could not be resolved.

In conclusion the combination of HLBs with FFS has proven to be a versatile tool to study processes that occur at electrically excitable membranes. To summarize the advantages of the presented setup it can be claimed that:

1. Bilayer preparation is reproducible and easily accomplished by the painting technique.
2. Since the bilayer is planar and free standing it is ideally suited for imaging and optical measurement without producing surface artefacts.
3. The diffusion properties of fluorescent molecules can be determined in short time with high statistical accuracy by FFS in the aqueous compartments as well as directly in the bilayer.
4. At the same time the electrical properties of the bilayer can be precisely controlled and membrane currents can be determined with single molecule resolution.
5. Both compartments can be perfused during a measurement to change the buffer conditions. Hence both sides of the bilayer are accessible during an experiment.

4.1 Limitations of HLBs in combination with FFS

Besides the introduced advantages, the presented combination of HLBs with FFS bears some technical limitations:

4.1.1 The size relation problem

Generally it is not feasible to study the same (freely diffusion) single molecule both optically and electrically simultaneously with the presented setup. This follows from using a confocal detection volume, which is about five orders of magnitude smaller than the area of the planar bilayer. Consequently, a single electrically active ion channel has a vanishing small probability to diffuse across a stationary excitation volume. Beam scanning may be used to image the single molecule, but it is much too slow to yield photon data of a single molecule in reasonable time resolution, which would be sufficient for correlation of electrical and optical signals. This limitation can be overcome by using wide field excitation, as has been demonstrated by other approaches [42-43].

In principle, an electro-optical correlation of a single ion channel could be achieved with the presented setup, if the fluorescent ion channel was immobilized in the bilayer. A scan would determine the position of the molecule. For the actual measurement the excitation volume would be placed directly at the stationary molecule [4-7]. The fast time resolution of the

single photon counting detectors would be more than sufficient for correlation of the electrical function of an ion channel with optical properties of the fluorescent probe. Unfortunately, to our knowledge no applicable method exists which can be used to completely immobilize a protein in a BLM [8]. Additionally, even if immobilization was feasible, the short photo stability of conventional fluorescent dyes would greatly restrict the measurement time.

Another approach for confocal electro-optical correlation of a single ion channel would be to miniaturize the planar bilayer to a size which is on the order of the confocal volume or even smaller. Currently, 25µm thick PTFE films with an aperture size of Ø = 150µm are used. The aspect ratio of thickness and diameter is 1:6 (thickness / diameter). If the bilayer is prepared from a lipid solvent solution by the painting technique, a high aspect ratio is advantageous, because smaller aspect ratios < 1:2 prevent the formation of the bilayer (the complete aperture is filled by the torus). Therefore, if it was desired to prepare a planar bilayer by the painting technique on an aperture of Ø = 1 µm the thickness of the film should not exceed 0.5 µm. Unfortunately, the effort to produce and handle such thin films (containing one small aperture) would demand a specialized material science expertise. Recent successful examples of producing small sized planar bilayer show that a miniaturization to nano-meter sized bilayer is possible. So called nano-BLMs can be formed on functionalized porous alumina with pore sizes of 50 – 400 nm [9]. However, since porous alumina films are arrays of numerous nano-pores opto-electrical correlation cannot be achieved using this material. A promising method to produce small sized planar bilayers is to use SLBs on glass-slides covering ≈ 1 µm sized apertures [10, 11]. GUVs containing reconstituted ion channels could be used to cover the apertures by spontaneous rupture on the glass-slide producing planar membranes.

4.1.2 Incorporation of functional ion channels into HLBs

To be able to apply FFS the concentration range of diffusing fluophores has to be in the range of 1-50 molecules per confocal volume. In a 2D planar bilayer (Ø ≈ 100µm) one fluophore per excitation volume (w_0 = 330 nm) is achieved if a total number of ≈ 25000 fluophores is present in the bilayer. Hence for an electro-optical study using FFS a large number of fluorescent ion channels have to be incorporated in the bilayer. In case of self-incorporating pore-forming toxins this number can be easily reached. However, more complex ion channels require proteo-liposome reconstitution and subsequent membrane fusion to be incorporated in the bilayer. Unfortunately, liposome fusion to the planar bilayer is a spontaneous event. Fusion can be induced by osmotical swelling [38], but usually the bilayer ruptures when liposomes fuse en masse with the planar membrane. Facilitating liposome fusion to the planar bilayer using peptides which have been shown to mediate liposome-liposome fusion [13, 14] did not succeed (data not shown). In other BLM studies proteo-liposomes containing the respective ion channel are spread to a monolayer at the air

water interface. From two monolayers (*Cis* and *Trans*) a BLM is folded which contains the ion channel proteins [15, 16]. Unfortunately, the monolayer folding technique is not applicable to the HLB setup, because the required air water interface cannot be produced on both sides of the aperture.

Even if one succeeds to incorporate a sufficient number of ion channel proteins in the bilayer to use FFS, the problem may be that a large fraction of proteins is not in an open conformation or is just not active, as has been observed in the presented Colicin A study. Hence, the quality of the protein preparation (purification, labeling, and reconstitution) has to meet the requirements of a homogenously active population of proteins [61]. In practice the protein preparation is the most laborious and unpredictable step in course of a BLM experiment.

In general the optical addressable horizontal bilayers would be well suited to study non ion channel membrane protein such as receptors, as well. Unfortunately, the insertion of non channel proteins in BLMs is even more complicated than ion channels, because the osmotic liposome fusion technique relies on open ion channels in the liposomes. New methods are required to overcome the problem of functional and quantitative protein incorporation in BLMs.

4.1.3 Detection of non electrolyte transport through the bilayer

Besides the direct study of electro-optical conformational changes of ion-channels, it would be of great interest to follow the binding and transport of non-electrolyte cargos through metabolite and protein conducting channels.

The electrical detection of macro-molecule transport through a single channel is based on transient ion current blocking events during channel passage of the macro-molecule. A stochastic analysis of the blocking events can be used to characterize the transport time and binding constants of the substrate [18, 19]. In some cases even a certain molecule type can be sensed [20]. Unfortunately the electrical blocking signals do not always correspond to molecule transport. Blocking can also be produced be transient binding to the pore. Thus interpretation of stochastic electrical current traces is difficult especially when transport of large macro-molecules wants to be studied. An electro-optical correlation of macro-molecule transport could overcome this limitation. Using the presented confocal setup the concentration of fluorescently labeled transport substrates can be determined down to pico-molar concentrations. Thus, if a transport substrate is added to the *Cis* side of a bilayer containing one channel, it may be detected on the *Trans* side with FFS when the concentration reaches the pico-molar range. The main parameters which affect the concentration increase in the *Trans* compartment during transport are the conductance of the respective pore for the cargo [mol/s] and the volume of the *Trans* compartment. For clearness the transport time of a 20 amino acid long peptide which should be transported through a beta barrel pore until the concentration threshold in *Trans* is reached can be

estimated. It is assumed that the conductance value of the channel for the peptide is ≈ 100 peptides/s [21]. The *Trans* compartment has a total volume of 200 µl. Using this parameters, it would take 4 years to reach a concentration of 100 pM of the peptide in *Trans* compartment, if only a single channel was present in the bilayer. If the *Trans* compartment volume was reduced to 1 nl, the transport would take only 10 min before the detection threshold of 100 pM is reached. Examples of nano-sized bilayer-enclosed compartments exist [22, 23], however in none of these studies an electrode was incorporated in the *Trans* compartment for electrical measurements.
Immobilization of an ion channel (discussed above) would be advantageous for transport studies, as well. If the confocal volume was positioned just beneath the channel, the transport of fluorescent cargo could be detected in real time. However, as has been already remarked total immobilization of proteins in BLMs has not been feasible so far.

4.1.4 Lifetime of HLBs

The main reason why BLMs have not been used in screening assays or other automated measurement systems is the instability of the bilayer. A vertical free standing planar bilayer (Ø ≈ 100µm), which is protected from mechanical stress (vibration dumping), has a mean lifetime of some hours. For some unknown reason the free standing horizontal bilayers are even more prone to rupture. Its lifetime is about half that of the vertical bilayers. Concepts to increase the stability of the bilayer include embedment of the membrane in a hydro-gel [2, 24-26], polymerization of specific lipids or miniaturization of the bilayer [27, 28]. Using the mentioned techniques the lifetime of BLMs can be prolonged to weeks.

4.2 Outlook

So far the presented studies using the electro-optical setup were of model character. Considering the presented limitations of HLBs in combination with FFS possible applications to biological relevant targets are discussed.

4.2.1 Lipid domain partitioning of KV-channels

The ternary lipid bilayer including liquid phase separation, which were presented in the first part of this thesis, may be readily used to study the function of (potential) lipid raft associated ion channels. For example, a major class of such ion channels are voltage gated potassium channels (KV) which are involved in membrane excitability [29]. From biochemical experiments (detergent resistant membranes) it is deduced that KV-channels are associated with lipid rafts [73]. However, direct observations of KV raft association do not exist and the functional role of a possible raft association is unknown. Functional reconstitution of KV-channels in BLMs has been demonstrated [31]. Additionally, a variety of single site mutations for specific fluorescence labeling are already available [32, 33]. In analogy to the gramicidin A partitioning experiments, fluorescent KV-channels may be

incorporated in ternary HLBs at 37°C. When the temperature is lowered to 24°C lipids phase separate and KV-channels will redistribute according to its affinity for lipid domains. Simultaneously, the effect on the electrical activity of the channels can be determined. Additionally, membrane cholesterol can be depleted by cyclodextrin or cholesterol oxidase to disrupt lipid phase separation during an electrical measurement [34]. In general domain partitioning experiments can be conducted with any electrically active membrane protein, which is thought to be involved in lipid raft association, to determine the influence of the lipid environment on the function of the respective protein. However, one has to be careful interpreting the results, because recent studies have indicated that lipid phase separation in cell membranes and ternary lipid bilayers may not be directly comparable [35, 36]. Probably the simple ternary lipid mixtures have to be modified by additional lipids and proteins to resemble the plasma membrane of eukaryotic cells more closely.

4.2.2 Calmodulin binding to Sec61

In conventional BLM experiments the effect of compounds and binding partners on ion channels is studied by a change in the electrical activity. However, the actual binding site and structural changes of the ion channel during binding cannot be determined. For example, in our lab it was found that the channel opening of Sec61, the protein translocase of the endoplasmic reticulum, is regulated by calcium dependent calmodulin binding (unpublished data [38]). A potential binding site for calmodulin is a conserved IQ motiv in the alpha subunit of Sec61. Using the opto-electrical setup the binding site and the impact of binding on the electrical activity could be determined at the same time. Therefore, Sec61 could be specifically labeled with a donor dye at positions near the IQ motif as well as far away from the motiv. If calmodulin was labeled with an acceptor dye (ideally non-fluorescent, since calmodulin has to be present in excess) the binding could be detected by quenching of the donor fluorescence. By mapping the distance of the donor acceptor pairs of different Sec61 mutants the binding site of calmodulin to Sec61 could be precisely determined.

4.2.3 Single particle tracking

Since it is hardly possible to study the electrical signal of a single ion channel and its fluorescent signal simultaneously using FFS (see limitations), wide field laser illumination in combination with a sensitive EM-CCD-camera will be used to image the whole area of the HLB at once with millisecond time resolution. Except for the fluorescence lifetime and the fast rotational diffusion all parameters which can be determined using FFS are also accessible using SPT (lateral and slow rotational diffusion constants, particle brightness, FRET, etc.). Thus a fast and statistical accurate characterization of an electro-optical experiment could be done using FFS and accordingly a detailed one to one correlation of electrical and optical signals may be approached using the SPT setup.

4.3 References

1. Ide, T., and T. Yanagida. 1999. An artificial lipid bilayer formed on an agarose-coated glass for simultaneous electrical and optical measurement of single ion channels. *Biochemical and Biophysical Research Communications*. 265:595–599.

2. Ide, T., Y. Takeuchi, T. Aoki, and T. Yanagida. 2002. Simultaneous optical and electrical recording of a single ion-channel. *Jpn J Physiol*. 52:429–434.

3. Borisenko, V., T. Lougheed, J. Hesse, E. Füreder-Kitzmüller, N. Fertig, J. C. Behrends, G. A. Woolley, and G. J. Schütz. 2003. Simultaneous optical and electrical recording of single gramicidin channels. *Biophys J*. 84:612–622.

4. Munro, J. B., R. B. Altman, N. O'Connor, and S. C. Blanchard. 2007. Identification of two distinct hybrid state intermediates on the ribosome. *Mol Cell*. 25:505–517.

5. Roy, R., S. Hohng, and T. Ha. 2008. A practical guide to single-molecule fret. *Nat Methods*. 5:507–516.

6. Theissen, B., A. R. Karow, J. Köhler, A. Gubaev, and D. Klostermeier. 2008. Cooperative binding of atp and rna induces a closed conformation in a dead box RNA helicase. *Proc Natl Acad Sci U S A*. 105:548–553.

7. Fiore, J. L., B. Kraemer, F. Koberling, R. Edmann, and D. J. Nesbitt. 2009. Enthalpy-driven RNA folding: single-molecule thermodynamics of tetraloop-receptor tertiary interaction. *Biochemistry*. 48:2550–2558.

8. Ichikawa, T., T. Aoki, Y. Takeuchi, T. Yanagida, and T. Ide. 2006. Immobilizing single lipid and channel molecules in artificial lipid bilayers with Annexin A5. *Langmuir*. 22:6302–6307.

9. Horn, C., and C. Steinem. 2005. Photocurrents generated by Bacteriorhodopsin adsorbed on nano-black lipid membranes. *Biophys J*. 89:1046–1054.

10. Fertig, N., R. H. Blick, and J. C. Behrends. 2002. Whole cell patch clamp recording performed on a planar glass chip. *Biophys J*. 82:3056–3062.

11. Fertig, N., M. Klau, M. George, R. H. Blick, and J. C. Behrends. 2002. Activity of single ion channel proteins detected with a planar microstructure. *Applied Physics Letters*. 81:4865.

12. Cohen, F. S., W. D. Niles, and M. H. Akabas. 1989. Fusion of phospholipid vesicles with a planar membrane depends on the membrane permeability of the solute used to create the osmotic pressure. *J Gen Physiol*. 93:201–210.

13. Top, D., R. de Antueno, J. Salsman, J. Corcoran, J. Mader, D. Hoskin, A. Touhami, M. H. Jericho, and R. Duncan. 2005. Liposome reconstitution of a minimal protein-mediated membrane fusion machine. *EMBO J*. 24:2980–2988.

14. Hofmann, M. W., B. C. Poschner, S. Hauser, and D. Langosch. 2007. pH-activated fusogenic transmembrane LV-peptides. *Biochemistry*. 46:4204–4209.

15. Schindler, H., and J. P. Rosenbusch. 1978. Matrix protein from *Escherichia Coli* outer membranes forms voltage-controlled channels in lipid bilayers. *Proc Natl Acad Sci U S A*. 75:3751–3755.

16. Schindler, H. 1980. Formation of planar bilayers from artificial or native membrane vesicles. *FEBS Lett*. 122:77–79.

17. Johnson, A. E. 2005. Fluorescence approaches for determining protein conformations, interactions and mechanisms at membranes. *Traffic*. 6:1078–1092.

18. Henrickson, S. E., M. Misakian, B. Robertson, and J. J. Kasianowicz. 2000. Driven DNA transport into an asymmetric nanometer-scale pore. *Phys Rev Lett*. 85:3057–3060.

19. Brun, L., M. Pastoriza-Gallego, G. Oukhaled, J. Mathe, L. Bacri, L. Auvray, and J. Pelta. 2008. Dynamics of polyelectrolyte transport through a protein channel as a function of applied voltage. *Phys Rev Lett*. 100:158302.

20. Bayley, H., and P. S. Cremer. 2001. Stochastic sensors inspired by biology. *Nature*. 413:226–230.

21. Movileanu, L., J. P. Schmittschmitt, J. M. Scholtz, and H. Bayley. 2005. Interactions of peptides with a protein pore. *Biophys J*. 89:1030–1045.

22. Hemmler, R., G. Böse, R. Wagner, and R. Peters. 2005. Nanopore unitary permeability measured by electrochemical and optical single transporter recording. *Biophys J*. 88:4000–4007.

23. Ganesan, P. V., and S. G. Boxer. 2009. A membrane interferometer. *Proc Natl Acad Sci U S A*. 106:5627–5632.

24. Lu, X., A. Leitmannova Ottova, and H. T. Tien. 1996. Biophysical aspects of agar-gel supported bilayer lipid nembranes: a new method for forming and studying planar bilayer lipid membranes. *Bioelectrochemistry and Bioenergetics*. 39:285–289.

25. Jeon, T.-J., N. Malmstadt, and J. J. Schmidt. 2006. Hydrogel-encapsulated lipid membranes. *J Am Chem Soc*. 128:42–43.

26. Kang, S. Cheley, A. C. Rice-Ficht, and H. Bayley. 2007. A storable encapsulated bilayer chip containing a single protein nanopore. *J Am Chem Soc*. 129:4701–4705.

27. White, R. J., E. N. Ervin, T. Yang, X. Chen, S. Daniel, P. S. Cremer, and H. S. White. 2007. Single ion-channel recordings using glass nanopore membranes. *J Am Chem Soc*. 129:11766–11775.

28. Heitz, B. A., J. Xu, H. K. Hall, C. A. Aspinwall, and S. S. Saavedra. 2009. Enhanced long-term stability for single ion channel recordings using suspended poly(lipid) bilayers. *J Am Chem Soc*. 131:6662–6663.

29. Bezanilla, F. 2005. Voltage-gated ion channels. *IEEE Trans Nanobioscience*. 4:34–48.

30. Martens, J. R., K. O'Connell, and M. Tamkun. 2004. Targeting of ion channels to membrane microdomains: localization of KV channels to lipid rafts. *Trends Pharmacol Sci*. 25:16–21.

31. Pantoja, R., D. Sigg, R. Blunck, F. Bezanilla, and J. R. Heath. 2001. Bilayer reconstitution of voltage-dependent ion channels using a microfabricated silicon chip. *Biophys J*. 81:2389–2394.

32. Blunck, R., J. F. Cordero-Morales, L. G. Cuello, E. Perozo, and F. Bezanilla. 2006. Detection of the opening of the bundle crossing in KcsA with fluorescence lifetime spectroscopy reveals the existence of two gates for ion conduction. *J Gen Physiol*. 128:569–581.

33. Blunck, R., H. McGuire, H. C. Hyde, and F. Bezanilla. 2008. Fluorescence detection of the movement of single KcsA subunits reveals cooperativity. *Proc Natl Acad Sci U S A*. 105:20263–20268.

34. Bacia, K., D. Scherfeld, N. Kahya, and P. Schwille. 2004. Fluorescence correlation spectroscopy relates rafts in model and native membranes. *Biophys J*. 87:1034–1043.

35. Kaiser, H.-J., D. Lingwood, I. Levental, J. L. Sampaio, L. Kalvodova, L. Rajendran, and K. Simons. 2009. Order of lipid phases in model and plasma membranes. *Proc Natl Acad Sci U S A*. 106:16645–16650.

36. Lingwood, D., and K. Simons. 2010. Lipid rafts as a membrane-organizing principle. *Science*. 327:46–50.

37. Rajendran, L., H.-J. Knölker, and K. Simons. 2010. Subcellular targeting strategies for drug design and delivery. *Nat Rev Drug Discov*. 9:29–42.

38. Erdmann, Frank. 2009. Zur Regulation der Protein Translokase des Endoplasmatischen Reikulums. *Dissertation*

5. Summary

The main results of the presented thesis are:

- A horizontal bilayer chip was constructed, which is suitable for simultaneous electrical and optical recordings using high numerical aperture objectives. The design of the chip allows changing the buffer solutions in the *Cis* and *Trans* compartments during a measurement. Furthermore a temperature control allows setting a temperature in the range of 5-45°C at the bilayer.
- The horizontal bilayer dynamics were characterized using fluorescent fluctuation techniques. Lipid diffusion constants (lateral and rotational) were found to be comparable to other membrane model membrane systems, with slightly higher values due to solvent partitioning in the horizontal bilayers.
    - Lipid temperature dependent lipid phase separation was studied using ternary lipid mixtures mimicking the plasma membrane of eukaryotic cells. The lipid dynamics in liquid ordered were found to be decreased compared to the liquid disordered phase.
    - The horizontal bilayers were electrically sealed during liquid-liquid phase separation of lipids. However, during liquid-solid phase separation transient current fluctuations were observed
- The partitioning of a simple ion channel (gramicidin A) in the lipid domains was found to influence its electrical activity. Gramicidin A (gA) was largely excluded from the liquid ordered phase resulting in an increased surface density of gA in the disordered phase. With the sorting of gA to the disordered phase the number of open gA ion channels (dimers) increased, because the dimerization constant is simply dependent on the surface density of gA monomers.
- The membrane binding and channel formation of the channel forming toxin Colicin A (ColA) was studied with the electro-optical setup. The binding of the water soluble protein to the bilayer was increased at acidic pH. Ion channel formation of ColA was induced by an application of trans-membrane potential of more than 60 mV on the side of ColA addition. The single channel conductance in 1M KCl was 20pS.
    - The structural changes during membrane binding and channel opening were studied using site specific labeling of different ColA mutants. During membrane binding ColA was found to stay monomeric. All tested labeling sites resided at the bilayer water interface. The fraction of open channel of the total membrane bound ColA population was very low when an appropriate membrane potential was applied for several minutes.

Unfortunately, the open channel conformation could not be analyzed, because the signal of the membrane bound ColA corrupted the measurements.

6. Appendix

6.1 Construction plans of the horizontal bilayer chip

6.1.1 Component assembly

Explosion View:

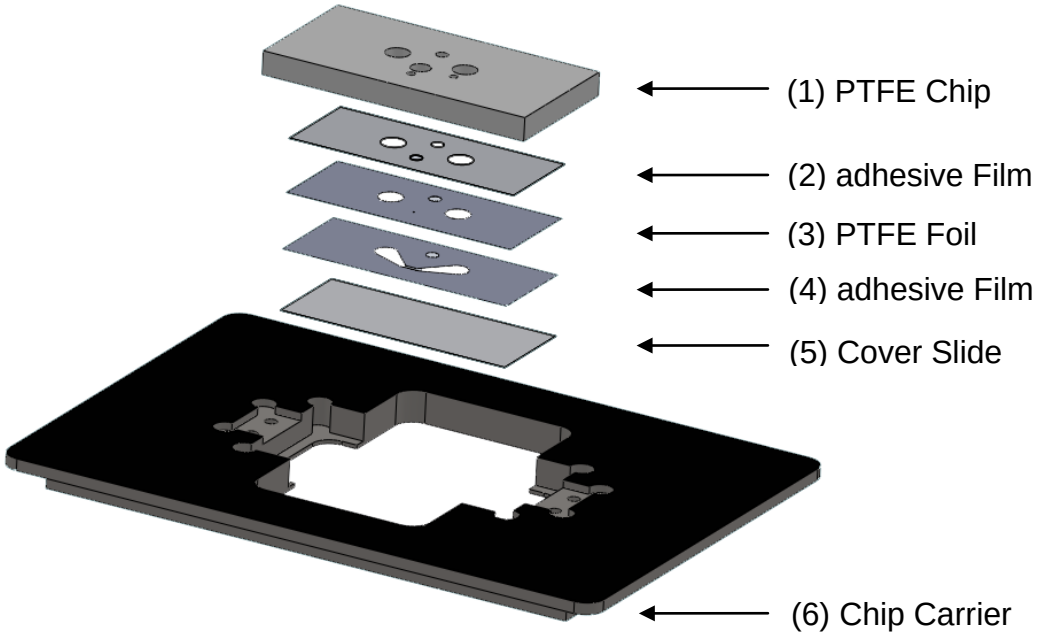

Top View:

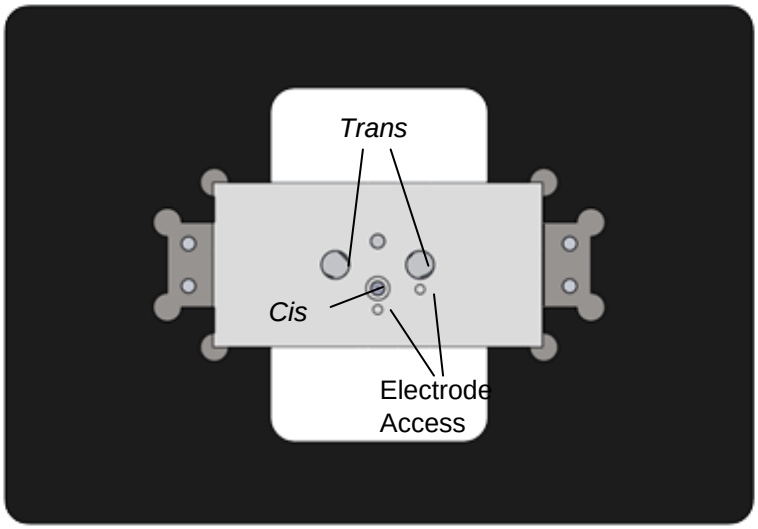

6.1.2 PTFE Chamber

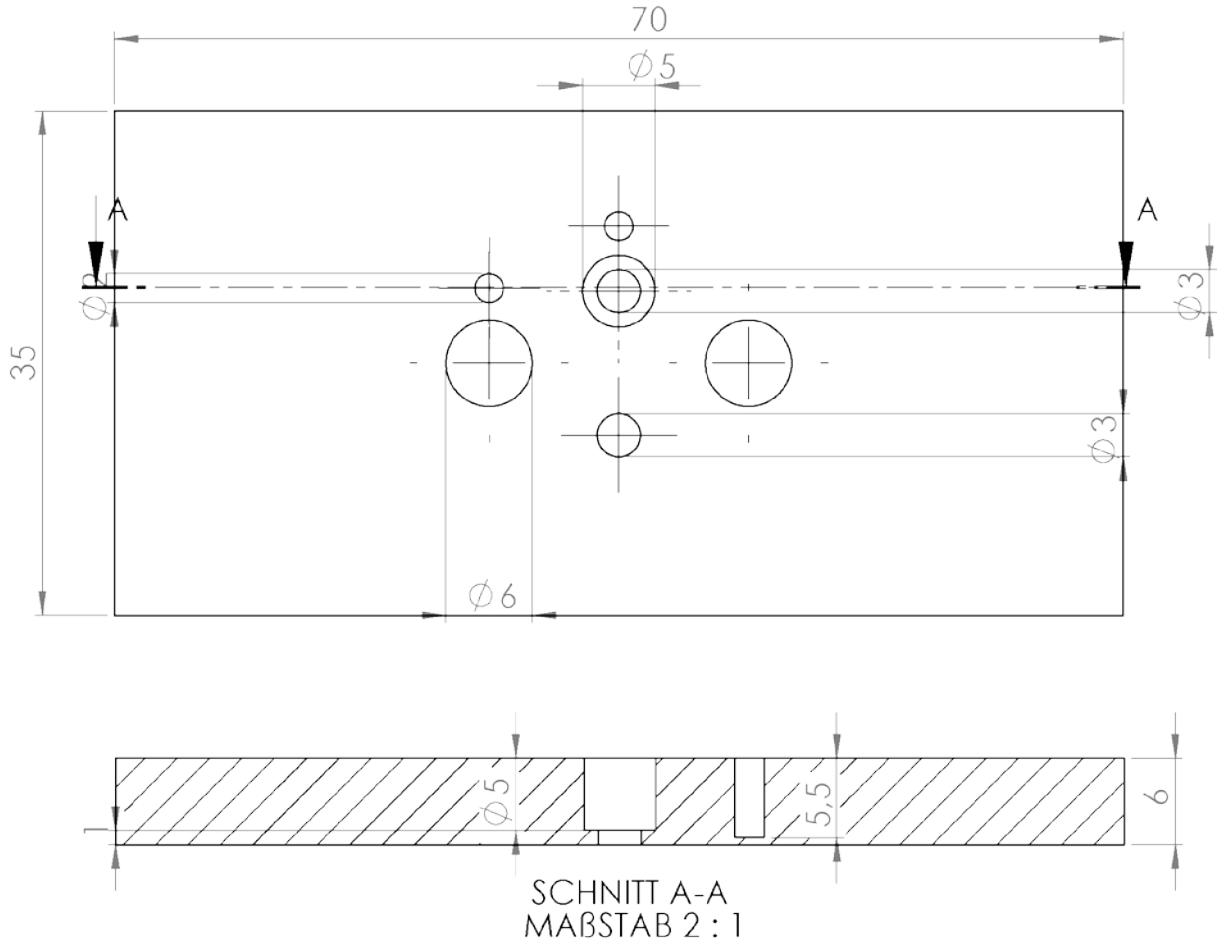

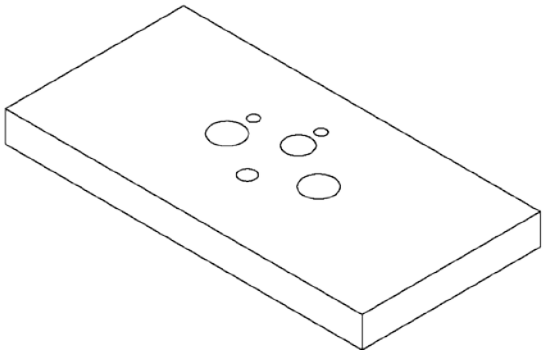

6.1.3 Upper adhesive tape

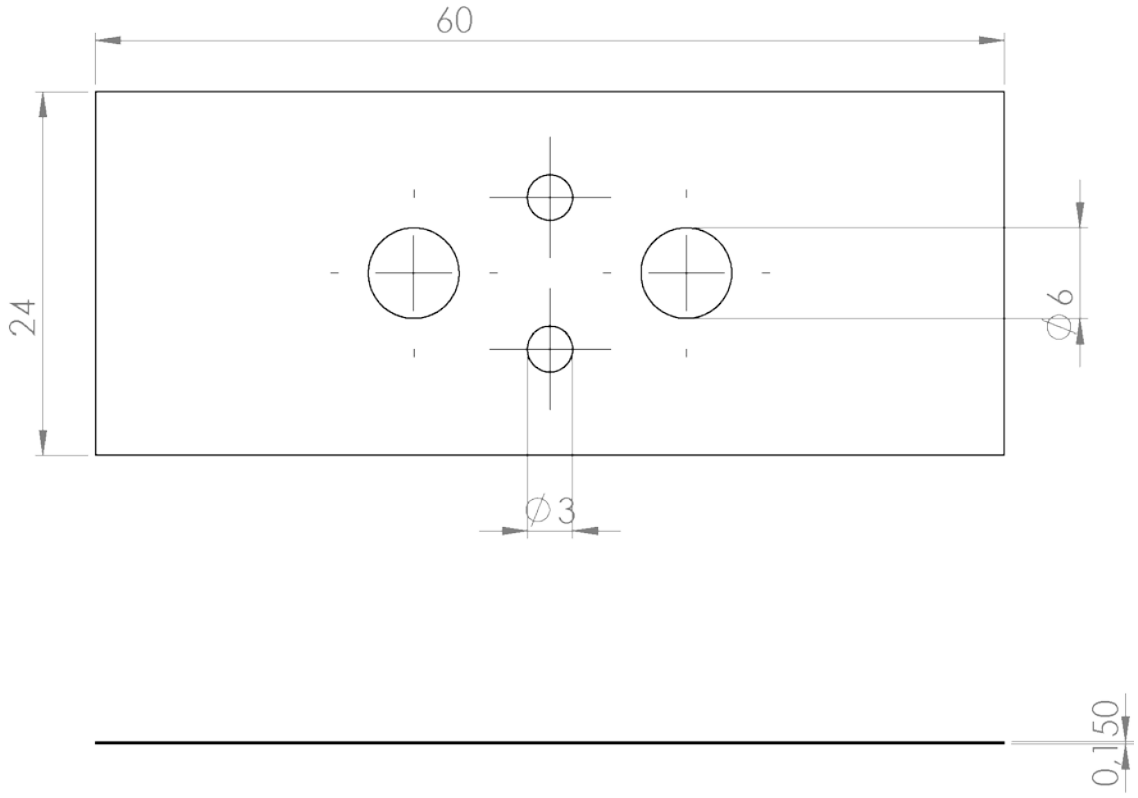

6.1.4 PTFE foil

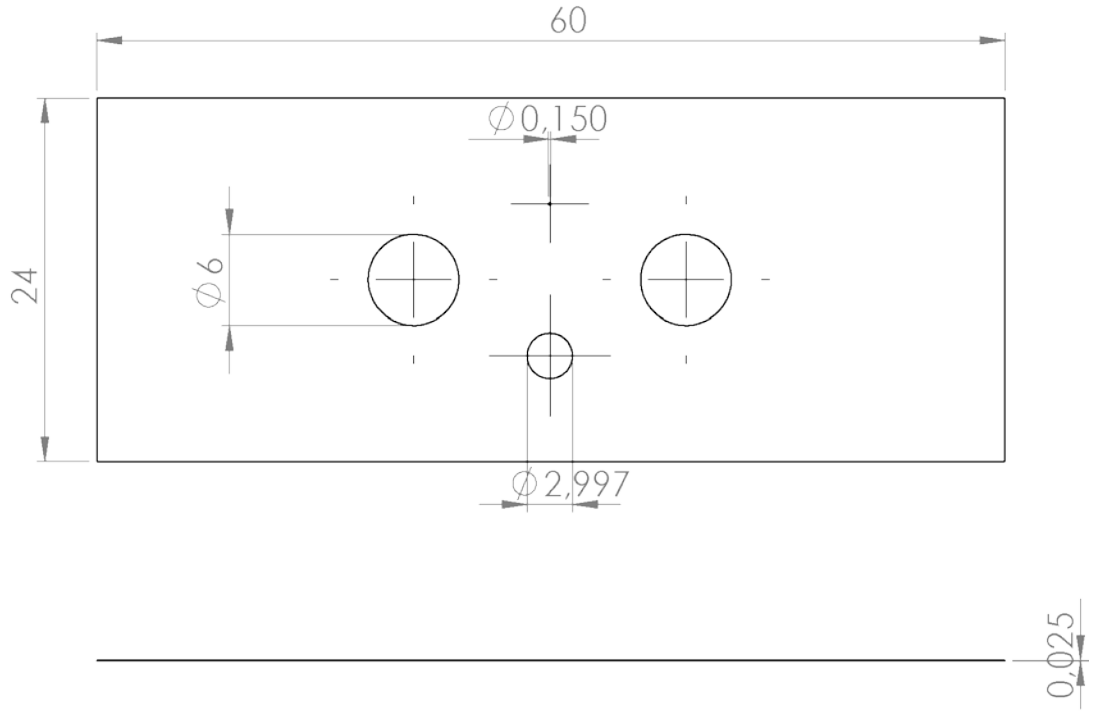

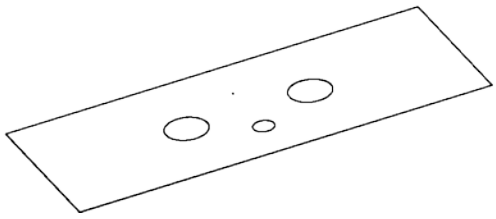

6.1.5 Lower adhesive film

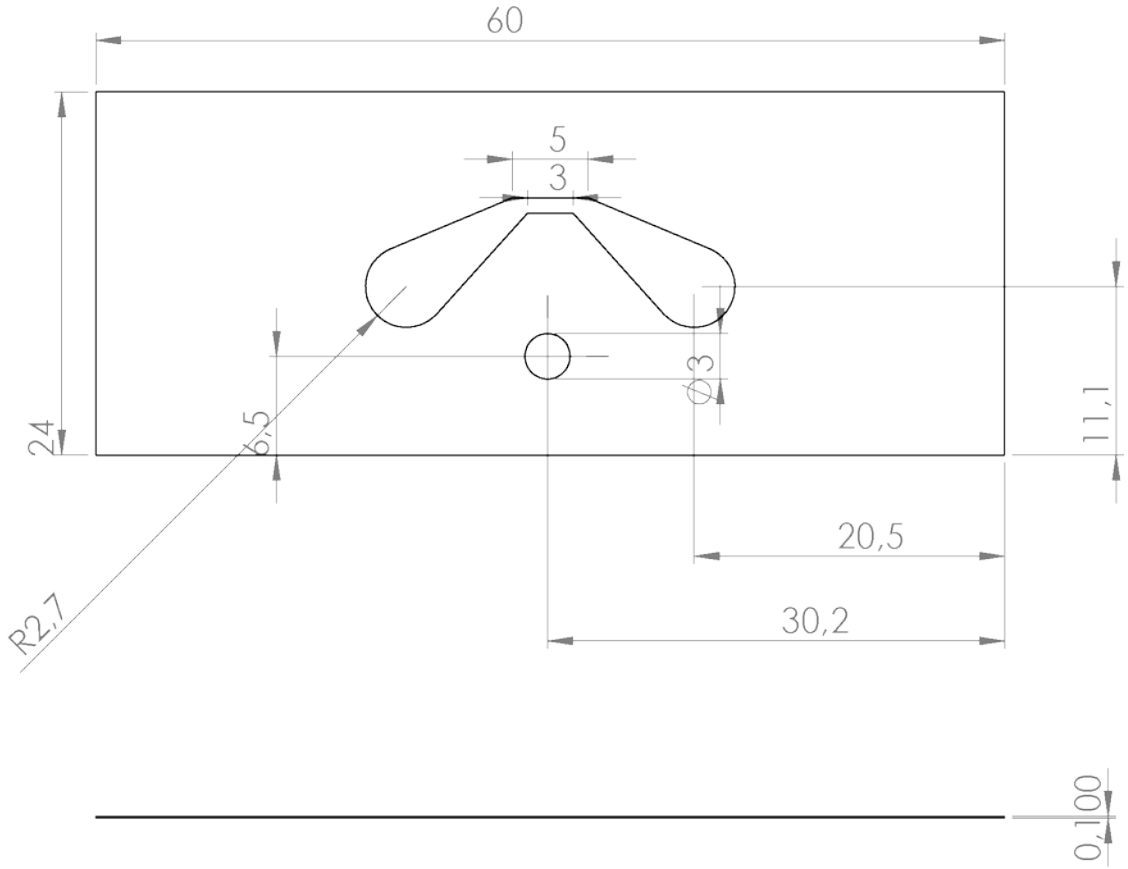

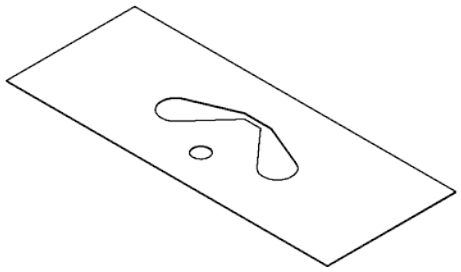

6.1.6 Temperature control

Explosion View:

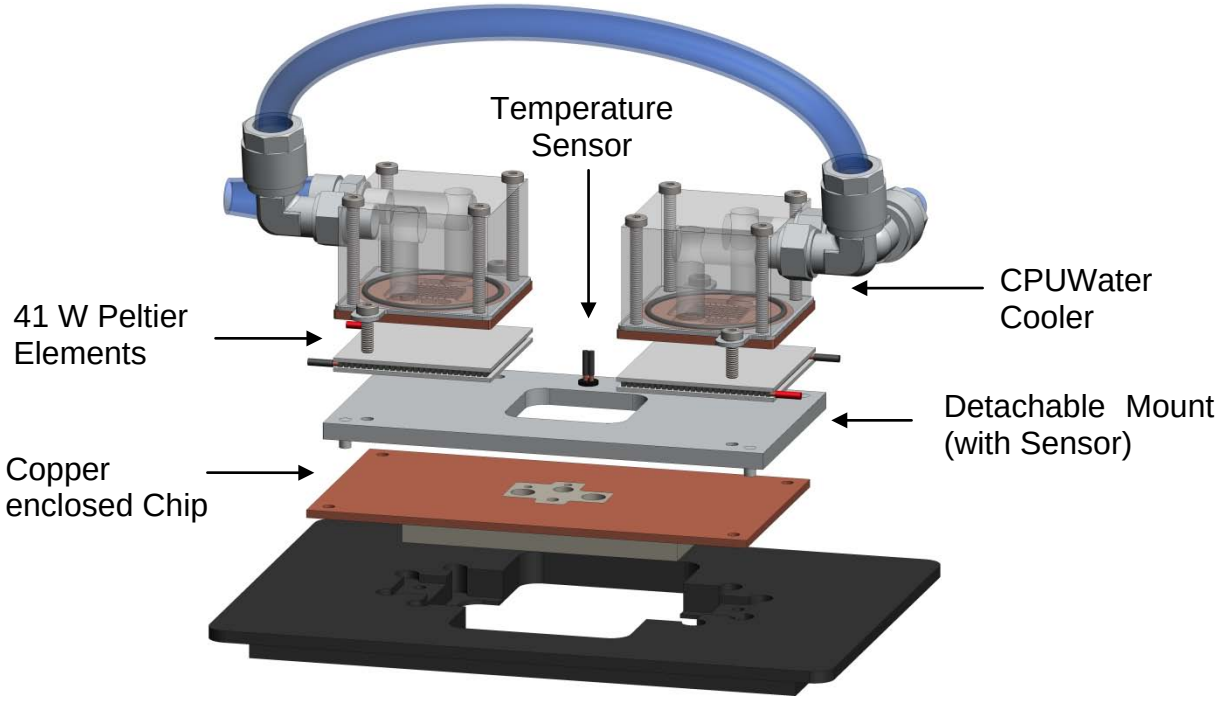

Assembled View:

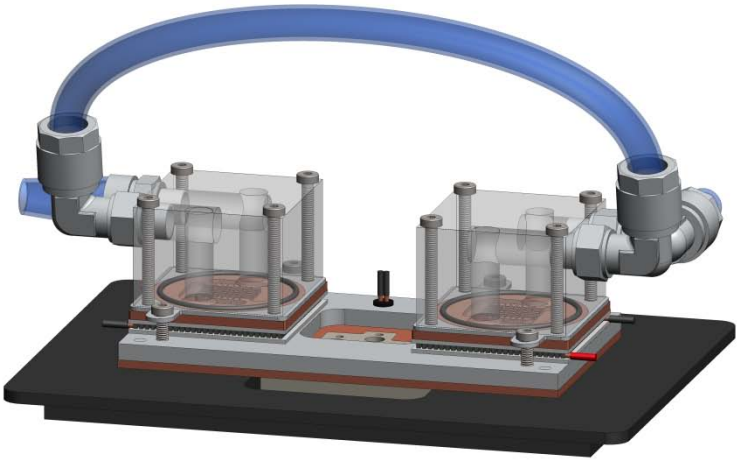

Top View:

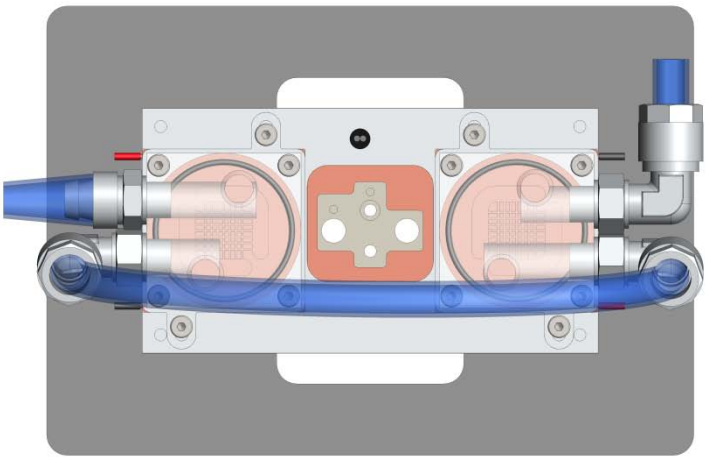

6.2 Publications

The results presented in this thesis are published in:

Ringemann, C., B. Harke, C. v. Middendorff, R. Medda, A. Honigmann, R. Wagner, M. Leutenegger, A. Schonle, S. W. Hell, and C. Eggeling. 2009. Exploring single-molecule dynamics with fluorescence nanoscopy. *New Journal of Physics*. 11:103054.

Honigmann, A, C. Walter, F. Erdmann, C. Eggeling, and R. Wagner. 2010. Characterization of horizontal lipid bilayers as a model system to study lipid phase separation. *Biophysical Journal.* in press

6.3 Index of figures and tables

FIGURE 1.1 CARTOON OF A EUKARYOTIC CELL. 2
FIGURE 1.2 MODEL MEMBRANE SYSTEMS. 4
FIGURE 1.3 BLM SETUP. 5
FIGURE 1.4 BLM FORMATION TECHNIQUES. 6
FIGURE 1.5 PROTEO-LIPOSOME FUSION TO A BLM. 7
FIGURE 1.6 SCHEME OF THE HORIZONTAL LIPID BILAYER SETUP. 9
FIGURE 1.7 FLUORESCENCE CORRELATION SPECTROSCOPY. 11
FIGURE 1.8 Z-SCAN FCS. 13
FIGURE 1.9 THE PRINCIPLE OF TIME-CORRELATED SINGLE PHOTON COUNTING. 14
FIGURE 1.10 THE PRINCIPLE OF TIME RESOLVES ANISOTROPY. 14
FIGURE 2.1 SETUP OF THE HORIZONTAL BILAYER CHAMBER. 26
FIGURE 2.2 DETERMINATION OF THE MINIMAL WAIST SIZE OF THE LASER FOCUS. 29
FIGURE 2.3 SETUP OF THE TEMPERATURE CONTROL. 30
FIGURE 2.4 INFLUENCE OF HYDROCARBON SOLVENTS ON THE DIFFUSION OF LIPIDS 32
FIGURE 2.5 LATERAL AND ROTATIONAL MOBILITY IN DOPC/DSPC/CO (2:1:1) BILAYERS 35
FIGURE 2.6 DIPOLE-ORIENTATION OF ATTO647N-LIPIDS. 36
FIGURE 2.7 STEADY STATE ANISOTROPY AND FCS DIFFUSION LAWS IN HLBS 38

FIGURE 2.8 TEMPERATURE DEPENDENT DIFFUSION OF THE LIPID PROBE SM647 40
FIGURE 2.9 HYDRODYNAMIC VISCOSITY OF HLBS. 41
FIGURE 2.10 CURRENT FLUCTUATIONS IN THE PHASE TRANSITION RANGE 43
FIGURE 2.11 PHASE PARTITIONING AND ELECTRICAL ACTIVITY OF GRAMICIDIN A. 44
FIGURE 3.1 RIBBON REPRESENTATIONS OF COLICIN IA 54
FIGURE 3.2 LABELING SITES OF COLICIN A. 56
FIGURE 3.3 PH DEPENDENT BINDING OF COLA TO HLBS. 62
FIGURE 3.4 PH DEPENDENT BINDING OF COLA-NBD TO LIPOSOMES. 63
FIGURE 3.5 ELECTROPHYSIOLOGICAL CHARACTERISTICS OF COLA IN LIPID BILAYERS. 64
FIGURE 3.6 STEADY STATE FRET MEASUREMENTS OF COLA-488 AND COLA-647. 65
FIGURE 3.7 OLIGOMERIZATION MEASUREMENTS OF COLA IN HLBS 67
FIGURE 3.8 CALCEIN RELEASE FROM LIPOSOME INCUBATED WITH COLA. 68
FIGURE 3.9 FLUORESCENCE LIFETIME OF COLA-NBD MUTANTS. 70
FIGURE 3.10 CONFORMATION OF THE PORE-FORMING DOMAIN OF COLA. 74

6.4 Abbreviations

AFM	Atomic force microscopy
BLM	Black lipid membrane
CER	Ceramide
cFLA	Confocal fluorescence lifetime analysis
CO	Cholesterol
ColA	Colicin A
cTRA	Confocal time-resolved anisotropy
DNA	Deoxyribonucleic acid
DOL	Degree of labeling
DOPC	Dioleoyl-sn-glycero-3-phosphocholine
DPPE	1,2-dihexdecanoyl-sn-glycero-3-phosphatidyl-ethanolamine
DSPC	Distereoyl-sn-glycero-3-phosphocoline
EDTA	Ethylenediaminetetraacetic acid
ESR	Electron spin resonance
FCCS	Fluorescence cross-correlation spectroscopy
FCS	Fluorescence correlation spectroscopy

FFS	Fluorescence fluctuation spectroscopy
FIDA	Fluorescence intensity distribution analysis
FPLC	Fast protein liquid chromatography
gA	Gramicidin A
GUV	Giant uni-lamellar vesicle
HeNe	Helium-Neon
HLB	Horizontal lipid bilayers
IRF	Instrument response function
KV	Voltage gated potassium channels
L_d	Liquid disordered
L_o	Liquid ordered
LSM	Laser scanning microscope
LUV	Large uni-lamellar vesicle
MOPS	3-(N-Morpholino)-propansulfonic-acid
NA	Numeric aperture
NBD	4-chloro-7-nitrobenz-2-oxa-1,3-diazole
NHS	N-hydroxysuccinimide
OD	Optical density
PAGE	Polyacrylamide gel electrophoresis
PCH	Photon counting histogram
PEEK	polyetheretherketon
PS	Petrov-Schwille
PTFE	Polytetrafluorethylene
RMS	Root mean square
SD	Saffman-Delbrueck
SDS	Sodium dodecyl sulfate
SLB	Supported lipid bilayer
SM	Sphingomyelin
smFRET	Single molecule fluorescence resonance energy transfer
SMPC	1-stearoyl-2-myristoyl-sn-glycero-3-phosphocholine
S_o	Solid ordered
STED	Stimulated emission depletion
SUV	Small uni-lamellar vesicle
TCEP	Tris(2-carboxyethyl)phosphine hydrochloride
TIRFM	Total internal reflection microscopy
T_m	Melting temperature
Tris	Tris(hydroxymethyl)amino-methan

6.5 Software

2D Image Editing	Image JA 1.43o Coral DrawX3 MATLAB R2008a
3D Modeling (artistic)	Blender 2.49b
3D Modeling (Proteins)	VMD 1.8.6
Data Evaluation	OriginPro 8 (OriginLab Corporation) MATLAB R2008a
FFS Acquisition/Analysis	SymphoTime (PicoQuant)

Curriculum Vitae

Surname:	Honigmann
First Name:	Oscar Alf
Date of Birth:	08.12.1979
Place of Birth:	Magdeburg
Address:	Bramscher Str. 53
	49088 Osnabrueck

2000	Abitur - Gymnasium Elmschenhagen Kiel
2000-2001	Alternative civilian service - Drachensee Stiftung in Kiel
2001-2006	Study of Biology at the University of Osnabrueck
	Certificate: Master of Science
2006-2010	Promotion at division of Biophysics (AG Wagner) – University Osnabrueck

Declaration

I hereby declare that the presented thesis ‘Simultaneous optical and electrical recordings in horizontal lipid bilayers: Membrane dynamics and protein interactions’ was prepared entirely on my own and I have not used outside sources without declaration in the text. Any concepts or quotations applicable to these sources are clearly attributed to them. I have not attempted a promotion before.

Osnabrueck, the 8th of June 2010

(Alf Honigmann)